# Challenge Journal of CONCRETE RESEARCH LETTERS

Vol.16 No.3 (2025)

acoustic emission aerated concrete artificial neural network compressive strength corrosion cracking ductility durability energy absorption ferrocement flexural strength fly ash fracture mechanics mechanical properties mortar nanoparticle reinforced concrete self-compacting concrete steam curing strengthening superplasticizer tensile strength workability waste disposal water absorption

ISSN 2548-0928

TULPAR ACADEMIC PUBLISHING

Challenge Journal of Concrete Research Letters

**E-mail:** *cjcrl@challengejournal.com*

**Web page:** *cjcrl.challengejournal.com*

**Tulpar Academic Publishing**
*www.tulparpublishing.com*

Challenge Journal of Concrete Research Letters

# CONTENTS



TULPAR ACADEMIC PUBLISHING

Challenge Journal of Concrete Research Letters

Research Article

# Experimental study on the mechanical performance of polypropylene fiber-reinforced concrete incorporating palm oil fuel ash as partial cement replacement

Alaa Omar Tanash [a], Ahmed Mokhtar Albshir Budiea [a,*], Mohd Faizal Md Jaafar [a], Khairunisa Muthusamy [a], Fahrizal Zulkarnain [b]

[a] *Faculty of Civil Engineering Technology, Universiti Malaysia Pahang Al-Sultan Abdullah, 26300 Kuantan, Pahang, Malaysia*
[b] *Department of Civil Engineering, Universitas Muhammadiyah Sumatera Utara, 20238 Medan, Sumatera Utara, Indonesia*

## ABSTRACT

Environmental pollution caused by the disposal of palm oil fuel ash, a type of waste from the palm oil trade, needs to be resolved. At the same time, activities involved in the manufacturing of cement, which is the primary binder in commonly used concrete, have undesirable impacts on the environment. In view of environmental sustainability, the approach of using palm oil fuel ash as a pozzolanic material would contribute towards a cleaner, greener environment. The present study aimed to investigate the fresh and mechanical properties of polypropylene fibre-reinforced concrete mixed with palm oil fuel ash as a cement replacement. Six different mixtures were tested with varying weight percentages of palm oil fuel ash as a cement substitute. Water absorption, workability, compressive strength, and splitting tensile strength were among the tests conducted. Concrete loses some of its workability when palm oil fuel ash is added. The strength of the concrete increases upon incorporating 10% palm oil fuel ash, benefiting from the pozzolanic reaction, which forms a compact internal structure. Notably, at this optimal level, compressive strength improved by approximately 9.5% compared to the control mix after 28 days of curing. This study provides new insights into the underexplored area of incorporating POFA in polypropylene fibre-reinforced concrete (PFRC), where limited prior research exists, thus expanding the understanding of sustainable composite materials. The utilization of palm oil fuel waste for concrete production contributes to the development of environmentally friendly construction materials and supports sustainable building practices.

## ARTICLE INFO

**Article history:**
Received – March 16, 2025
Revision requested – April 14, 2025
Revision received – May 16, 2025
Accepted – May 28, 2025

**Keywords:**
Palm oil fuel ash
Cement replacement
Fibre-reinforced concrete
Mechanical properties
Water absorption



**Citation:** Tanash AO, Budiea AMA, Md Jaafar MF, Muthusamy K, Zulkarnain F (2025). Experimental study on the mechanical performance of polypropylene fiber-reinforced concrete incorporating palm oil fuel ash as partial cement replacement. *Challenge Journal of Concrete Research Letters*, 16(3), 115–124.

## 1. Introduction

Concrete has a high load-bearing capacity and can be used for various construction purposes. The fragile material cannot transfer stresses after fractures. Due to their brittle failure mechanism, fibres make concrete ductile (Hossain et al. 2019). Due to advances in fibre technology and their mechanical strength and endurance, fibres are used in concrete (Liu et al. 2019). Research shows that fibres improve the performance and durability of concrete. Thus, a new composite material has been created by integrating fibres. A cement-based matrix with uniformly and randomly distributed fibres for discontinuous reinforcement forms fibre-reinforced

* *Corresponding author*. Tel.: +60-9-431-5014 ; E-mail address: ahmedbudieea@umpsa.edu.my (A. M. A. Budiea)
ISSN: 2548-0928 / DOI: https://doi.org/10.20528/cjcrl.2025.03.001

concrete (FRC) (Xin et al. 2019). In modern and promising polypropylene fibre-reinforced concrete, fibres in different shapes and geometries are randomly integrated into the cement matrix. The aim is to minimise the susceptibility to fracture and brittleness of cement composites. Due to their low weight, low thermal conductivity, and resistance to acids and alkalis, polypropylene fibres are better than other synthetic fibres (Hesami et al. 2016). FRC is becoming increasingly popular in the construction industry due to increased durability and reduced brittleness, but it also presents challenges in dealing with the environmental impact of cement production. Combining waste materials with FRC is one promising solution to look at.

In 2020, the cement industry produced 4.3 gigatonnes of cement and is expected to increase by 23% by 2050 (EMR, 2025). This growth presents difficulties in meeting the United Nations Sustainable Development Goals in the areas of environment, economics, and society. The main goal of Sustainable Development Goal (SDG) 13 is to tackle and alleviate the consequences of climate change. Meanwhile, cement industry accounts for around 7 to 8% of worldwide carbon emissions (Shah et al. 2022). The use of carbonate minerals harvested from the hills, which involves the removal of green areas, blasting and crushing the rock, and finally calcining it at the factory, causes environmental pollution. By incorporating waste materials from different industries into cement production, the amount of trash being disposed of in landfills can be reduced. This promotes cleanliness (Mohamad et al. 2025). This practice would help to maintain the environment and contribute to the creation of a sustainable and environmentally friendly ecosystem, ultimately leading to improved public health.

On the other hand, both Indonesia and Malaysia more than 85% of world palm oil production (Abdulkadir et al. 2025). Malaysia's palm oil business has grown since the 1970s, extending to rural and suburban regions. Malaysia has 5.9 million hectares of oil palm, 18% of its total land area (MPOC 2021). Malaysian palm oil production is 19.14 million tonnes and is predicted to reach 26.6 million tonnes by 2035 (Gan and Li 2014). Malaysia has 457 oil palm mills that generate biomass waste (Ghulam Kadir et al. 2020). Biomass waste from palm oil farms and mills exceeded 311 million tonnes in 2020 (Terry et al. 2021). Empty bunches, fibres, shells, and liquid effluents are among the waste generated at palm oil mills. Palm oil mills burn palm oil fibres and shells to provide energy for mill operations, producing palm oil fuel ash (POFA). The rise of the palm oil sector will increase palm oil mill byproducts, especially POFA. Disposal of POFA at dumping site pollutes the environment (Patah et al. 2025) and would consume larger space at landfill as it continues to accumulate over the year. The probable harm of POFA disposal to the environment owing to leaching and accidental fire has also been pointed out by Olivia et al. (2024). Thus, using these materials as raw materials in many sectors can help maintain this business and offer a management solution.

Researchers have recently focused on POFA as a viable alternative to cement in the construction industry. Utilising POFA instead of cement in concrete may significantly mitigate the adverse environmental impacts associated with the concrete industry and POFA disposal. The integration of a suitable percentage of ground POFA, which is a pozzolanic ash, as a partial cement replacement, contributes towards an increase in the strength of conventional concrete (Katte et al. 2023; Johan et al. 2023), lightweight concrete (Alnahhal et al. 2021), self-compacting concrete (Mujedu et al. 2020), ultra-high-performance concrete (Abdul Kudus et al. 2023) and paving block (Dasar et al. 2025) via the pozzolanic reaction. The densification of the concrete internal structure, owing to the formation of a larger amount of CSH gel and a reduction in calcium hydroxide, enhances cement-based concrete durability and makes it an attractive waste material to be used in other types of concrete production. So far, the impact of utilising POFA as a cement replacement in polypropylene fibre-reinforced concrete (PFRC) has been explored in a limited scope of research. This study investigates the mechanical performance of PFRC with POFA as a partial cement alternative.

This study addresses that research gap by systematically evaluating the influence of POFA as a partial cement replacement in PFRC across key performance metrics, including compressive strength, splitting tensile strength, workability, and water absorption. The findings aim to advance the development of greener, high-performance cementitious composites and contribute new knowledge to the limited existing literature on POFA-integrated PFRC. While POFA has been extensively studied in self-compacting and lightweight concretes, its role in fibre-reinforced concrete, particularly polypropylene fibre reinforced concrete (PFRC), remains underexplored. This study addresses this gap by investigating the performance of PFRC incorporating varying levels of ground POFA. The research intentions to evaluate the combined effects of POFA's pozzolanic characteristics and fibre reinforcement, offering a novel efforts toward sustainable, durable, and ductile concrete composites suitable for structural applications.

## 2. Methodology

### *2.1. Materials*

The materials used in producing the PFRC are ordinary Portland cement (OPC), palm oil fuel ash (POFA), aggregate, sand, water, polypropylene fibres, and superplasticizer. Ordinary Portland cement, according to ASTM C150 (2020), was used as the primary binder in the concrete mixture. The POFA, shown in Fig. 1, was gathered from a palm oil mill in West Malaysia. The POFA was then dried in an oven at 110 °C for 24 hours to remove its moisture. It was ground into a fine powder using a grinding machine that meets the ASTM C618 (2019) specifications for particle size (66% of the particles pass through a 45 μm sieve) so that it can be used as a pozzolanic ash. Table 1 tabulates the oxide composition of the POFA used. In this study, polypropylene fibre with a length of 12 mm and a diameter of 0.18 mm, which was purchased from a local supplier, was used. Crushed granite aggregates were obtained from a nearby quarry and utilised

as coarse material. River sand was used as fine aggregate. The particle size distribution of the sand is shown in Fig. 2. Tap water was utilised for the preparation and curing of concrete specimens. Superplasticizer was included to sustain a low water-to-cement ratio while preserving the workability of the mixture.

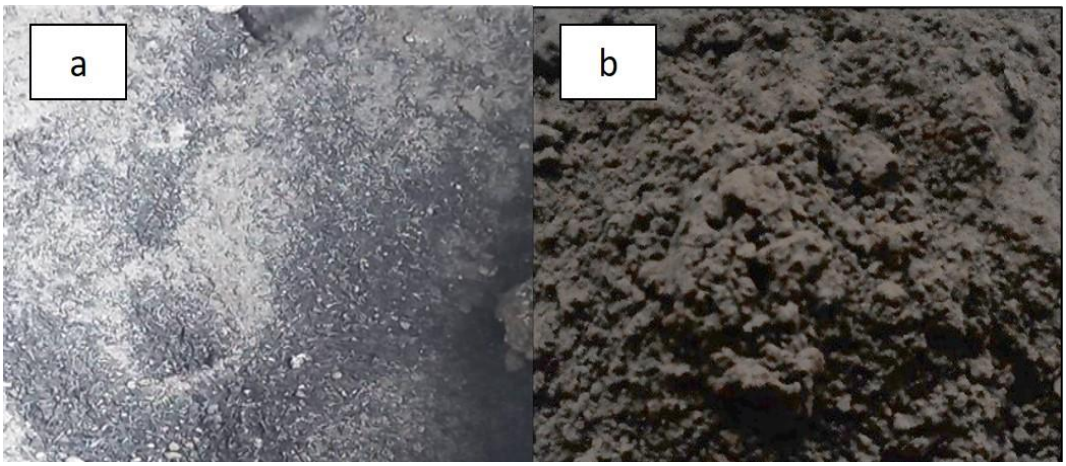


**Fig. 1.** POFA: (a) As received from the mill; (b) After grinding process.

**Table 1.** Oxide composition of binders.

| Type of bnder | $SiO_2$ | $Al_2O_3$ | $Fe_2O_3$ | $K_2O$ | $P_2O_5$ | MgO | $SO_3$ | CaO |
|---|---|---|---|---|---|---|---|---|
| Ordinary portland cement | 17.66 | 3.00 | 3.64 | 0.69 | – | – | 3.16 | 70.92 |
| POFA | 58.4 | 3.24 | 7.85 | 10.2 | 4.96 | 3.71 | 0.90 | 9.58 |

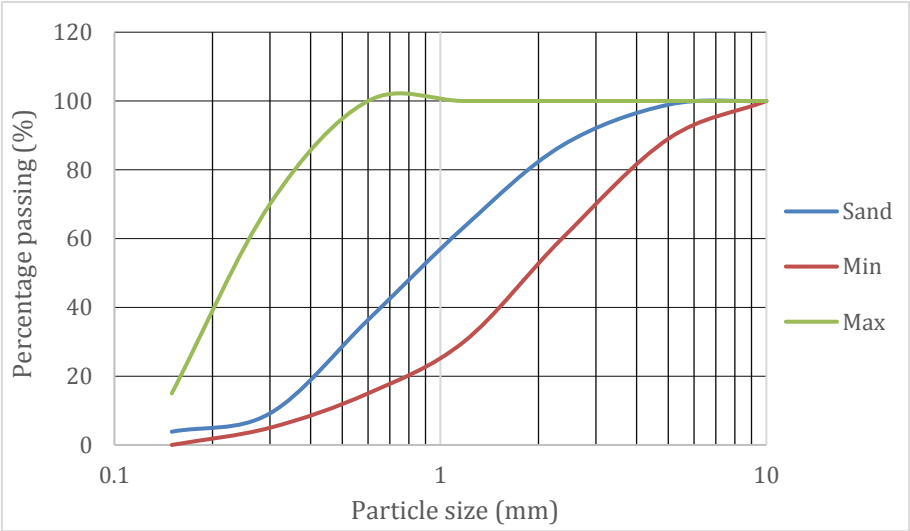


**Fig. 2.** The particle size distribution of the sand.

### *2.2. Mix proportion and specimen preparation*

In this present study, six different concrete mixes were prepared. A control mixture sample with target strength of 42MPa was prepared with no replacement of OPC with POFA. Five further mixes were prepared, each containing a proportion of POFA as a partial cement replacement comprising 10%, 20%, 30%, 40%, and 50% of the total weight of OPC. An identical water-to-cement ratio was used for all combinations. The mixture proportions are specified in Table 2.

All carefully measured components were mixed in a concrete mixer. Crushed coarse aggregate, sand, POFA, OPC, and polypropylene fibre were mixed in a dry state. The concrete was then fully mixed with the addition of water and superplasticizer before being placed in the prepared moulds. A vibrating table was used to compact the concrete mix. Then, the moulds were covered with wet gunny sacks and left overnight. The next day, the concrete was removed from the moulds, labelled, and then immersed in water for curing purposes.

**Table 2.** Mix proportion (kg/m$^3$).

| Mix designation | Cement | POFA | Coarse aggregate | Fine aggregate | Water | Superplasticizer | Fibre |
|---|---|---|---|---|---|---|---|
| 0%POFA | 550 | 0 | 825 | 975 | 216 | 5.8 | 1.5 |
| 10%POFA | 495 | 55 | 825 | 975 | 216 | 5.8 | 1.5 |
| 20%POFA | 440 | 110 | 825 | 975 | 216 | 5.8 | 1.5 |
| 30%POFA | 385 | 165 | 825 | 975 | 216 | 5.8 | 1.5 |
| 40%POFA | 340 | 210 | 825 | 975 | 216 | 5.8 | 1.5 |
| 50%POFA | 340 | 265 | 825 | 975 | 216 | 5.8 | 1.5 |

### *2.3. Testing*

The concrete workability was tested using a slump test following BS EN 12350-2 (2009). The slump test involves filling a metallic slump cone with fresh concrete in three layers, each tamped 25 times with a steel rod. After filling, the cone carefully lifted vertically, and the subsidence of the concrete was measured to evaluate workability.

The compressive strength test was carried out by BS EN 12390-3 (2009). Standard 150 mm × 150 mm × 150 mm cube specimens were cast and cured in water. The test was conducted at 7, 28, and 90 days. Before testing, the cubes were surface-dried, and each sample was placed between the compression platens of a calibrated testing machine and loaded continuously at a rate of 0.5 MPa/s until failure. The average value of three specimens was recorded as the compressive strength for each mix and age.

The splitting tensile strength test followed BS EN 12390-6 (2009). For this, 150 mm diameter × 300 mm cylindrical specimens were used. Each cylinder was placed horizontally between the compression platens of the testing machine. A line load was applied along the length of the cylinder via wooden or steel strips to distribute the load uniformly. The load was applied continuously at a controlled rate until the specimen split along its vertical diameter.

The water absorption test was performed on water-cured concrete cubes following BS 1881-122 (1983). The specimens were oven-dried at 105±5 °C for 24 hours and then cooled in a desiccator to room temperature. The dry weight was recorded. The specimens were then fully immersed in water for 24 hours, surface-dried, and the wet weight was measured. Then the water absorption was calculated following the standard. This procedure helps assess the porosity and permeability characteristics of the concrete.

## 3. Results and Discussion

### *3.1. Workability*

Fig. 3 depicts the impact of including POFA as cement replacement in polypropylene fibre-reinforced concrete (PFRC) on slump values. The alterations in the slump pattern correspond to an increase in POFA quantity. The results indicated a substantial association between the rise in POFA content and a marked reduction in the workability of the PFRC. The slump values for samples with proportions of 0%, 10%, 20%, 30%, 40%, and 50% were 160 mm, 150 mm, 145 mm, 130 mm, 120 mm, and 100 mm, respectively. Substitution of 50% of the cement content with POFA, resulted in a 62.5% reduction compared to the reference samples. The workability of PFRC is affected using POFA, which possesses distinct features compared to OPC. The reduction in workability with the incorporation of POFA may be attributed to its higher carbon content, which absorbs more superplasticizer than alternative particles (Johari et al. 2012; Jimma et al. 2015). In addition, Islam et al. (2016a) indicated a continuous trend when cement was partially replaced with POFA, with the maximum substitution limit set at 10% POFA. The study's findings suggested that increasing the POFA content to 25% led to a reduction in slump levels. Comparable behaviour has also been seen with the incorporation of POFA of several types of concrete (Islam et al. 2016b; Khankhaje et al. 2016). However, there are researcher who observed increment in concrete workability upon blending ground POFA and highlighted the coarser size of POFA in comparison to OPC is one of the contributing factor.

### *3.2. Compressive strength*

The compressive strength of the PFRC is affected by the POFA concentration, as depicted in Fig. 4. The compressive strength values of all PFRC mixtures vary in the different phases of curing. After 7 days they range from 23 MPa to 46.39 MPa, after 28 days from 31.55 MPa to 50.79 MPa and after 90 days from 34.8 MPa to 62.5 MPa. The compressive strength was enhanced when 10% POFA was employed as a cement substitute compared to the control mix. The increase in compressive strength at 10% POFA concentration can be attributed to the creation of a more robust CSH gel resulting from hydration and pozzolanic reactions. A beneficial impact of 10% POFA as pozzolanic ash on the mechanical strength of construction materials has been noted in high-strength lightweight aggregate concrete (Muthusamy et al. 2019). Nonetheless, the strength decreased as the POFA level exceeded 20%. The reduction in strength of cement-based composites containing a higher proportion of pozzolanic ash is attributable to the lowered cement content, which results in a reduced formation of CSH gel and

a lesser amount of calcium hydroxide necessary for the pozzolanic reaction. The total quantity of CSH gel generated from both hydration and pozzolanic reactions is lower than that of the mixture containing a lower amount of POFA (Muthusamy et al. 2016). The strength of PFRC diminishes by 35.9% when 50% POFA is utilised as a cement alternative. Previous studies by Hamada et al. (2020) and Mujedu et al. (2020) have discovered a similar tendency in the investigation of the compressive strength of concrete with the incorporation of high levels of POFA.

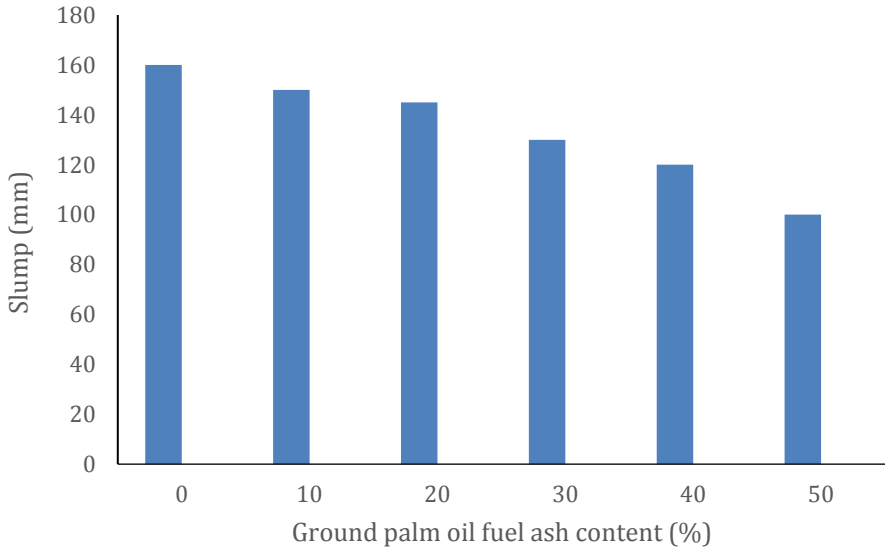


**Fig. 3.** Workability of PFRC containing diverse content of ground POFA.

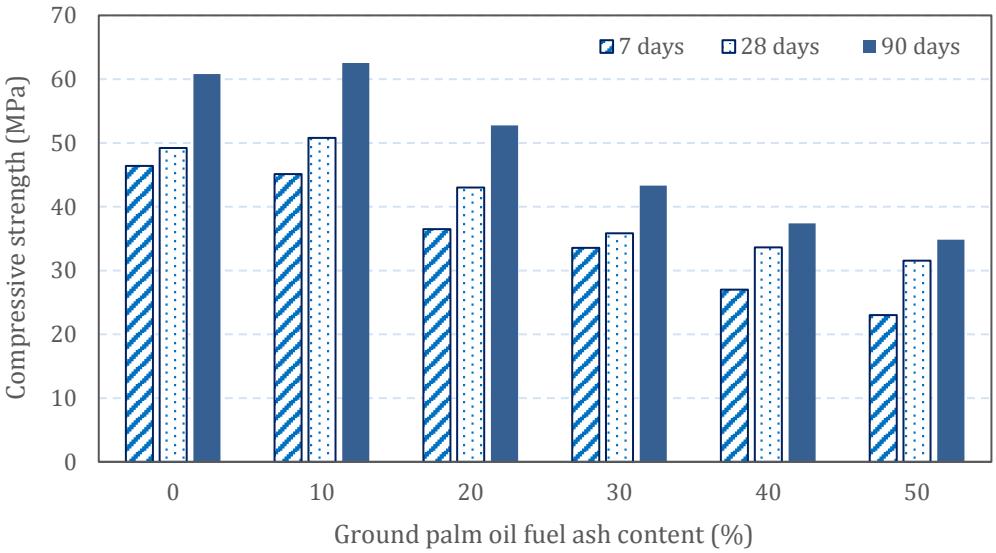


**Fig. 4.** Compressive strength result of concrete mixes.

### *3.3. Splitting tensile strength*

Fig. 5 depicts the splitting tensile strength test results at diverse curing ages. The splitting tensile strength of all mixes increases as curing age become longer. The splitting tensile strength values of all PFRC mixtures vary across different curing phases.

After 7 days, they range from 2.29 MPa to 3.2 MPa, after 28 days from 2.38 MPa to 3.55 MPa, and after 90 days from 3.43 MPa to 4.03 MPa. The PFRC containing 10% POFA demonstrated superior tensile strengths among all mixes. The results demonstrated a 6.2% and 9.2% enhancement in tensile strength following the replacement of 10% of the cement with POFA at 28 and 90 days, respectively. The most significant reduction of 35% and 7% was observed in the PFRC mix containing 50% POFA at 28 and 90 days, respectively. The noted reduction in strength with a cement substitution above 20% by POFA can be ascribed to the lowered generation of hydration products, linked to the decreased cement content.

Interfacial transition zone (ITZ) qualities, which affect concrete tensile strength, may explain the observed phenomenon (Islam et al. 2016). Similar behaviour has been seen in other types of concrete by previous researchers, Muthusamy et al. (2016) and Hamada et al. (2022).

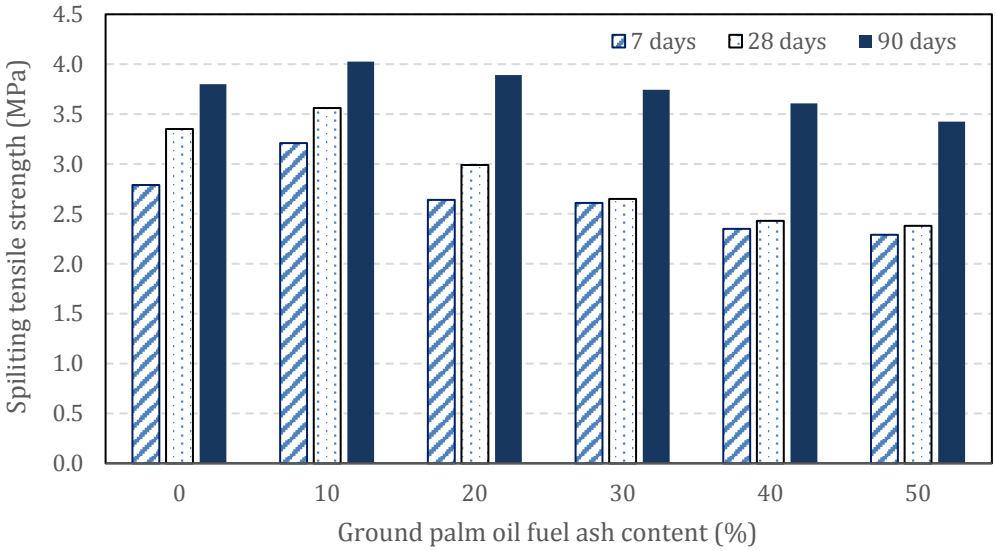


**Fig. 5.** Splitting tensile strength result of concrete mixes.

### *3.4. Water absorption*

Fig. 6 depicts the outcomes of the water absorption test results. 10% replacement levels demonstrated reduced water absorption values relative to the control concrete. Application of up to 10% POFA results in a slight reduction in water absorption relative to the control samples. The PFRC with sustained 10% ground POFA exhibits a slightly reduced water absorption capacity relative to the PFRC without POFA. However, beyond this threshold, the utilization of POFA resulted in a significant rise in the water absorption of the PFRC specimens. The 50% increase in ground POFA content blended led to a substantial enhancement in water absorption, with an increase of up to 50% relative to the control samples. Overuse of POFA causes significant elimination of a high amount of cement, resulting in lower hydration process, forming less calcium hydroxide, which in turn disturbed the pozzolanic reaction. Nonetheless, all concrete mixes exhibit water absorption of less than 2%, indicating it can be classified as good quality concrete. According to Neville and Brooks (2010), concrete with water absorption not exceeding 10% can be classed as a good quality type.

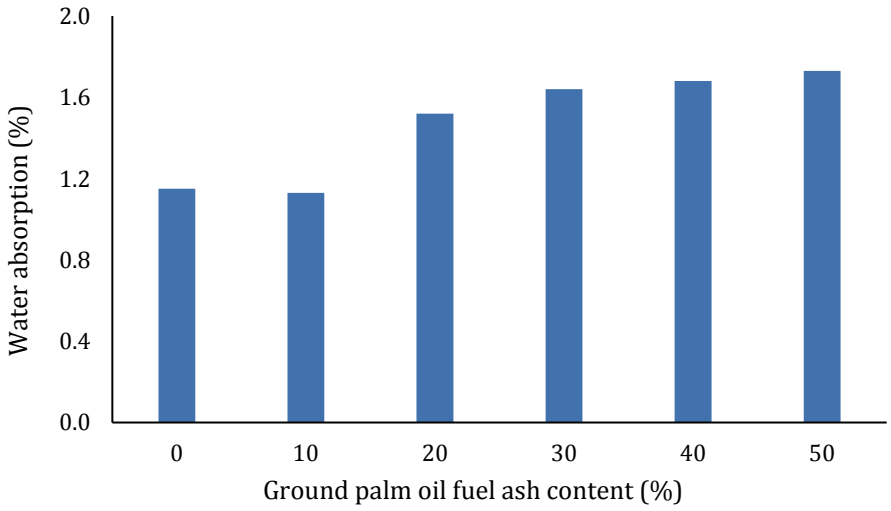


**Fig. 6.** Water absorption result of concrete mixes.

### *3.5. Predictive model using ANOVA and response surface methodology*

The relationship between the compressive strength of PFRC to the curing age and the different percentage levels of POFA using ANOVA is presented in Table 3. The results showed that the sum of squares (1894.01) and *F*-value (107.58) indicate that the model is significant. The corresponding *p*-value of %POFA and curing age obtained from ANOVA is < 0.0001 (less than 0.05) and it indicates the POFA and curing age significantly affect the compressive strength. The results also show that POFA content may contribute to the overall performance of compressive strength of PFRC when compared to curing

age. The sum of squares for %POFA (1368.49) was found to be higher than the curing age (525.52), indicating that POFA content significantly influences the compressive strength of PFRC. The linear regression model using ANOVA yielded that curing age and altered POFA content significantly affected the compressive strength of PFRC as tabulated in Table 4. It also indicates that the relationship between compressive strength and those factors is very strong, where $R^2$ is 0.9348. The model has explained about 93.48% of the variance in compressive strength is explained by the linear model. The empirical relationship between compressive strength (*CS*) against curing age (*A*) and POFA content (*B*) is expressed by Eq. (1), which is only appropriate within the range of POFA content and curing ages adopted in the present research work.

$$CS\,(\text{MPa}) = 47.88544 + 0.153347 \cdot A - 0.51055 \cdot B \quad (1)$$

**Table 3.** Interaction on the responses to the compressive strength of PFRC using ANOVA.

| Source | Sum of squares | df | Mean square | *F*-value | *p*-value | Remark |
|---|---|---|---|---|---|---|
| Model | 1894.01 | 2 | 947.01 | 107.58 | < 0.0001 | significant |
| *A*-Age | 525.52 | 1 | 525.52 | 59.7 | < 0.0001 | |
| *B*-POFA | 1368.49 | 1 | 1368.49 | 155.46 | < 0.0001 | |
| Residual | 132.04 | 15 | 8.8 | | | |
| Cor. Total | 2026.05 | 17 | 947.01 | | | |

**Table 4.** ANOVA fit statistic for compressive strength of PFRC towards curing age and %POFA.

| Model | Std. deviation | $R^2$ | Adjusted $R^2$ | Predicted $R^2$ |
|---|---|---|---|---|
| Linear | 2.97 | 0.9348 | 0.9261 | 0.9029 |

The 3D response surface and perturbation plots offer an understanding of the relationship between curing age, %POFA and compressive strength (CS) of polypropylene fibre reinforced concrete (PFRC) as presented in Fig. 7. The 3D surface in Fig. 7(a) shows a positive relationship between concrete compressive strength (CS) and curing age. The compressive strength increases dramatically as the curing time increases from 7 to 90 days. This pattern is consistent with the behaviour of normal concrete where the process of hydration continues and strengthens after prolonged curing. Interestingly, the effect of POFA content on compressive strength looks like a non-linear relationship.

The inclusion of POFA in PFRC has a significant influence at lower POFA content (10% POFA). However, the compressive strength behaves to decrease for higher contents. This indicated an adverse impact on the strength of PFRC from higher percentages of POFA up to 50%. This occurs through the use of only a partial replacement for cement by POFA that either does not bind well or affects positively strength development. Fig. 7(b) demonstrates perturbation plots visualize the individual effects on compressive strength. Line A (Age) shows an upward slope compared to Line B (%POFA), confirming that curing age consistently enhances its compressive strength. The steepness of Line B indicates that POFA content has a strong and direct impact on the compressive strength of the PFRC. The slope is downward for Line B reflecting the influence of lower content of POFA associated with the highest compressive strength. This line of argument is logical as it reflects the behaviour of POFA, which is not always highly reactive when compared to cement itself and could result in strength loss at higher replacement levels.

A summary of the ANOVA to evaluate the significance of the curing age and POFA replacement to splitting tensile strength of PFRC is provided in Table 5. This model was significant with a *p*-value of 0.0001 and an *F*-value of 65.96. Moreover, it shows that when the p-value is less than 0.05, meaning that the combination of factors has a statistically significant effect on the splitting tensile strength of the PFRC. Obviously, their combined effect is more pronounced when the sum of squares for curing age is higher than %POFA. The results revealed that different levels percentage of POFA have a smaller effect on the splitting tensile strength of the PFRC compared to curing age. This suggests that as the curing age increases, the splitting tensile strength increases significantly, confirming the positive relationship.

On the other hand, the model accounts for 89.79% of the variance in splitting tensile strength ($R^2$ is 0.8979), and thus provides a good relationship as tabulated in Table 6. The linear model is significant meaning that the combination of curing age and POFA content effectively explains the variation in splitting tensile strength. There is only 10.21% of other factors not included in the model contribute very little. From the linear equation, the predicted splitting tensile strength (*STS*) for PFRC at different curing ages (*A*) and integration of POFA (*B*) is shown in Eq. (2). However, this equation is applicable only within the range of POFA content and curing ages used in this experimental work.

$$STS\,(\text{MPa}) = 2.94313 + 0.013379 \cdot A - 0.01614 \cdot B \quad (2)$$

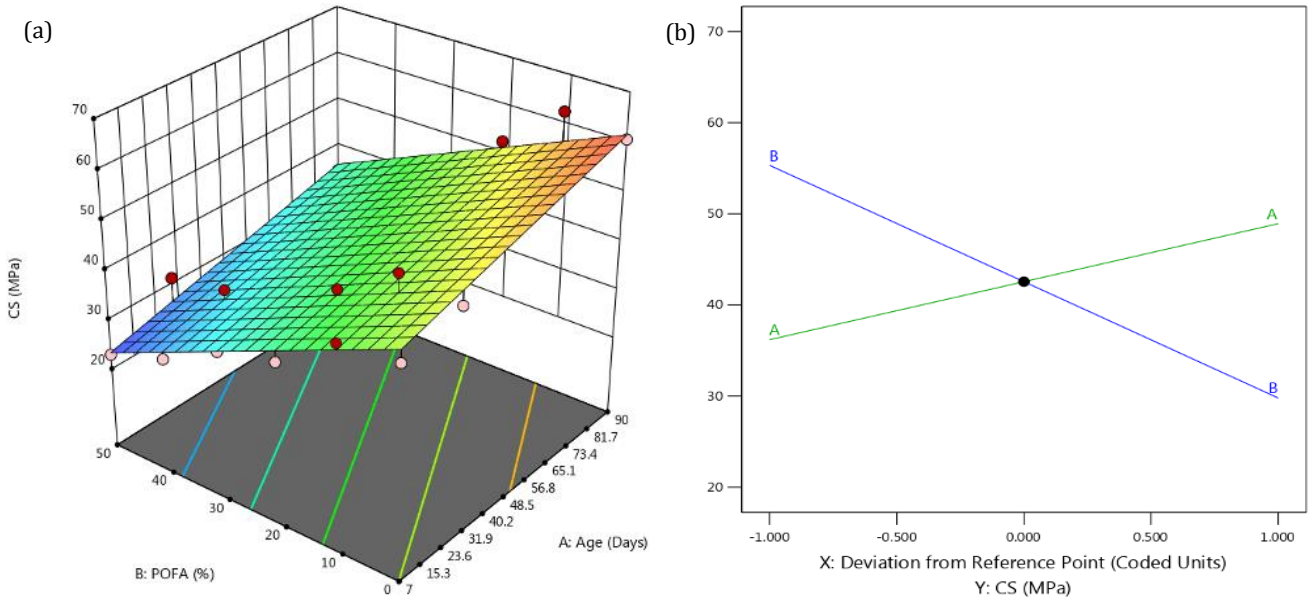


**Fig. 7.** (a) Effects of curing age and %POFA on the compressive strength of PFRC using 3D response surface; (b) Perturbation plots.

**Table 5.** Interaction on the responses to the splitting tensile strength of PFRC using ANOVA.

| Source | Sum of squares | df | Mean square | *F*-value | *p*-value | Remark |
|---|---|---|---|---|---|---|
| Model | 5.37 | 2 | 2.68 | 65.96 | < 0.0001 | significant |
| *A*-Age | 4 | 1 | 4 | 98.3 | < 0.0001 | |
| *B*-POFA | 1.37 | 1 | 1.37 | 33.63 | < 0.0001 | |
| Residual | 0.6104 | 15 | 0.0407 | | | |
| Cor. Total | 5.98 | 17 | | | | |

**Table 6.** ANOVA fit statistic for splitting tensile strength of PFRC towards curing age and %POFA.

| Model | Std. deviation | $R^2$ | Adjusted $R^2$ | Predicted $R^2$ |
|---|---|---|---|---|
| Linear | 0.2017 | 0.8979 | 0.8843 | 0.8325 |

Fig. 8 depicts the 3D response surface and perturbation plots for splitting tensile strength of PFRC containing various percentages of POFA over the different curing ages. The plot in Fig. 8(a) shows a positive correlation between curing age and splitting tensile strength. It shows that prolonged curing age boosts splitting tensile strength due to the continued hydration process. Meanwhile, PFRC incorporating different levels of POFA content had a less significant effect on splitting tensile strength. However, PFRC containing 10% POFA developed strength compared to control PFRC and modified PFRC incorporating 20%, 30%, 40% and 50% POFA. At lower POFA content, splitting tensile strength tends to be higher as the curing age increases. This indicates that although the curing age improves the overall splitting tensile strength performance, POFA can only replace a certain percentage of cement without affecting the strength performance, particularly when exceeding 20% POFA. The negative effect of POFA content on splitting tensile strength is also supported by the perturbation plot in Fig. 8(b), emphasizing that a higher level of POFA replacement reduces strength. The steepness of Line A representing the curing age shows an upward trend, indicating the splitting tensile strength increases as the curing age increases. The sharp slope of Line B (%POFA) demonstrates a downward trend, a considerable negative effect on the splitting tensile strength. It is evident from the perturbation plot that the percentage of POFA causes a decrease in splitting tensile strength when the replacement percentage exceeds the optimum range. This is because when POFA is used in higher proportions, the lower pozzolanic reactivity of POFA compared to conventional cement contributes to the reduction of splitting tensile strength.

### *3.6. Economic analysis*

In addition to mechanical performance, the economic feasibility of incorporating POFA in polypropylene fibre-reinforced concrete (PFRC) was briefly assessed. Based

on local pricing, POFA sourced from palm oil mills is significantly less expensive than ordinary Portland cement (OPC), primarily due to its status as an industrial waste byproduct. According to market estimates (e.g., OPC at USD 100/tonne and POFA at USD 20/tonne), a 10% replacement level results in approximately 8–12% reduction in binder cost per cubic metre of concrete, depending on processing and transport expenses. Furthermore, utilizing POFA contributes to waste reduction and may provide long-term savings through reduced environmental charges and sustainability incentives. This cost-effectiveness, combined with the improved mechanical performance at 10% POFA, highlights the practical potential of this technique in sustainable construction applications.

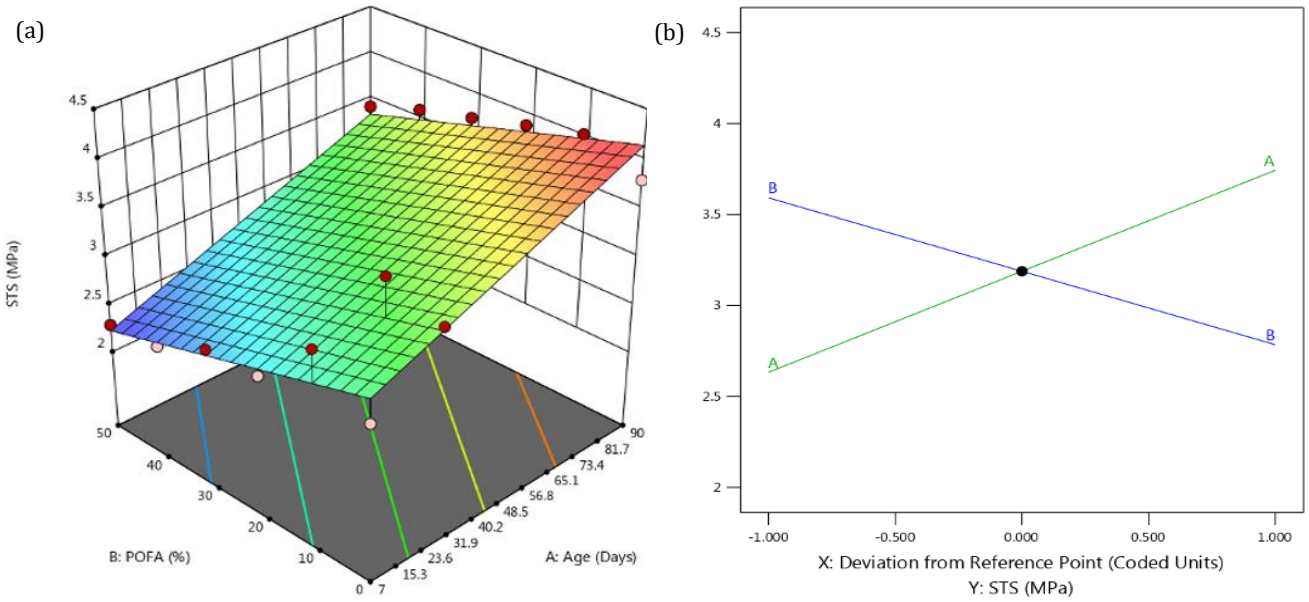


**Fig. 8.** (a) Effects of curing age and %POFA on the splitting tensile of PFRC using 3D response surface; (b) Perturbation plots.

## 4. Conclusions

This study explored the impact of incorporating palm oil fuel ash (POFA) as a partial cement replacement on the performance of polypropylene fibre reinforced concrete (PFRC).

The findings highlight that using POFA at a 10% replacement level enhances the mechanical strength. Notably, compressive and splitting tensile strengths improved at this dosage, while water absorption was slightly reduced compared to the control mix. These improvements are attributed to the pozzolanic activity of POFA, which contributes to the formation of additional calcium silicate hydrate (C–S–H) gel. However, beyond the 10% replacement level, the benefits began to diminish. At higher substitution rates, particularly above 20%, the concrete exhibited lower strength and workability. This decline is likely due to the reduced availability of cementitious materials and the limited reactivity of excess POFA. While all mixes remained within the acceptable range for water absorption, the loss in mechanical strength at higher POFA contents suggests a clear performance trade-off. Statistical analysis using ANOVA confirmed that both curing age and POFA content significantly affect strength development. Curing age showed a consistently positive influence, especially on splitting tensile strength, while POFA's effect was more variable, with a peak at 10%. Regression models showed strong predictive accuracy, accounting for over 93% and 89% of the variability in compressive and tensile strengths, respectively. Visual analyses through 3D surface and perturbation plots reinforced these trends, illustrating the optimal performance at low POFA levels and a drop-off as the replacement percentage increased. In summary, POFA can be a viable, sustainable cement substitute in PFRC when used in moderation. A replacement level of around 10% offers the best balance between mechanical strength and sustainability, making it a practical option for improving the environmental footprint of concrete without compromising its structural performance. This places POFA-blended PFRC as a promising material for sustainable construction, particularly in regions with a plentiful palm oil industry byproducts.

## References

Abdul Kudus S, Mustafa NK, Shahidan S (2022). Influence of palm oil fuel ash on mechanical properties of ultra-high-performance concrete. *International Journal of Sustainable Construction Engineering and Technology*, 13(4), 44–53.

Abdulkadir I, Wong LS, Ean LW, Mohammed BS, Kong SY (2025). Optimizing environmentally efficient mortar properties through synergistic integration of cellulose microfibers and calcined palm oil fuel ash: A response surface methodology technique. *Construction and Building Materials*, 458, 139687.

ASTM C150 / C150M – 20 (2020). Standard specification for Portland cement. ASTM International, West Conshohocken, PA, USA.

ASTM C618 – 19 (2019). Standard specification for coal fly ash and raw or calcined natural pozzolan for use in concrete. ASTM International, West Conshohocken, PA, USA.

***Acknowledgements***

*The financial support by Universiti Malaysia Pahang Al-Sultan Abdullah, under the International Matching Grant Scheme, was gratefully acknowledged. The contribution from Universitas Muhammadiyah Sumatera Utara was equally acknowledged and appreciated.*

***Funding***

*This research was supported by Universiti Malaysia Pahang Al-Sultan Abdullah under grant number UIC231507.*

***Conflict of Interest***

*The authors declared no potential conflicts of interest with respect to the research, authorship, and/or publication of this manuscript.*

***Author Contributions***

*All of the authors made substantial contributions to conception and design, or acquisition of data, or analysis and interpretation of data; were involved in drafting the manuscript or revising it critically for important intellectual content; and gave final approval of the version to be published.*

***Data Availability***

*The datasets created and/or analyzed during the current study are not publicly available, but are available from the corresponding author upon reasonable request.*

Alnahhal AM, Alengaram UJ, Yusoff S, Singh R, Radwan MKH, Deboucha W (2021). Synthesis of sustainable lightweight foamed concrete using palm oil fuel ash as a cement replacement material. *Journal of Building Engineering*, 35, 102047.

BS 1881-122 (1983). Testing concrete – Method for determination of water absorption. British Standards Institution (BSI), London, UK.

BS EN 12350-2 (2009). Testing fresh concrete – Part 2: Slump test. British Standards Institution (BSI), London, UK.

BS EN 12390-3 (2009). Testing hardened concrete – Part 3: Compressive strength of test specimens. British Standards Institution (BSI), London, UK.

BS EN 12390-6 (2009). Testing hardened concrete – Part 6: Tensile splitting strength of test specimens. British Standards Institution (BSI), London, UK.

Dasar A, Patah D, Okviyani N (2025). Impact of incorporating nano-palm oil fuel ash on the mechanical properties and durability of paving blocks prepared with seawater and sea sand for sustainable construction. *Construction Building Materials*, 481, 141539.

EMR (2021). Global Cement Market Report and Forecast 2021–2026. https://www.expertmarketresearch.com/reports/cement-market [accessed 10-02-2025].

Gan PY, Li ZD (2014). Econometric study on Malaysia's palm oil position in the world market to 2035. *Renewable and Sustainable Energy Reviews*, 39, 740–747.

Ghulam Kadir AP, Hishamuddin E, Loh SK, Ong-Abdullah M, Kamalrudin MS, Mohd Zanal Bidin MNI, Sundram S, Azizul Hasan ZA, Idris Z (2020). Oil Palm Economic Performance in Malaysia and R&D Progress in 2019. *Journal of Oil Palm Research*, 32(2), 159–190.

Hamada HM, Al-attar AAA, Yahaya FM, Muthusamy K, Tayeh BA, Humada AM (2020). Effect of high-volume ultrafine palm oil fuel ash on the engineering and transport properties of concrete. *Case Studies in Construction Materials*, 12, e00318.

Hamada HM, Al-attar AAA, Tayeh BA, Yahaya FM (2022). Optimizing the concrete strength of lightweight concrete containing nano palm oil fuel ash and palm oil clinker using response surface method. *Case Studies in Construction Materials*, 16, e01061.

Hesami S, Salehi Hikouei I, Emadi SAA (2016). Mechanical behavior of self-compacting concrete pavements incorporating recycled tire rubber crumb and reinforced with polypropylene fiber. *Journal of Cleaner Production*, 133, 228–234.

Hossain M, Shahjalal K, Islam M, Tiznobaik MS, Alam M (2019). Mechanical properties of recycled aggregate concrete containing crumb rubber and polypropylene fiber. *Construction and Building Materials*, 225, 983–996.

Islam MMU, Islam Mo, KH Alengaram UJ, Jumaat MZ (2016a). Mechanical and fresh properties of sustainable oil palm shell lightweight concrete incorporating palm oil fuel ash. *Journal of Cleaner Production*, 115, 307–314.

Islam MMU, Islam Mo, KH Alengaram UJ, Jumaat MZ (2016b). Durability properties of sustainable concrete containing high volume palm oil waste materials. *Journal of Cleaner Production*, 137, 167–177.

Jimma B, Rangaraju PR (2015). Chemical admixtures dose optimization in pervious concrete paste selection–A statistical approach. *Construction and Building Materials*, 101, 1047–1058.

Johan NHS, Khalid FS (2023). Strength of concrete containing POFA and fine recycled concrete as partial cement replacement. *Recent Trends in Civil Engineering and Built Environment*, 4(2), 126–134.

Johari MM, Zeyad A, Bunnori NM, Ariffin K (2012). Engineering and transport properties of high-strength green concrete containing high volume of ultrafine palm oil fuel ash. *Construction and Building Materials*, 30, 281–288.

Katte AR, Mwero J, Gibigaye M, Koteng DO (2023). Recycling palm oil wastes for the production of a pozzolanic cement replacement material for concrete. *Results in Engineering*, 17, 100903.

Khankhaje E, Hussin MW, Mirza J, Rafieizonooz M, Salim MR, Siong HC, Warid MNM (2016). On blended cement and geopolymer concretes containing palm oil fuel ash. *Materials & Design*, 89, 385–398.

Liu J, Jia Y, Wang J (2019). Experimental study on mechanical and durability properties of glass and polypropylene fiber reinforced concrete. *Fibers and Polymers*, 20, 1900–1908.

Mohamad N, Embong R, Othman NH, Muthusamy K, Md Jaafar MF (2025). Flowability and compressive strength of ternary blended cement mortar of coal bottom ash and ground cockle shell ash. *Challenge Journal of Concrete Research Letters*, 16(1), 25–32.

MPOC (2021). Fact Sheets Malaysian Palm Oil. https://mpoc.org.my/fact-sheets-malaysian-palm-oil/ [accessed 29-12-2021].

Mujedu KA, Ab-Kadir MA, Ismail M (2020). A review on self-compacting concrete incorporating palm oil fuel ash as a cement replacement. *Construction and Building Materials*, 258, 119541.

Muthusamy K, Mirza J, Zamri NA, Hussin MW, Majeed APA, Kusbiantoro A, Budiea AMA (2019). Properties of high strength palm oil clinker lightweight concrete containing palm oil fuel ash in tropical climate. *Construction and Building Materials*, 199, 163–177.

Muthusamy K, Zamri NA (2016). Mechanical properties of oil palm shell lightweight aggregate concrete containing palm oil fuel ash as partial cement replacement. *KSCE Journal of Civil Engineering*, 20, 1473–1481.

Neville AM, Brooks JJ (2010). Concrete Technology (2nd edition). Pearson Education Limited, Harlow, England.

Olivia M, Maulidi MA, Fadhlurrahman, Wibisone G (2024). Characteristics of palm oil fuel ash concrete admixed with precipitated silica and silica fume. *Cleaner Engineering and Technology*, 19, 100738.

Patah D, Dasar D, Okviyani N (2025). Sustainable concrete using seawater, sea-sand, and ultrafine palm oil fuel ash: Mechanical properties and durability. *Case Studies in Construction Materials*, 22, e04129.

Shah IH, Miller SA, Jiang D, Myers J (2022). Cement substitution with secondary materials can reduce annual global CO2 emissions by up to 1.3 gigatons. *Nature Communications*, 13, 5758.

Terry LM, Li C, Chew JJ, Aqsha A, How BS, Loy ACM, Chin BLF, Khaerudini DS, Hameed N, Guan G, Sunarso J (2021). Bio-oil production from pyrolysis of oil palm biomass and the upgrading technologies: A review. *Carbon Resources Conversion*, 4, 239–250.

Xin CL, Wang ZZ, Zhou JM, Gao B (2019). Shaking table tests on seismic behavior of polypropylene fiber reinforced concrete tunnel lining. *Tunnelling and Underground Space Technology*, 88, 1–15.

Challenge Journal of Concrete Research Letters

Research Article

# Predictive modelling of acoustic emission signal data for corrosion assessment: A modified dimensional analysis based approach

Shilpa Vishal Patil [a,*]

[a] *Department of Civil Engineering, Vishwakarma Institute of Technology, Pune, 411037 Maharashtra, India*

**ABSTRACT**

Acoustic emission (AE) technique has been proved as a powerful technique for structural health monitoring. AE technique can also be efficiently used for evaluation of corrosion activity in concrete. Despite its advantages, an effective analysis of data recorded by AE technique still founds to be a challenging task demanding an appropriate damage assessment methodology. For quantification of damages, various methods for analysis of AE data have been proposed but not a single method has found to be standardized for specific application. In this paper, a procedure for analysis of AE signals is proposed using modified dimensional analysis method. Many times, it becomes difficult to choose the appropriate AE parameter which can be effectively co-related to the physical feature for development of accurate prediction model. Hence, in the present research work an attempt has been made to develop a model by incorporating primary characteristic AE waveform parameters. A corrosion rate prediction model using modified dimensional analysis of AE signals is developed and compared with the model developed using non-linear regression analysis. The performance of two models is further assessed using different statistical parameters. The study demonstrated that the methodology of modified dimensional analysis indicated improvement in the corrosion rate predictions. Thus, modified dimensional analysis can be implemented as a promising method for analysis of complex AE signal data as well as for development of statistical modelling of corrosion phenomenon in reinforced concrete based on recorded AE parameters.

**ARTICLE INFO**

**Article history:**
Received – March 21, 2025
Revision requested – May 21, 2025
Revision received – June 4, 2025
Accepted – June 17, 2025

**Keywords:**
Acoustic emission signals
Modified dimensional analysis
Non-linear regression analysis
Corrosion prediction
Statistical measures



**Citation:** Patil SV (2025). Predictive modelling of acoustic emission signal data for corrosion assessment: A modified dimensional analysis based approach. *Challenge Journal of Concrete Research Letters*, 16(3), 125–132.

## 1. Introduction

Cracking of concrete due to corrosion of steel embedded in concrete is a major cause for deterioration of reinforced concrete (RC) structures. The risk of corrosion increases with the increase in age of the structure. Deterioration of the structure due to corrosion is of a great concern in the maintenance and repair of many civil structures in the coastal regions. Hence, for safety of RC structures, early detection of damages and appropriate prediction of corrosion status is the need of the day. For such damage detection, use of non-destructive techniques is on the rise as it is non-invasive in nature. The non-destructive techniques like half-cell potential, linear polarization resistance method, Tafel extrapolation technique and infrared thermograph are some of the practically adopted techniques for corrosion monitoring of RC structures (Song and Saraswathy 2007). Acoustic emission (AE) technique is one of the non-invasive techniques used for detection of corrosion and subsequent cracking of concrete. AE technique detects corrosion by capturing energy released by micro-cracks generated in concrete due to corrosion reaction (Ing et al. 2005; Idrissi and Limam 2003; Patil et al. 2014). The past studies by Ohtsu and Tomoda (2008), Kawasaki et al. (2010, 2013) and Di Benedetti et al. (2013) have revealed that

* *Corresponding author*. E-mail address: shilpa.patil@vit.edu (S. V. Patil)
ISSN: 2548-0928 / DOI: https://doi.org/10.20528/cjcrl.2025.03.002

AE technique can indicate an early warning of corrosion as compared to well-established electrochemical techniques. Idrissi and Limam (2003) showed a good correlation between the acoustic emission activity and corrosion current density. It is also reported in the literature that AE is a very powerful technique used for structural health monitoring which provides adequate information about the condition of structures for executing maintenance work in RC structures (Fricker and Vogel 2007; Di Benedetti and Nanni 2014; Patil et al. 2017; Nair and Cai 2010; Verstrynge et al. 2022).

Different methods are being used for analysis of data collected using AE technique. Usually, two main approaches namely parameter-based analysis and signal-based analysis of AE data are used in practice to characterize the damage due to corrosion. The parameter-based analysis includes study of variation of different AE parameters like cumulative signal strength, RA value & average frequency, b-value or Ib-value as well as intensity analysis based on historic index and severity index. The second approach of signal-based analysis mainly includes evaluation of the entire waveform recorded in AE system on the basis of three-dimensional localization of the AE source. One of the effective signal-based AE techniques is SiGMA analysis which identifies 3D AE source location based on moment tensor analysis (Zaki et al. 2015). Another method of a cluster analysis of AE data is also being used to correlate with the failure mechanisms of the material under study (Yu et al. 2023). Various machine learning tools are also being used now a days for corrosion rate prediction in cementitious mortars (Ji and Ye 2023; Thirumalaiselvi and Sasmal 2024). Thus, various researchers have proposed various methods in AE technique for quantification of damage and not a single method yet has found to be universally approved or standardized for specific application.

Although, AE technique is known as a qualitative technique, Ing et al. (2005) had tried to correlate absolute energy parameter of AE data with gravimetrical mass loss; but they could not establish any confirm relationship. On the other hand, Patil et al. (2015) have demonstrated the implementation of AE technique for quantification of corrosion in RC elements by establishing a nonlinear relationship between AE parameter and loss in mass of steel rebars. This relationship was obtained by performing non-linear regression analysis on the data collected through laboratory-based experimentation under accelerated corrosion condition. The mathematical expression formulated by Patil et al. (2015) is based on only one AE parameter namely "cumulative signal strength" (CSS). Even though analysis based on one AE parameter is easy and practicable, the evaluation of the entire AE waveform may provide wider perception to understand the failure mechanism. Many times, it also becomes difficult to choose the appropriate AE parameter which can be effectively co-related to the physical feature for development of accurate prediction model. Hence, in the present research work an attempt has been made to develop a model by incorporating five primary characteristic AE waveform parameters namely - amplitude, AE counts, rise time, duration and signal strength for prediction of corrosion rate of reinforcing steel in concrete. A comprehensive approach of modified dimensional analysis is used here to develop the model based on AE parameters. Although the method of dimensional analysis is a well-established mathematical method, its application for the analysis of AE signal data has not been explored yet.

## 2. Modified Dimensional Analysis

Dimensional Analysis is a mathematical technique which has been used in varied engineering and non-engineering applications. The technique is based on Buckingham Pi theorem but, it involves certain limitations such as need of accurate selection of number of parameters for the analysis, accurate selection of dimensionless groups and accurate elimination of redundant variables. To overcome these limitations, Butterfield (1999) had suggested modification in the method which is less complex and comprehensive. The major advantage of this modified Buckingham Pi theorem suggested by Butterfield (1999) is that it helps to maintain the dimensional homogeneity and mathematical stability of the final formulation. Thus, due to less complexity involved, this modified method has been applied to predict various engineering properties such as: to predict load settlement characteristic of large spread footings in sand (Phatak and Dhonde 2000), to predict ultimate torsional strength of RC beams (Phatak and Dhonde 2003), to predict 28-days compressive strength of cement (Phatak and Deshpande 2005; Pawar et al. 2024), to predict mechanical behaviour of plastic hinges developed in RC beams at ultimate loading conditions (Corrado and Carpinteri 2009) and to determine ultimate load capacity of shell foundations (Esmaili and Hataf 2013). The method of modified dimensional analysis has been also used for corrosion rate prediction of various grades of stainless steel in marine oil environment (Akpa 2013) as well as magnesium and related alloys in sodium chloride environment (Jayabharathy et al. 2017).

Despite of application of modified dimensional analysis in the fields of metal corrosion, its application for prediction of corrosion of steel embedded in concrete identified using AE parameters has not been investigated yet. Hence, the current research paper proposes a unique procedure of application of modified dimensional analysis (MDA) using AE signal parameters to predict the corrosion of steel embedded in concrete. The efficacy of the model developed using MDA is compared with the earlier model developed by author using non-linear regression analysis as explained in Patil et al. (2015). The performance of both the models is evaluated further based on statistical measures.

## 3. Data Used for Modified Dimensional Analysis

The data utilised in the current study is obtained from the earlier experimental work performed by Patil et al. (2014, 2015) for assessment of corrosion in RC elements using AE technique. As reported in earlier publications (Patil et al. 2014, 2015), the researchers performed an experimental study by subjecting the cylindrically

shaped RC specimens having diameter of 6 cm and height of 10 cm to accelerated corrosion. The experimental programme consisted of testing specimens made of different cement type (OPC and PPC), steel type (TMT and CRS) and rebar diameter (12 mm, 16 mm, and 20 mm). An impressed current technique with constant voltage of 3V was used for achieving accelerated corrosion of specimens as explained in Patil et al. (2014). The accelerated corrosion process was carried out till the specimen develops visible crack on the concrete surface due to corrosion. During the entire testing process, the corrosion activity in specimen was continuously monitored using AE technique. All the measurements were recorded at room temperature and with 100% humidity level under chloride induced accelerated corrosion conditions. A schematic diagram of the AE measurement system followed in earlier experimental work is presented in Fig. 1.

After completion of the test, the loss in mass of steel rebars removed from concrete specimens were recorded. A statistical tool - Analysis of Variance was used further to understand the significance of all material variables on recorded AE signal parameters and inferred that the influence of material variation on AE parameters is insignificant. Further the non-linear regression analysis (NLRA) was executed to establish the mathematical relation in between maximum CSS parameter recorded by AE and measured mass loss of steel rebars (Patil et al. 2015). In the current study, the AE data recorded during this laboratory based experimental work is used for performing MDA. The AE parameters used for MDA includes maximum cumulative duration, maximum cumulative count, maximum cumulative rise time, maximum cumulative signal strength and maximum cumulative amplitude along-with the other parameters like initial and final weight of rebar. These specific AE parameters are selected for analysis as these are primary characteristic AE parameters and can be easily obtained from AE waveform. Table 1 presents the data used for MDA.

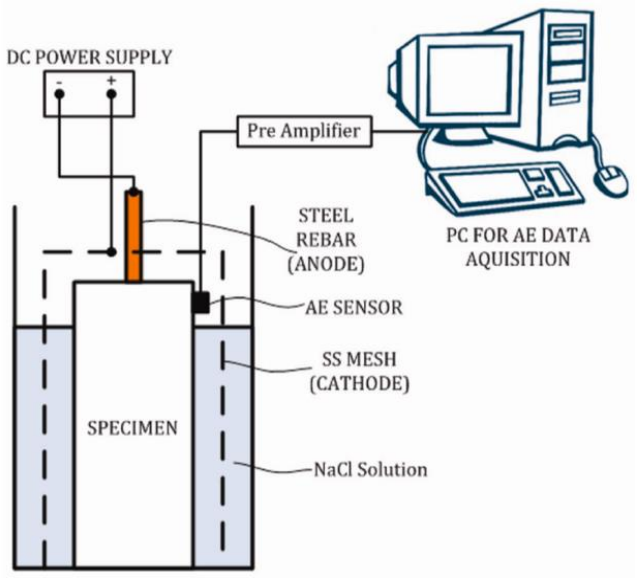


**Fig. 1.** Acoustic emission measurement system – schematic diagram (Patil et al. 2015).

**Table 1.** Data used for MDA.

| Sr. No. | Initial weight of rebar before corrosion ($g$) ($W_i$) | Maximum cumulative amplitude values (pico-volt) ($A_f$) | Maximum cumulative signal strength values (picovolt-second) ($S_f$) | Maximum cumulative rise time values (second) ($R_f$) | Maximum cumulative count values (nos.) ($C_f$) | Maximum cumulative duration values (second) ($D_f$) | Final weight of rebar after corrosion ($g$) ($W_f$) |
|---|---|---|---|---|---|---|---|
| 1 | 91.47 | 5.25E+10 | 8.04E+06 | 2.80E+04 | 2.19E+03 | 7.59E+04 | 88.86 |
| 2 | 91.50 | 6.61E+11 | 7.49E+07 | 3.20E+05 | 2.46E+04 | 8.23E+05 | 87.97 |
| 3 | 94.31 | 3.26E+11 | 3.48E+07 | 1.16E+05 | 1.58E+04 | 3.69E+05 | 88.63 |
| 4 | 164.01 | 4.05E+10 | 5.38E+06 | 1.99E+04 | 1.57E+03 | 5.61E+04 | 160.83 |
| 5 | 169.36 | 1.02E+11 | 1.39E+07 | 5.33E+04 | 4.06E+03 | 1.47E+05 | 165.75 |
| 6 | 261.60 | 6.38E+13 | 1.18E+10 | 6.26E+07 | 3.92E+06 | 1.28E+08 | 249.23 |
| 7 | 268.14 | 8.12E+13 | 1.37E+10 | 1.10E+08 | 3.93E+06 | 1.55E+08 | 256.36 |
| 8 | 248.60 | 2.55E+13 | 3.90E+09 | 1.55E+07 | 9.54E+05 | 3.69E+07 | 233.62 |
| 9 | 269.24 | 1.89E+11 | 2.64E+07 | 4.64E+04 | 6.12E+03 | 1.89E+05 | 263.72 |
| 10 | 266.83 | 1.79E+11 | 2.70E+07 | 4.58E+04 | 7.10E+03 | 1.76E+05 | 260.92 |
| 11 | 268.07 | 5.42E+10 | 6.00E+06 | 2.04E+04 | 3.33E+03 | 7.51E+04 | 263.78 |
| 12 | 269.12 | 1.93E+11 | 1.29E+07 | 3.59E+04 | 5.96E+03 | 1.30E+05 | 264.34 |
| 13 | 265.33 | 2.86E+11 | 2.73E+07 | 1.45E+05 | 1.12E+04 | 3.24E+05 | 256.70 |
| 14 | 266.93 | 9.31E+11 | 1.19E+08 | 6.49E+05 | 3.72E+04 | 1.43E+06 | 259.34 |

## 4. Modelling Technique Adopted Using MDA

Butterfield (1999) states that a specific system consisting of *n* parameters can be described by set (*K*) = ( $K_1$ , $K_2$ , $K_3$ , ..., $K_n$ ), consisting of total m primary dimensions as (*D*) = ($D_1$, $D_2$, $D_3$, $D_4$, ..., $D_m$). This system always has a minimum set - $D_{\min}$ which can dimensionally define all the parameters in the set *K*. Next, the number of dimensionless groups can be considered as difference between number of parameters in K and number of parameters in $D_{\min}$. The dimensionless groups ($\pi_1, \pi_2, \pi_3, \pi_4, \ldots \pi_N$) can be further assembled to determine the dependent parameter of interest. Thus, by applying this methodology, the set *K* for corrosion prediction of steel embedded in concrete using AE parameters is given as follows:

*K* = (final weight of rebar ($W_f$), initial weight of rebar ($W_i$), maximum cumulative duration ($D_f$), maximum cumulative count ($C_f$), maximum cumulative rise time ($R_f$), maximum cumulative signal strength ($S_f$), maximum cumulative amplitude ($A_f$)).

The units for all these parameters considered are: weight of rebar in gram; maximum cumulative duration in second; maximum cumulative rise time in second; maximum cumulative signal strength in volt-second; maximum cumulative amplitude in volt, whereas maximum cumulative count is unitless term.

Thus, the set defined in terms of their respective dimensions is, *K*=($M^1$, $M^1$, $T^1$, 0, $T^1$, $M^1L^2T^{-3}A^{-1}T^1$, $M^1L^2T^{-3}A^{-1}$). Here, n = 7 and m = 3 which is also set *D*. Hence, the number of isolated variables as well as dimensionless Pi-groups are obtained as, $N = n - m = 4$. In the current study $D_{\min} = D$. Now, the set R is selected such that all the variables of set R have distinct dimensions. Therefore, selecting $R = (Wi, Sf, Rf)$. Subsequently, $Q$ is selected from *R* following the modified Buckingham Pi theorem protocol. Therefore:

$$\mathrm{Q} = (Wi, Sf, Rf) \tag{1}$$

$$\mathrm{NOTQ} = (Wf, Df, Cf, Af) \tag{2}$$

Now, the dimensionless Pi-groups are generated by considering combinations of variables from Q and NOTQ sets. Hence, the dimensionless Pi-groups are:

$$\pi_1 = (Wi, Sf, Rf, Wf)$$

$$\pi_2 = (Wi, Sf, Rf, Cf)$$

$$\pi_3 = (Wi, Sf, Rf, Af)$$

$$\pi_4 = (Wi, Sf, Rf, Df) \tag{3}$$

Now solving for $\pi_1$,

$$\pi_1 = (W_i^a, S_f^b, R_f^c, D_f^1) \tag{4}$$

Eq. (4) can be presented in dimensional form as below:

$$[M^0L^0A^0] = [[M^1]^a, [M^1L^2T^{-3}A^{-1}T^1]^b, [T^1]^c, [M]^1 \tag{5}$$

Now, by comparing the indices of both sides of equation we get:

*M*: $0 = a + b + 1$

*L*: $0 = 2b$

*T*: $0 = b + c$

*A*: $0 = -b$

Hence, $a = -1$, $b = 0$, $c = 0$. By replacing these values of *a, b* and *c* in Eq. (4) we get:

$$\pi_1 = \left(\frac{W_f}{W_i}\right) \tag{6}$$

Similarly solving for the remaining Pi-terms we get:

$$\pi_2 = C_f \tag{7}$$

$$\pi_3 = \left(\frac{R_f \cdot A_f}{S_f}\right) \tag{8}$$

$$\pi_4 = \left(\frac{D_f}{R_f}\right) \tag{9}$$

Now to find final weight of rebar, articulating $\pi_1$ as a function of ( $\pi_2, \pi_3, \pi_4$ ), such that $\pi_1 = \psi(\pi_2, \pi_3, \pi_4)$ where $\psi$ is an undetermined function. From Eqs. (6), (7), (8) and (9), substituting the Pi-terms in above equation we get:

$$\left(\frac{W_f}{W_i}\right) = \psi\left(C_f, \left(\frac{R_f \cdot A_f}{S_f}\right), \left(\frac{D_f}{R_f}\right)\right. \tag{10}$$

To determine the precise nature of ($\psi$), the power-product relationship of the dimensionless group is exercised as follows:

$$\pi_1 = \beta_1 \pi_2^{\beta_2} \pi_3^{\beta_3} \pi_4^{\beta_4} \tag{11}$$

or

$$\left(\frac{W_f}{W_i}\right) = \beta_1 \left(C_f\right)^{\beta_2} \left(\frac{R_f \cdot A_f}{S_f}\right)^{\beta_3} \left(\frac{D_f}{R_f}\right)^{\beta_4} \tag{12}$$

$$W_f = W_i\, \beta_1 \left(C_f\right)^{\beta_2} \left(\frac{R_f \cdot A_f}{S_f}\right)^{\beta_3} \left(\frac{D_f}{R_f}\right)^{\beta_4} \tag{13}$$

The values of constants ($\beta_1, \beta_2, \beta_3, \beta_4$) are further calculated by performing non-linear analysis using SOLVER function of MS Excel. The final equation obtained is as shown in Eq. (12).

$$W_f = W_i \cdot 1.143\left(C_f\right)^{0.00379} \left(\frac{R_f \cdot A_f}{S_f}\right)^{-0.009} \left(\frac{D_f}{R_f}\right)^{-0.001249} \tag{14}$$

Thus, Eq. (14) represents the model developed for prediction of final weight of rebars using MDA.

## 5. Results and Discussion

Using the model developed based on dimensional analysis as presented in Eq. (14), the final weight of steel rebars, mass loss and corrosion rate values are calculated. The details of calculations and comparative assessment with the results of NLRA model are discussed in detail in following sections.

### *5.1. Prediction of the final weight of steel rebar*

Based on the developed model using MDA, the final weights of rebar are calculated. The final weights of rebar are also calculated using the NLRA model presented by Patil et al. (2015) which is as shown in Eq. (15).

$$y = 1.05 \cdot 10^6 \cdot e^{0.711x} \quad (15)$$

In Eq. (15), $y$ indicates maximum CSS value whereas $x$ represents mass loss of steel rebar calculated by gravimetric method. The values so calculated are compared with actual final weight of the rebar measured after completion of the experimental work as mentioned in earlier work of Patil et al. (2015). Fig. 2 presents the comparative graph for final weights of rebar measured and calculated using NLRA as well as MDA model.

From Fig. 2 it can be clearly noticed that the final weights of rebar calculated using MDA model are perfectly in agreement with that of values calculated using earlier developed NLRA model as well as with measured values. These predicted final weight values of steel bars are further used to compute the mass loss and then the corrosion rate as described in ASTM G1-03 (2017).

### *5.2. Prediction of corrosion rate*

Figs. 3 and 4 represents the scatter plot between actual corrosion rate and predicted corrosion rate using MDA and NLRA models respectively.

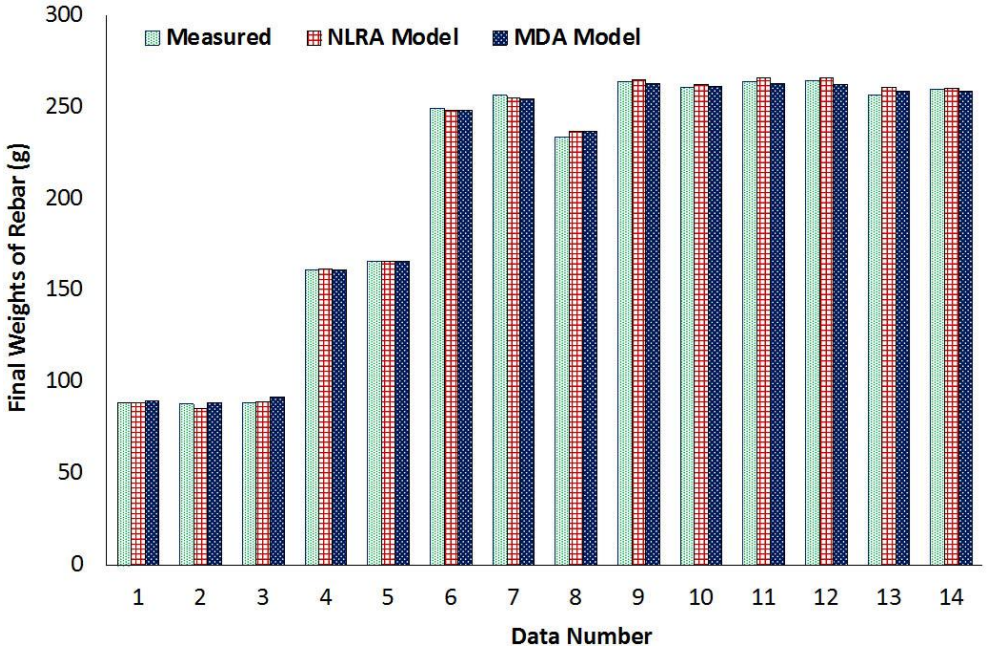


**Fig. 2.** Final weights of rebars using MDA model and earlier NLRA model.

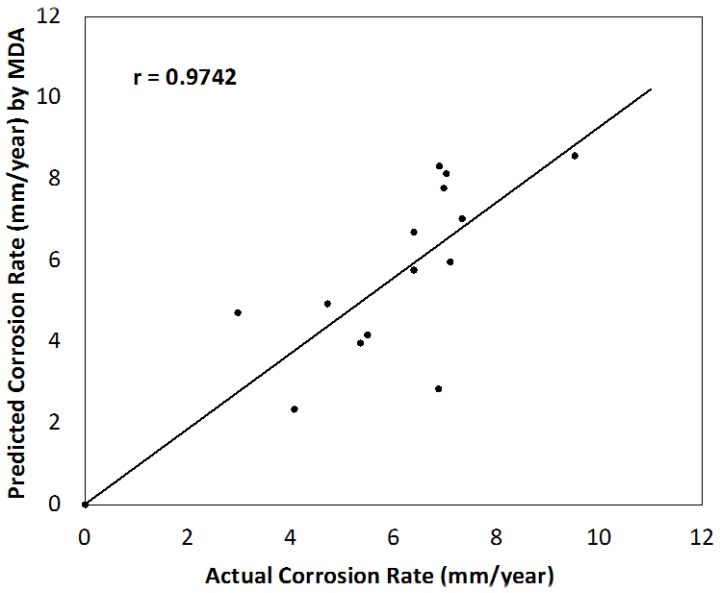


**Fig. 3.** Predicted values vs. actual values of corrosion rate using MDA model.

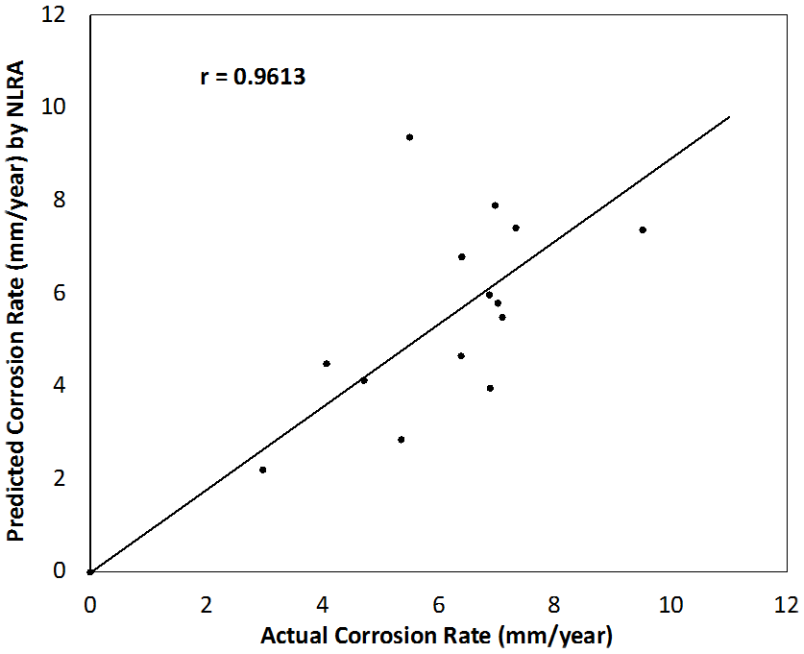


**Fig. 4.** Predicted values vs. actual values of corrosion rate using NLRA model.

From Fig. 3, it can be observed that for MDA model, the scatter of points is less from the equality line between predicted and actual corrosion rate values with a high correlation coefficient value ($r$=0.97) as compared to NLRA model shown in Fig. 4. To understand the performances of both the developed models, various statistical measures are calculated as presented in Table 2. The commonly adopted statistical measure is the correlation coefficient ($r$) which computes the degree of relatedness of the variables. The value of r nearer to 1.0 denotes a linear relationship between the two variables. The square of correlation coefficient is termed as coefficient of determination ($R^2$). The value of $R^2$ varies from zero to one and the higher value represents better concurrence between predicted and observed values. However, $R^2$ value remains unaffected to proportional/additive differences between the predicted and observed data. This may result in obtaining higher value of $R^2$ even if predicted values fluctuate considerably in magnitude, exhibiting major flaws in the model. Another most commonly adopted measure for evaluating the quality of predictions is Root Mean Square Error (RMSE). It specifies how far model simulations fall from observed true values with lower value indicating good predictions. But similar to $R^2$, this parameter is also influenced by the higher error values. A statistical measure - Mean Absolute Error (MAE) explains the difference between the modelled and observed values. It has been observed that the extent by which RMSE surpasses the MAE implies the range of outliers in the data. Another statistical measure – coefficient of efficiency or Nash-Sutcliffe Efficiency ($E$) is also broadly used to estimate the performance of models. It is expressed as the ratio between mean square error and the variance in the observed data, deducted from one. Its value varies between -infinity to one and values closer to 1.0 denotes better agreement in observed data and model. The negative value of $E$ implies that the observed mean is a better predictor than the model (Legates and McCabe 1999). Based on the above definitions, the values of all above mentioned statistical measures for both the models are calculated to evaluate the performance of MDA and NLRA model as presented in Table 2.

**Table 2.** Performance of models.

| Model | MDA Model | NLRA Model |
|---|---|---|
| Correlation Coefficient - $r$ | 0.9742 | 0.9613 |
| Coefficient of Determination - $R^2$ | 0.9491 | 0.9241 |
| Root Mean Square Error - RMSE | 2.0993 | 4.2051 |
| Mean Absolute Error - MAE | 1.1615 | 1.4339 |
| Nash-Sutcliffe Efficiency - $E$ | 0.1302 | - 0.3161 |

From Table 2 it can be observed that there is a marginal difference in $r$ as well as $R^2$ values of the two models. Thus, correlation coefficient and coefficient of determination value implies that both the models are relatively good with no prominent differences. On the other hand, RMSE value for the NLRA model is nearly twice that of the MDA model indicating better prediction by MDA model. Moreover, the extent by which RMSE exceeds MAE is approximately three times greater for the NLRA model than that of the model developed using MDA signifying existence of greater outlier in NLRA model. The Nash-Sutcliffe Efficiency – $E$ value for the NLRA model is negative implying that the observed mean is a better predictor than the model, whereas for the MDA model, E value being positive and close to zero, infers that the observed mean is as good a predictor as the model. Thus, the statistical measures calculated for both these models indicate lesser extent of outliers in the data predicted by MDA model than that of the model based on NLRA implying better performance of MDA model as compared to NLRA model.

## 6. Conclusions

The study presented in this paper is the first approach towards modelling the rate of corrosion of steel rebar in concrete using a comprehensive method of MDA implemented for AE parameters. A model is developed using MDA for AE parameters collected for quantification of corrosion and the performance of developed model is compared with the model based on NLRA. The performance of both the models is evaluated further using statistical measures like $r$, $R^2$, RMSE, MAE and Nash-Sutcliffe Efficiency – $E$. The outcomes of the study can be summarized as below.

- Based on the selected data for performing MDA, the developed model is presented as:

$$W_f = W_i \cdot 1.143\left(C_f\right)^{0.00379}\left(\frac{R_f \cdot A_f}{S_f}\right)^{-0.009}\left(\frac{D_f}{R_f}\right)^{-0.001249}$$

  This equation predicts the weight of steel rebar after corrosion based on weight of rebar before corrosion and the primary characteristic AE parameters recorded during the active corrosion process. Using these predicted values of weight of steel rebars after corrosion, corrosion rate can be calculated using procedure described in ASTM G1-03 (2017).
- The model developed using MDA exhibited higher values of $r$, $R^2$ as well as E and lower values of MAE and RMSE, demonstrating better performance than the NLRA model.
- Instead of using few energy-based AE parameters for analysis, primary characteristic AE waveform parameters namely - amplitude, counts, rise time, duration and signal strength can be efficiently used combinedly for successful formulation of corrosion prediction models using MDA.
- MDA is a promising tool for analysis of AE parameters which can be successfully used to formulate predictive model using few datasets unlike other machine learning based approaches which demands large datasets for training and testing of models.

Thus, the current study reveals that the presented methodology for application of MDA using AE signal parameters can be promisingly used to formulate the corrosion prediction model for RC elements by ensuring mathematical stability. With the help of MDA, it is also demonstrated that, the dimensional homogeneity helps to check the accuracy of the relationship between different variables and improves the predictions of physical phenomena. The procedure for analysis of AE signal data using MDA is a simplified process as compared to other AE data analysis methods as it uses simple tools like spreadsheets. The dataset used in the current study is limited to laboratory-based experiments in accelerated condition. However, it is necessary to extend the study further to check the applicability of developed model to variable field data considering real world environment conditions.

***Acknowledgements***
*None declared.*

***Funding***
*The author received no financial support for the research, authorship, and/or publication of this manuscript.*

***Conflict of Interest***
*The author declared no potential conflicts of interest with respect to the research, authorship, and/or publication of this manuscript.*

***Author Contributions***
*The author confirms sole responsibility for all aspects of the study including conception and design, acquisition of data, analysis and interpretation of data, drafting the manuscript, revising it critically for important intellectual content; and gave final approval of the version to be published.*

***Data Availability***
*The datasets created and/or analyzed during the current study are not publicly available, but are available from the corresponding author upon reasonable request.*

## REFERENCES

Akpa JG (2013). Modeling of the corrosion rate of stainless steel in marine oil environment. *ARPN Journal of Engineering and Applied Sciences*, 8(8), 656–662.

ASTM G1-03 (2017). Standard practice for preparing, cleaning, and evaluating corrosion test specimens. ASTM International, West Conshohocken, PA, USA.

Butterfield R (1999). Dimensional analysis for geotechnical engineers. *Geotechnique*, 49(3), 357–366.

Corrado M, Carpinteri A (2009). Dimensional analysis of over-reinforced concrete beams in bending. *Atti del XIX Congresso Nazionale di Meccanica Teorica ed Applicata*, Ancona, Italy, no.110.

Di Benedetti M, Loreto G, Matta F, Nanni A (2013). Acoustic emission monitoring of reinforced concrete under accelerated corrosion. *Journal of Materials in Civil Engineering,* 25(8), 1022–1029.

Di Benedetti M, Nanni A (2014). Acoustic emission intensity analysis for in situ evaluation of reinforced concrete slabs. *Journal of Materials in Civil Engineering*, 26(1), 6–13.

Esmaili D, Hataf N (2013). Determination of ultimate load capacity of conical and pyramidal shell foundations using dimensional analysis. *Iranian Journal of Science and Technology - Transactions of Civil Engineering*, 37, 423–435.

Fricker S, Vogel T (2007). Site installation and testing of a continuous acoustic monitoring. *Construction and Building Materials,* 21(3), 501–510.

Idrissi H, Limam A (2003). Study and characterization by acoustic emission and electrochemical measurements of concrete deterioration caused by reinforcement steel corrosion. *NDT&E International*, 36, 563–569.

Ing M, Austin S, Lyons R (2005). Cover zone properties influencing acoustic emission due to corrosion. *Cement and Concrete Research,* 35, 284–295.

Jayabharathy S, Pushparaj S, Mathiazhagan P (2017). Prediction of corrosion rate of magnesium and its alloy-modeling. *International Journal of Advanced Research in Basic Engineering Sciences and Technology*, 3(32), 55–61.

Ji H, Ye H (2023). Machine learning prediction of corrosion rate of steel in carbonated cementitious mortars. *Cement and Concrete Composites*, 143, 105256.

Kawasaki Y, Tomoda Y, Ohtsu M (2010). AE monitoring of corrosion process in cyclic wet–dry test. *Construction and Building Materials*, 24(12), 2353–2357.

Kawasaki Y, Wakuda T, Kobarai T, Ohtsu M (2013). Corrosion mechanisms in reinforced concrete by acoustic emission. *Construction and Building Materials*, 48, 1240–1247.

Legates DR, McCabe Jr. GJ (1999). Evaluating the use of "goodness of fit" measures in hydrological and hydro climatic model validation. *Water Resources Research*, 35(1), 233–241.

Nair A, Cai CS (2010). Acoustic emission monitoring of bridges: Review and case studies. *Engineering Structures*, 32, 1704–1714.

Ohtsu M, Tomoda Y (2008). Phenomenological model of corrosion process in reinforced concrete identified by acoustic emission. *ACI Materials Journal,* 10, 5194–5199.

Patil S, Karkare B, Goyal S (2014). Acoustic emission vis-à-vis electrochemical techniques for corrosion monitoring of reinforced concrete element. *Construction and Building Materials,* 68, 326–332.

Patil S, Goyal S, Karkare B (2015). Acoustic emission-based mathematical procedure for quantification of rebar corrosion in reinforced concrete. *Current Science*, 109(5), 943–948.

Patil S, Karkare B, Goyal S (2017). Corrosion induced damage detection of in-service RC slabs using acoustic emission technique. *Construction and Building Materials*, 156, 123–130.

Pawar NM, Gujar S, Dhonde HB, Valles D (2024). Early prediction of characteristic compressive strength of concrete based on mix proportions using modified dimensional analysis. *2024 IEEE 14th Annual Computing and Communication Workshop and Conference (CCWC)*, Las Vegas, NV, USA, 0043–0052.

Phatak DR, Deshpande NP (2005). Prediction of 28-days compressive strength of 53-grade using dimensional analysis. *Journal of Materials in Civil Engineering*, 17(6), 733–735.

Phatak DR, Dhonde HB (2000). Behaviour of five large spread footing in sand. *Journal of Geotechnical and Geoenvironmental Engineering*, 126(10), 940–942.

Phatak DR, Dhonde HB (2003). Dimensional analysis of reinforcement concrete beams subjected to pure torsion. *Journal of Structural Engineering*, 129(11), 1559–1563.

Song H, Saraswathy V (2007). Corrosion monitoring of reinforced concrete structures – a review. *International Journal of Electrochemical Science,* 2, 1–28.

Thirumalaiselvi A, Sasmal S (2024). Machine learning-based acoustic emission technique for corrosion-induced damage monitoring in reinforced concrete structures*. Engineering Applications of Artificial Intelligence*, 137(Part A), 109–121.

Verstrynge E, Van Steen C, Vandecruys E, Wevers M (2022). Steel corrosion damage monitoring in reinforced concrete structures with the acoustic emission technique: A review. *Construction and Building Materials*, 349, 128-732.

Yu X, Montrésor S, Bentahar M, Mechri C (2023). Cluster analysis of acoustic emission signals for the damage pattern recognition of polymer concrete. *Applied Acoustics*, 211, 109533.

Zaki A, Chai HK, Aggelis DG, Alver N (2015). Non-destructive evaluation for corrosion monitoring in concrete: A review and capability of acoustic emission technique. *Sensors*, 15, 19069–19101.

Challenge Journal of Concrete Research Letters

Research Article

# Impact of wrap quantity on strength of damaged and undamaged CFRP-reinforced structural members

Serdal Ünal [a], Ahmet Burak Kurt [a], Mehmet Canbaz [a,*]

[a] *Department of Civil Engineering, Eskişehir Osmangazi University, 26480 Eskişehir, Türkiye*

**ABSTRACT**

In this study, the effect of carbon fiber reinforced polymer (CFRP) wrapping on the compressive and bending behavior of damaged reinforced concrete structural elements located in high earthquake risk areas was investigated in detail. The main objective was to evaluate the potential of CFRP wraps as an effective strengthening technique for improving the mechanical performance of concrete members that have already sustained damage. During the experimental phase, concrete specimens in the form of 15×15×15 cm cubes and 10×10×50 cm prisms were prepared using CEM IV 32.5 pozzolanic cement, which is commonly used in structural applications due to its durability and environmental benefits. After subjecting these specimens to controlled damage to simulate real-life structural degradation, they were reinforced using single and double layers of CFRP wrapping. The mechanical performances of these wrapped specimens were then assessed through compressive and bending strength tests. The results demonstrated that CFRP wrapping significantly enhanced the compressive strength of the specimens, with double-layer applications showing the greatest improvements. However, the effect on flexural strength was found to be more limited, indicating that although CFRP is 60.83% effective in resisting compressive loads, its contribution to flexural capacity may require additional considerations. Furthermore, double-layer CFRP wrapping not only improved strength but also increased deformation capacity, indicating enhanced ductility and energy absorption. Despite the relatively high cost of CFRP materials, these findings highlight the technique as a practical and efficient solution for the rehabilitation and strengthening of compression load-bearing members, particularly in regions vulnerable to seismic activity.

**ARTICLE INFO**

**Article history:**
Received – April 25, 2025
Revision requested – May 21, 2025
Revision received – June 4, 2025
Accepted – June 17, 2025

**Keywords:**
Carbon fiber reinforced polymer
Composite materials
Reinforced concrete strengthening
Damaged structural elements



**Citation:** Ünal S, Kurt AB, Canbaz M (2025). Impact of wrap quantity on strength of damaged and undamaged CFRP-reinforced structural members. *Challenge Journal of Concrete Research Letters*, 16(3), 133–141.

## 1. Introduction

Earthquakes are natural disasters that can have severe destructive effects on structures, especially in countries located on active fault lines (Bird and Bommer 2004). Most of the loss of life and property from earthquakes is caused by weaknesses in the structural systems of buildings (Wu et al. 2019; Çelik et al. 2024). The primary causes of these weaknesses include the use of substandard materials, inadequate design practices, nonstandard construction practices, and structural wear and tear over time. Such deficiencies cause serious damage, especially to the main load-bearing elements such as columns and beams, and reduce the overall strength of the structure. Identifying the structural weaknesses of buildings susceptible to earthquake damage is essential to ensure that such structures experience minimal damage—and, most importantly, avoid collapse—during seismic events (Zardari et al. 2024). Therefore, the evaluation of existing buildings and their retrofitting, where necessary, is of great importance for both life safety and economic sustainability. Rather than constructing a new

* *Corresponding author*. Tel.: +90-222-239-3750 ; E-mail address: mcanbaz@ogu.edu.tr (M. Canbaz)
ISSN: 2548-0928 / DOI: https://doi.org/10.20528/cjcrl.2025.03.003

building, retrofitting existing structures is a less costly and more environmentally friendly solution (Jagarajan et al. 2017; Ma et al. 2012). Structural strengthening is significantly more cost-effective than demolishing and rebuilding existing structures, offering a major economic advantage. Additionally, it minimizes downtime, reducing labor and time losses (Keshmiry et al. 2024). In this context, the need for retrofitting methods that can be applied quickly and increase strength is growing every day.

One of the most effective ways to meet this need is through CFRP wrapping applications (Hegde et al. 2019). Fiber-reinforced polymer (FRP) materials can be manufactured in various geometries and possess a wide range of applications, spanning from industrial uses to construction-related implementations (Eryılmaz Yıldırım et al. 2024). CFRP is a composite material with many advantages such as high tensile strength (usually 2500–5000 MPa), low specific gravity (~1.6 g/cm$^3$), corrosion resistance and ease of application (Mitra 2000; Heidarzadeh 2022). CFRP has high tensile strength, low weight, and excellent corrosion resistance due to its carbon fiber content and polymer matrix. It also exhibits high stiffness and dimensional stability under varying environmental conditions (Kim et al. 2023). First used in the aerospace and automotive industries, this material has been widely used in the construction industry in recent years, especially for structural reinforcement. The high modulus of elasticity of CFRP allows it to increase the deformation capacity of reinforced concrete elements (Mousa et al. 2019; Xue et al. 2010). CFRP offers significant advantages over other strengthening materials due to its high strength-to-weight ratio, excellent corrosion resistance, and ease of application. It can also be easily bonded with epoxy-based adhesives, allowing for quick and effective reinforcement of existing structures. It is increasingly being used in structural elements such as columns, beams and shear walls to provide strength against both compressive and tensile loads (Rashid and Bahrami 2023). The high strength-to-weight ratio makes CFRP more advantageous than conventional steel reinforcements. Although the cost of CFRP is high, this is offset by its long life and maintenance-free nature (Younis et al. 2018).

This study investigated the effect of CFRP wrapping on severely damaged reinforced concrete members and addressed an important gap in the literature in this area. While many studies in the literature have focused on the strengthening effects of CFRP applications on intact members, this study experimentally evaluated the strengthening of controlled-damage concrete specimens with CFRP. This study addresses the gap in the literature regarding the performance of CFRP wrapping on previously damaged concrete elements, particularly under both compressive and bending loading conditions. The experiments conducted on the strength and deformation behavior of structural elements reveal how effective the application of CFRP wrapping is. As a result of compressive and bending tests performed on 15x15x15 cm cube and 10x10x50 cm prism specimens, it was observed that especially double-layer CFRP wrapping applications provided a significant increase in compressive strength. The effects on bending strength were found to be limited. In this respect, the study contributes to the structural engineering literature and applications by demonstrating that CFRP can be effective, within certain limits, not only in intact but also in partially damaged structural elements.

## 2. Experimental Study

### *2.1. Materials*

Cement: CEM IV/B 32.5N pozzolanic cement was used as binder in the study. The cement used is the product of Eskisehir Cement Factory (Eskişehir, Türkiye), which is produced according to TS EN 197-1 (2012) standard. The chemical and physical properties of the cement used in the production are given in Table 1.

Water: Municipal water was used in the mixtures. Properties of the mix-water is given in Table 2.

**Table 1.** Properties of cement.

| Chemical content, mg/dm$^3$ | | | | | | | | | |
|---|---|---|---|---|---|---|---|---|---|
| CaO | $Al_2O_3$ | $SiO_2$ | $Fe_2O_3$ | MgO | CI- | $Na_2O$ | $K_2O$ | LOI | $SO_3$ |
| 40.50 | 10.60 | 35.41 | 2.70 | 1.81 | 0.042 | 0.93 | 0.96 | 4.21 | 2.84 |
| Physical properties | | | | | | | | | |
| Specific surface, cm$^2$/g | | Expansion, mm | | Initial setting, min. | | Final setting, min. | | Density, g/cm$^3$ | |
| 4800–5300 | | 1 | | 180–220 | | 230–280 | | 2.85 | |

**Table 2.** Properties of water.

| Cu, % | Mn, % | Al, % | $NH_4$, % | Fe, % | $NO_3$, % | K, % | Ni, % | As, % | Conductivity, µS/cm | pH | Hardness, Fd$^0$ |
|---|---|---|---|---|---|---|---|---|---|---|---|
| 0.015 | 0.014 | 0.05 | 0.07 | 0.005 | 11.3 | 6.7 | 5.11 | 1.21 | 623 | 7.4 | 30.23 |

Aggregates: Concrete cube specimens were created by using three types of crushed aggregates. Fig. 1 shows an analysis of the particle size of the aggregate mixture. The commercial quartz sand as fine aggregate (specific gravity of 2.65). Further, the densities of the fine aggregates were 2.69, 2.70, and 2.71 g/cm$^3$, for fine aggregate sizes of (0–4 mm), (4–11.2 mm), and (11.2–22.4 mm) respectively.

CFRP: MegaKarbon Wrap K918-K923 brand CFRP was used in the study. The mechanical properties of the material used are given in Table 3.

Resin: MegaPro Epo Y501 is a two component epoxy based laminating resin specially formulated for MegaKarbon Wrap 300 K918. MegaKarbon Wrap 300 K918 is used to bond the carbon reinforced fiber polymer MegaKarbon Wrap 300 K918 to the surfaces of structural elements in reinforcement applications. The chemical properties of the material used are given in Table 4. The CFRP and resin material used in production is shown in Fig. 2.

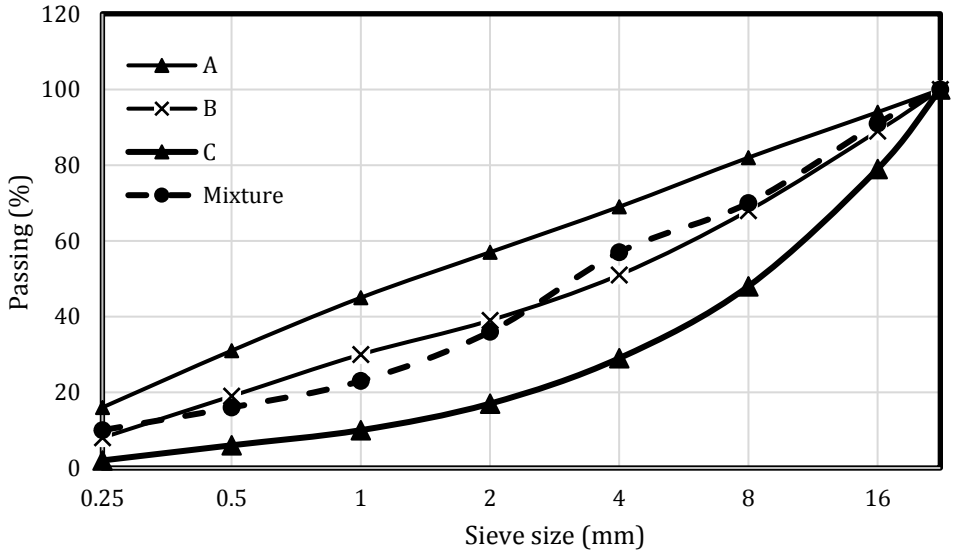


**Fig. 1.** Granulometry of the aggregate mixture according to EN 12620 (2002).

**Table 3.** Properties of CFRP.

| Width, mm | Tensile strength, MPa | Modulus of elasticity, MPa | Elongation at break, % | Fabric nominal thickness, mm$^2$/mm |
|---|---|---|---|---|
| 501 | 4000-5000 | >235 | ~2 | 0.169 |

**Table 4.** Properties of resin.

| Specific weight, g/cm$^3$ | Working time, min. | Compressive strength, MPa | Shear strength, MPa | Tensile adhesion strength, MPa |
|---|---|---|---|---|
| 1.08 | 60 | 79 | >6 | 52 |


**Fig. 2.** CFRP and resin material used in the production of the concrete specimens.

### *2.2. Method and tests*

During the production phase, the concrete was prepared in the mixing ratios given in Table 5. The vibration process was used to evenly distribute the concretes in the mold and to obtain a homogeneous structure. A total of 12 cube (15x15x15 cm) and 12 prism (10x10x50 cm) specimens were produced. The specimens were left outdoors for 3 days for a short setting period, and after setting, the specimens were carefully removed from the molds.

To ensure that the specimens reached their maximum strength, the removed specimens were placed in the specimen curing bath. The specimens were kept in the hardening pool for 28 days, and after full strength development, the specimens were removed from the pool and allowed to dry for 2 days. The specimens were then prepared for testing.

**Table 5.** Mix ratio of 1 $m^3$ of concrete mixture by weight.

| Cement, kg | Water, kg | Aggregate, kg | | |
|---|---|---|---|---|
| | | 0–4 mm | 4–11.2 mm | 11.2–22.4 mm |
| 300 | 180 | 920 | 410 | 570 |

Half of the concrete specimens produced prior to the wrapping process were damaged to test the performance of the damaged structural elements. After the production stage, the CFRP was cut as follows for single and double wrapping for the cube and prism specimens, with an overlap of 10 cm to wrap the specimens.

- For single wrapping cube specimen: (60+10)×15 cm
- For double wrapping cube specimen: (120+10)×15 cm
- For single wrapping prism specimen: (40+10)×50 cm
- For double wrapping prism specimen: (80+10)×50 cm

To wrap the intact specimens, the necessary wrapping materials were first prepared. Then, the two-part epoxy-based laminating resin (MegaPro Epo Y-501) to be applied to the concrete surface and wrapping material was prepared and the application process started. At this stage, mixing the resin in the correct proportions and applying it properly will improve the performance and structural integrity of the material. To mix the epoxy components, component A and B were combined in a bucket and mixed at a slow speed using a low speed hand mixer. High speed mixing should be avoided. When mixing the components, the ratio of component A and B was poured into the container so that 1/3=B/A. The resin used is approved according to TS EN 1504-4 (2006). Unit weight, ultrasonic pulse and compression tests were carried out on 28 day old specimens as hardened concrete tests.

After the production process, tests such as unit weight, ultrasound transmission rate, compressive strength and bending strength were performed to determine the mechanical and physical properties of the specimens before and after wrapping. Unit weight is determined by dividing the weight by the total volume. The ultrasonic pulse velocity is obtained by dividing the sample length by the time it takes for the vibration generated by the transmitting probe to reach the receiving probe in the specimen. Compressive strength is obtained by dividing the compressive force by the specimen area. Fig. 3 shows the bending strength test and some of the damaged specimens while the cube and prism specimens wrapped with CFRP are demonstrated in Fig 4.

**Fig. 3.** Damaged and undamaged concrete specimens.

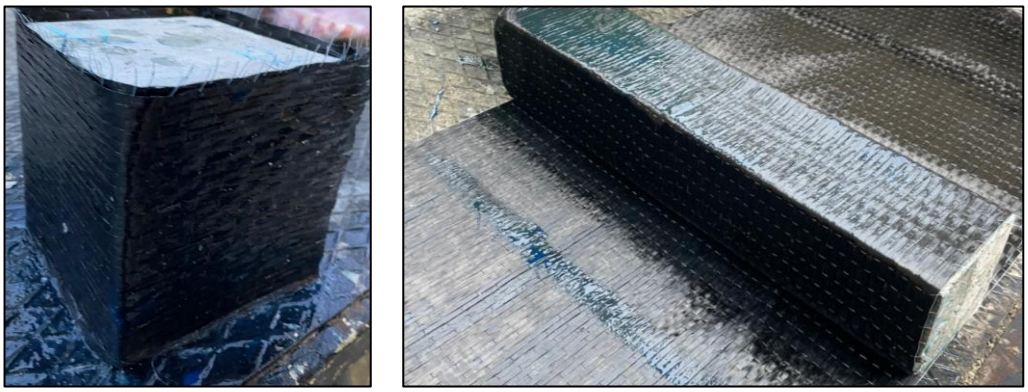

**Fig. 4.** Cube and prism concrete specimens wrapped with CFRP.

## 3. Results and Discussion

### *3.1. Reinforcement test results of low-strength undamaged concrete*

The data presented in Fig. 5 shows the results of unit weight and ultrasound transmission velocity tests performed on undamaged concrete specimens with CFRP wraps. In terms of unit weight, while the weight of the unwrapped specimen was 2,198.03 kg/dm$^3$, this value increased by 0.32% to 2,204.99 kg/dm$^3$ with single layer CFRP wrapping and by 0.73% to 2,214.02 kg/dm$^3$ with double layer CFRP. These increases can be explained by the CFRP layers adding additional mass to the outer surface of the concrete. Although the internal density of the structure remains unchanged, the carbon fiber layers applied externally increase the total mass, although at small rates. The ultrasound transmission velocity results provide more information about the internal structural continuity of the material. In the unwrapped specimen, the transit velocity was 3.24 km/h, whereas this value increased by 2.78% to 3.33 km/h with a single layer of CFRP and by 4.01% to 3.37 km/h with a double layer of CFRP. These increases indicate that the tight wrapping effect of CFRP on the surface of the concrete maintains the continuity in the internal structure, preventing the formation of microcracks and allowing a more uninterrupted passage of ultrasonic waves. Especially in the undamaged specimens, the better adhesion and homogeneous wrapping effect of CFRP resulted in an improvement in wave passage. As a result, the CFRP winding increases the unit weight to a limited extent, but it seems to contribute to the internal structural integrity, especially through increases in the ultrasound transmission rate. This shows that CFRP not only improves the mechanical strength but also the elastic properties and integrity of the material.

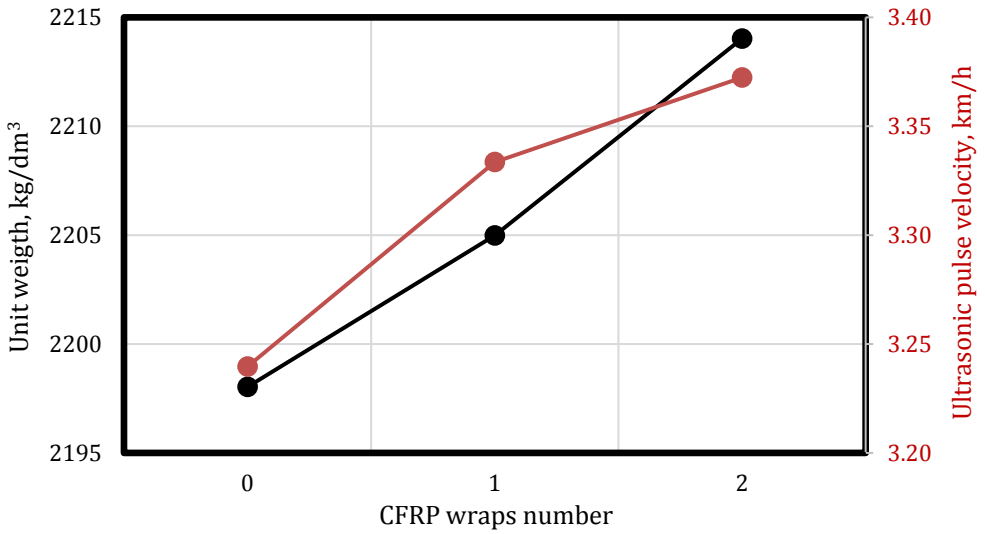


**Fig. 5.** Unit weight and ultrasound pulse velocities of the undamaged concrete specimens.

The effect of CFRP wrapping on the undamaged specimens is stronger and directly observed in Fig. 6. While the compressive strength of the unwrapped specimens was 10.37 MPa, this value increased by 48.17% to 15.36 MPa with single layer CFRP wrapping. Double layer CFRP wrapping increased the strength by 61.84% to 16.79 MPa. These results show that CFRP wrapping is much more effective in undamaged structures and that the wrapping can work effectively on the entire surface in the absence of existing micro cracks. Therefore, strengthening with CFRP provides higher performance in undamaged structural elements and the strength increase is more efficient, especially in double layer applications.

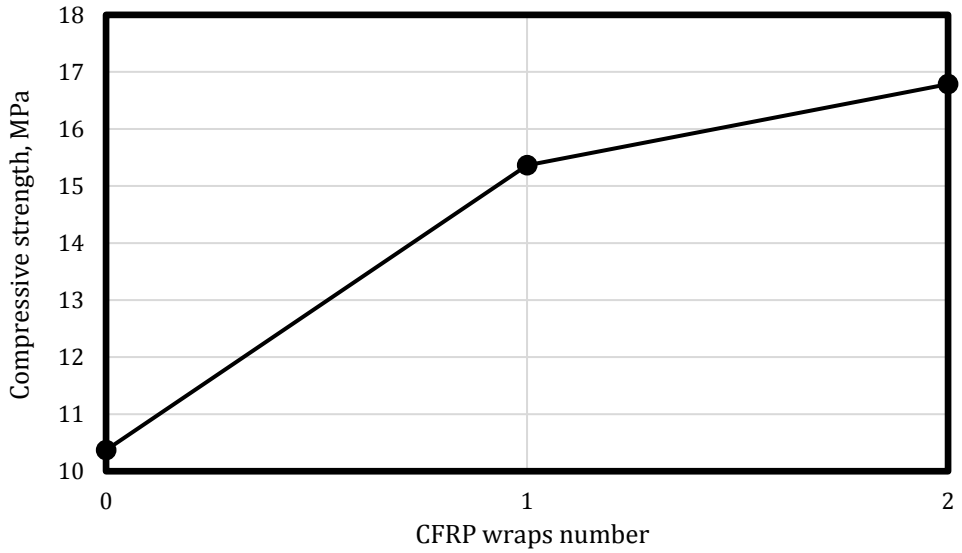


**Fig. 6.** Compressive strength of the undamaged concrete specimens.

Fig. 7 shows the effect of CFRP wrapping on the bending strength of 15 cm cube-shaped concrete specimens. In the undamaged specimens, the effect of CFRP wrapping is very positive. Single layer CFRP application increased the bending strength by 17.13% to 2.8845 MPa, while double layer wrapping increased this increase by 22.37% to 3.01275 MPa. These increases indicate that the CFRP wrap directly contributes to the load carrying capacity by adhering properly on undamaged surfaces. In conclusion, CFRP wrapping is an effective method to increase bending strength in undamaged specimens.

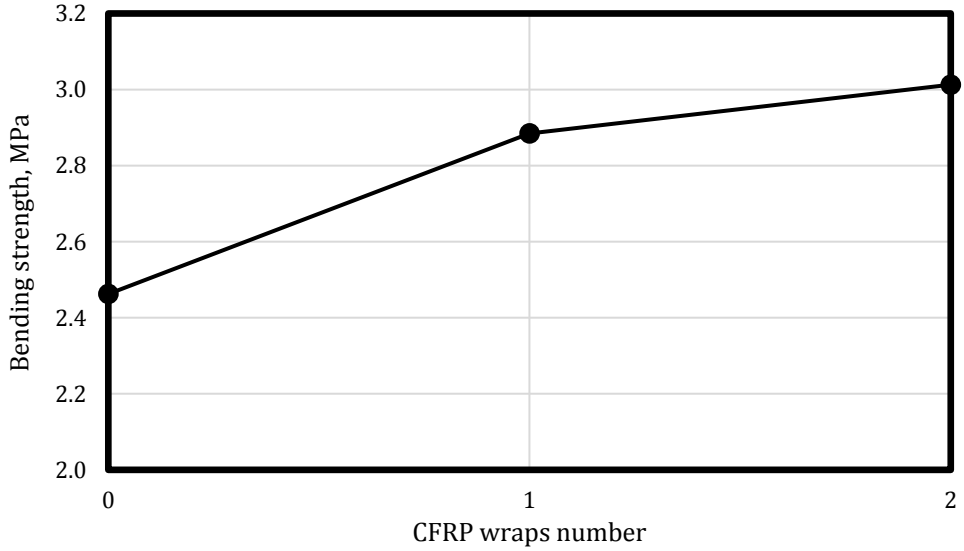


**Fig. 7.** Bending strength of the undamaged concrete specimens.

### *3.2. Reinforcement test results of damaged concrete*

The results shown in Fig. 8 are from the unit weight and ultrasound transmission velocity tests performed on the damaged concrete specimens after CFRP wrapping. While the unit weight was 2,198.03 kg/dm$^3$ for the specimens without CFRP wraps, this value increased by 0.10% to 2,200.33 kg/dm$^3$ with single layer of CFRP and by 0.23% to 2,203.16 kg/dm$^3$ with double layer of CFRP. These small increases indicate that the CFRP winding provides a slight contribution to the concrete mass and this contribution naturally increases with increasing winding number. However, this change is due to the effect of the CFRP layer applied on the surface rather than the internal structure of the concrete. Ultrasound transmission rate results provide information about the internal structural integrity of the material. The ultrasound transmission velocity of the specimens without CFRP wraps and with a single layer of CFRP wraps remained the same and was measured as 3.24 km/s. This indicates that the application of a single layer of CFRP has no significant effect on the closure of cracks or the improvement of the continuity of the internal structure. However, with double layer CFRP wrapping, the ultrasonic transmission velocity increased by 2.16%

to 3.31 km/h. This increase indicates that the double layer of CFRP provides a more effective wrapping in the damaged areas, resulting in the closure of cracks, reduction of micro voids and therefore more efficient wave passage. While the application of CFRP has a limited effect on the unit weight, especially double-ply applications can increase the ultrasonic transmission rate by contributing to the internal structural improvement. This shows that CFRP can partially improve not only superficial but also structural integrity.

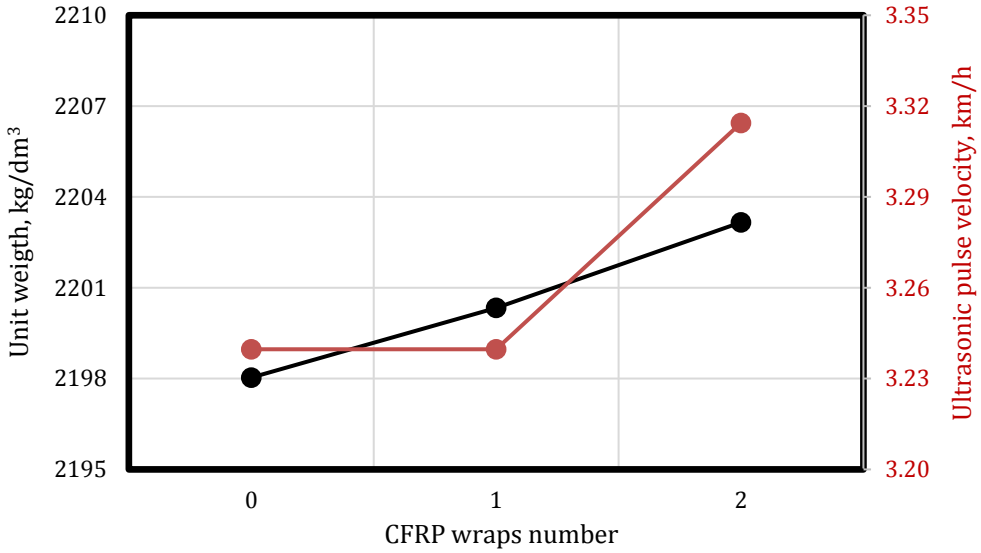


**Fig. 8.** Unit weight and ultrasound pulse velocities of the damaged concrete specimens.

The effect of CFRP wrapping on damaged concrete specimens is shown in Fig. 9. The compressive strength was measured as 10.37 MPa in the unwrapped condition. When a single layer of CFRP wrapping was applied, the strength increased by 22.99% to 12.76 MPa. The double layer CFRP application provided a more significant increase, increasing the strength by 60.83% to 16.68 MPa. These increases demonstrate the potential of CFRP to partially strengthen damaged structures. However, it should be noted that the effect of CFRP wrapping may be limited on damaged surfaces and existing cracks may partially reduce the effectiveness of CFRP. Nevertheless, it is seen that this limited effect can be overcome to a great extent with multi-layer wrapping applications.

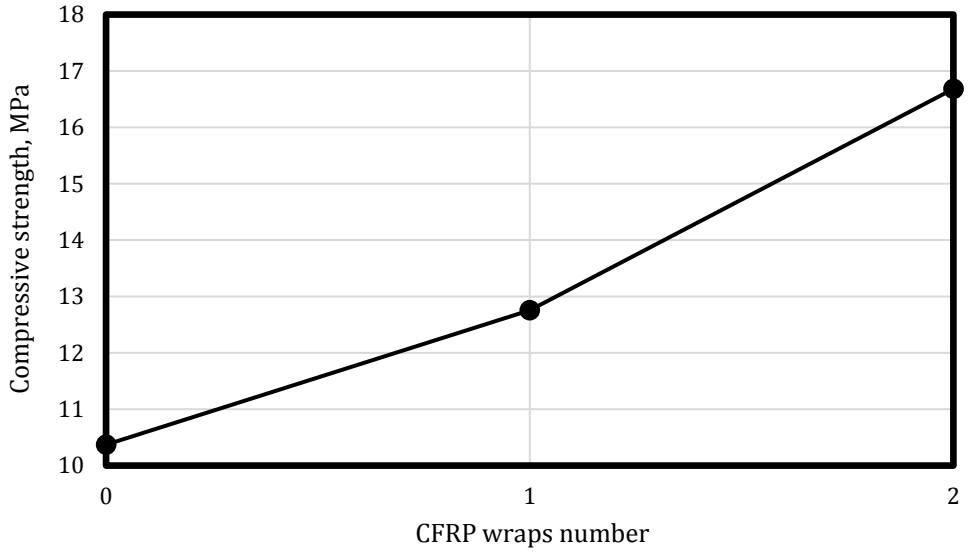


**Fig. 9.** Compressive strength of the damaged concrete specimens.

The bending test results in Fig. 10 show the effect of CFRP wrapping on the bending strength of 15 cm cube-shaped concrete specimens. The bending strength of both damaged and undamaged specimens without CFRP wrapping was 2.46 MPa. In the damaged specimens, the strength decreased by 33.41% to 1.64 MPa with a single layer of CFRP wrapping, which can be explained by the inability of CFRP to provide sufficient adherence in the cracked areas and adversely affect the load transfer similar to the literature (Alabdulhady et al. 2022). However,

in the double layer CFRP application, the strength increased again to 2.30 MPa and showed a decrease of only 6.66% compared to the unwrapped condition. This result shows that the double layer of wrapping can restore the bearing capacity to a large extent by creating sufficient wrapping effect in the damaged areas. While CFRP wrapping is an effective method to increase bending strength in undamaged specimens, positive results can be obtained in damaged specimens only with multi-layer applications. This shows that the effectiveness of CFRP is directly related to the integrity of the specimen surface.

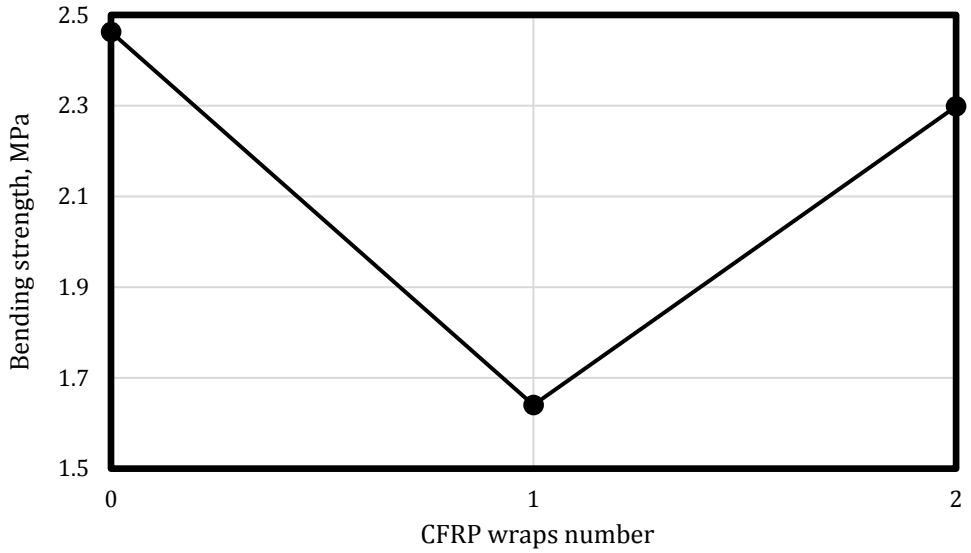


**Fig. 10.** Bending strength of the damaged concrete specimens.

Fig. 11 shows the fracture mechanisms of the concrete specimens after bending and compressive tests with CFRP wrapping. It was observed that CFRP was effective in maintaining the structural integrity of the prisms in the mid-point loaded bending effect, where the prisms broke in the middle as expected. In the cube specimens, it was observed that the concrete did not crumble due to the CFRP, where shear stresses at approximately 45 degrees were effective as expected in compression.

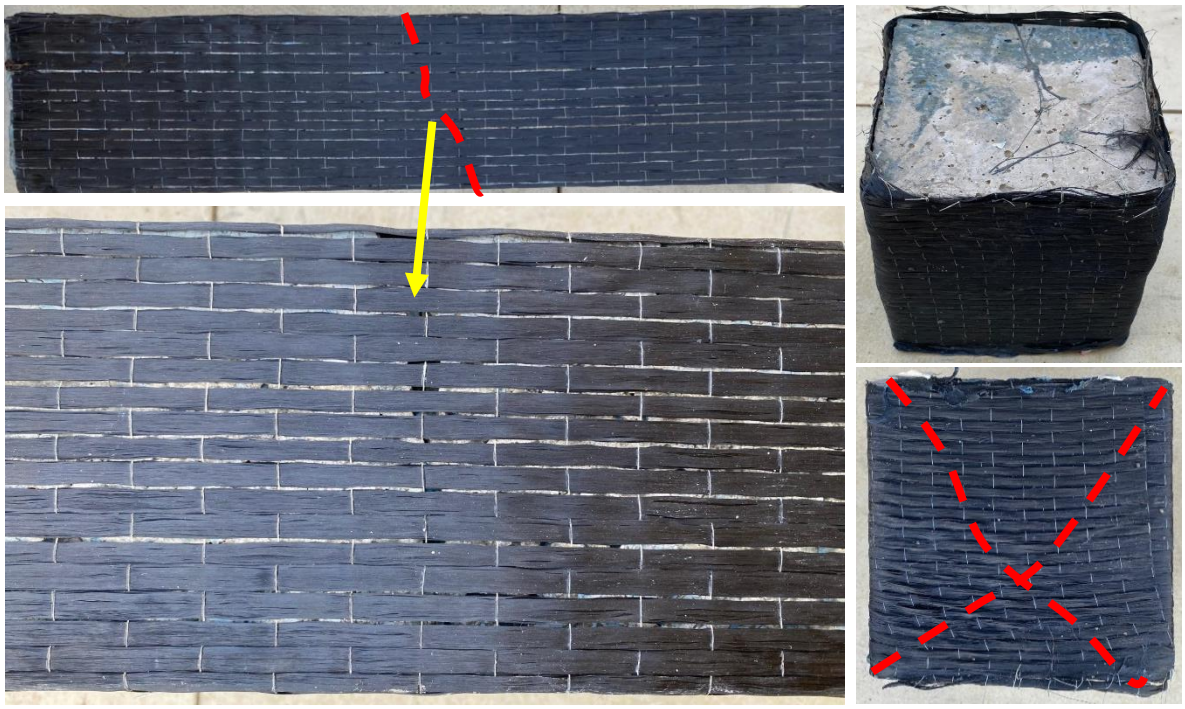

**Fig. 11.** Fracture mechanism of the concrete specimens.

## 4. Conclusions

The conclusions of the study are summarized as follows:

- CFRP wrapping applications significantly increase the compressive strength of both damaged and undamaged reinforced concrete elements. Especially double layer wrapping gives much more effective results than single layer wrapping.
- Although the effect on bending strength is not as significant as that on compressive strength, a partial improvement was achieved by CFRP wrapping in undamaged specimens. However, this effect was limited in damaged specimens.
- In damaged specimens, a single layer of CFRP wrapping was insufficient to completely cover the micro cracks, which limited the increase in strength. On the contrary, double layer wrapping more effectively closes the micro cracks and increases the strength.
- Ultrasonic pulse velocity tests show that the double layer of CFRP, in particular, contributes to the internal structural continuity of the concrete and reduces micro voids.
- The unit volume weight increased slightly with the application of CFRP. This increase is directly related to the superficial contribution of CFRP and does not adversely affect the performance of the structure.
- The CFRP wrapping shows higher performance, especially in previously undamaged elements, as it is possible to achieve a more homogeneous and effective adhesion of the wrapping to the concrete surface.

As a result of this study, double layer CFRP wrapping is considered to be a feasible and effective method for reinforcement of damaged and undamaged reinforced concrete members, increasing both strength and strain capacity. Therefore, double layer wraps is recommended for areas where reinforcement is needed.

***Acknowledgements***

*The authors would like to thank KYK (Kütahya Construction Chemicals), Türkiye for material support.*

***Funding***

*The authors received no financial support for the research, authorship, and/or publication of this manuscript.*

***Conflict of Interest***

*The authors declared no potential conflicts of interest with respect to the research, authorship, and/or publication of this manuscript.*

***Author Contributions***

*All of the authors made substantial contributions to conception and design, or acquisition of data, or analysis and interpretation of data; were involved in drafting the manuscript or revising it critically for important intellectual content; and gave final approval of the version to be published.*

***Data Availability***

*The datasets created and/or analyzed during the current study are not publicly available, but are available from the corresponding author upon reasonable request.*

## REFERENCES

Alabdulhady MY, Ojaimi MF, Chkheiwer AH (2022). The efficiency of CFRP strengthening and repair system on the flexural behavior of RC beams constructed with different concrete compressive strength. *Results in Engineering*, 16, 100763.

Bird JF, Bommer JJ (2004). Earthquake losses due to ground failure. *Engineering Geology*, 75(2), 147-179.

Çelik Z, Turan E, Oltulu M, Öner G (2024). Reinforcement of concrete beams using waste carbon-nanoclay-fiberglass laminate pieces. *Challenge Journal of Concrete Research Letters*, 15(1), 1-6.

EN 12620 (2002). Aggregates for concrete. European Committee for Standardization (CEN), Brussels, Belgium.

Eryılmaz Yıldırım M, Aybar K, Canbaz M (2024). Size effect on compressive behavior of GFRP bars. *Challenge Journal of Structural Mechanics*, 10(1), 14-20.

Hegde S, Shenoy BS, Chethan, KN (2019). Review on carbon fiber reinforced polymer (CFRP) and their mechanical performance. *Materials Today: Proceedings*, 19, 658-662.

Heidarzadeh G (2022). Numerical Modelling of Bond Behaviour of FRP Bar Reinforced Concrete Beam Under High Strain Rate Impact Load. *Ph.D. thesis*, City St George's, University of London, London, UK.

Jagarajan R., Asmoni MNAM, Mohammed AH, Jaafar MN, Mei JLY, Baba M (2017). Green retrofitting–A review of current status, implementations and challenges. *Renewable and Sustainable Energy Reviews*, 67, 1360-1368.

Keshmiry A, Hassani S, Dackermann U, Li J (2024). Assessment, repair, and retrofitting of masonry structures: A comprehensive review. *Construction and Building Materials*, 442, 137380.

Kim, NI, Kwon DY, Burenkhangai D., Lee KM, Bae SY, Chu YS (2023). A study on manufacturing CFRP rebar with a high tensile strength. *Journal of the Korean Ceramic Society*, 60(3), 488-495.

Ma Z, Cooper P, Daly D, Ledo L (2012). Existing building retrofits: Methodology and state-of-the-art. *Energy and Buildings*, 55, 889-902.

Mitra P (2000). Advanced polymer composites with special reference to carbon fibre reinforced polymer (CFRP). *Proceedings of National Conference on Composites: Science & Technology*, IIT Bombay, 31–48.

Mousa S, Mohamed HM, Benmokrane B (2019). Strength and deformability aspects of circular concrete members reinforced with hybrid carbon-FRP and glass-FRP under flexure. *Journal of Composites for Construction*, 23(2), 04019005.

Rashid SP, Bahrami A (2023). Structural performance of infilled steel–concrete composite thin-walled columns combined with FRP and CFRP: A comprehensive review. *Materials*, 16(4), 1564.

TS EN 197-1 (2012). Cement – Part 1: Composition, specifications and conformity criteria for common cements. Turkish Standards Institution, Ankara, Türkiye.

TS EN 1504-4 (2006). Products and systems for the protection and repair of concrete structures – Part 4: Structural bonding. Turkish Standards Institution, Ankara, Türkiye.

Wu J, He X, Li Y, Shi P, Ye T, Li N (2019). How earthquake-induced direct economic losses change with earthquake magnitude, asset value, residential building structural type and physical environment: An elasticity perspective. *Journal of Environmental Management*, 231, 321-328.

Xue W., Tan Y, Zeng L (2010). Flexural response predictions of reinforced concrete beams strengthened with prestressed CFRP plates. *Composite Structures*, 92(3), 612-622.

Younis A, Ebead U, Judd S (2018). Life cycle cost analysis of structural concrete using seawater, recycled concrete aggregate, and GFRP reinforcement. *Construction and Building Materials*, 175, 152-160.

Zardari S, Kutlu İ, Nayeb A (2024). Investigation of structural performances of historical building elements made with local materials using the finite element method. *Challenge Journal of Concrete Research Letters*, 15(3), 101-111.

Challenge Journal of Concrete Research Letters

Research Article

# Design of reactive powder concrete mortar mixes through high strength and durability

Yousry B. I. Shaheen [a], Zeinab A. Etman [a], Hanan Lotfy Sabiha [b,*]

[a] *Department of Civil Engineering, Menoufia University, 32511 Shebin ElKoum, Menofia, Egypt*
[b] *Higher Institute of Engineering and Technology, Menoufia University, 32511 Shebin ElKoum, Menofia, Egypt*

## ABSTRACT

This research investigates the characteristics of reactive powder concrete (RPC) through comprehensive analysis. The primary methodology involved evaluating both fresh (uncured) and hardened RPC specimens. The initial phase incorporated silica fume (SF) as a cement replacement at concentrations of 5, 10, 15, 20, and 25%, fly ash (FA) substitution at levels of 5, 10, 20, 25, and 30% of the cement content, plus binary combinations where SF constituted 10% cement replacement while FA proportions ranged from 10 to 30%. Material behavior was assessed through slump flow testing procedures. Hardened concrete evaluation encompassed dry density measurements, compressive strength analysis conducted at 7, 28, 56, and 90-day intervals, along with tensile splitting strength and flexural strength determination at 28 days. Results demonstrate that FA substitution alone provides superior workability compared to SF+FA combinations and pure SF, whereas SF replacement individually exhibits enhanced compressive, tensile splitting, and flexural strength performance relative to standalone FA and binary SF+FA mixtures. The subsequent investigation phase examined the influence of nano-silica (NS) on fresh and hardened RPC characteristics. NS replaced cement at 1, 2, 3, 4, and 5% levels, combined with 10% SF and 20% FA. Findings revealed that increased NS content diminishes workability due to elevated water demand for hydration and mixing processes as particle fineness increases. Regarding hardened properties, the optimal composition comprises 10% SF, 20% FA, and 3% NS, attributed to NS's effective interaction with calcium hydroxide generated during cement hydration, which facilitates additional C-S-H formation through enhanced pozzolanic reactions. This mechanism results in improved mixture performance and strength development.

## ARTICLE INFO

**Article history:**
Received – January 1, 2025
Revision requested – March 25, 2025
Revision received – June 2, 2025
Accepted – June 25, 2025

**Keywords:**
Reactive powder concrete
Blast furnace slag cement
Silica fume
Fly ash
Nano silica



**Citation:** Shaheen YBI, Etman ZA, Sabiha HL (2025). Design of reactive powder concrete mortar mixes through high strength and durability. *Challenge Journal of Concrete Research Letters*, 16(3), 142–154.

## 1. Introduction

Reactive powder concrete (RPC) belongs to the group of ultrahigh-performance concretes. All the components in RPC are chemically active, which is why it is referred to as reactive powder. Several studies have found that ultra high performance concrete (UHPC) is not considered concrete because it is not made with coarse aggregate (Sadrekarimi 2004). The word "concrete" is used for ultrahigh-performance concrete because it contains steel fibers to make it stronger and more flexible (Aïtcin 2000). On the other hand, RPC development does not require fibers. RPC was created by applying microstructural modification techniques, which changed its characteristics, including remarkable durability, high compressive strength, and toughness (Richard and Cheyrezy 1995). Currently, specific methods and raw materials need to be used in RPC production in order to obtain outstanding mechanical performance. These include (Sarika and Elson 2015):

* *Corresponding author*. E-mail address: hanan_lotfy85@yahoo.com (H. L. Sabiha)
ISSN: 2548-0928 / DOI: https://doi.org/10.20528/cjcrl.2025.03.004

- Removing coarse aggregate from the concrete to increase homogeneity.
- Making composite materials more ductile by adding steel tubes or metal fibers.
- Using large quantities of quartz and premium superplasticizer to create a low water/binder ratio, which reduces porosity and increases strength.
- Applying pressure both prior to and during the setting process to increase compactness.
- Utilizing cementitious materials containing highly active micro-silica and/or precipitated silica to accelerate cement hydration and catalyze a strong pozzolanic reaction.
- Applying steam curing to achieve greater strength.

To develop UHPC that achieves target strength performance, carefully selected raw materials and advanced processing methods are necessary. In recent years, multiple researchers have studied RPC characteristics and behavior. Numerous successful RPC applications include the Sherbrooke Bridge in Canada (60-meter span), the Future Bridge in the United States (25-meter length), seawall anchor systems in Portugal, various automotive bridges in Australia, and the manufacture of structural beam elements, manhole covers, roadway accessories, and other products. Presently, extensive research is conducted on RPC to investigate its response and behavior.

Silica fume (SF), a supplementary cementitious material (SCM), is a byproduct of silicon and ferrosilicon manufacturing. It appears in powder form as spherical particles approximately 200 nm in diameter. Since less cement is used in the composition, SF enhances hardened concrete properties while promoting environmental compatibility. SF addition has been associated with increased C-S-H gel formation and reduced $Ca(OH)_2$ content, which significantly improves matrix microstructural density and reduces porosity (Chandra and Berntsson 1996; Aïtcin 2016; Kurdowski 2014; Ullah et al. 2022). SF substantially improves the mechanical characteristics of RPC. It increases RPC packing density and enhances the interfacial transition zone between paste and aggregate. Compared to SCM formulations using fly ash (FA) or ground granulated blast-furnace slag, the primary limitation of RPC compositions with SF is reduced workability at higher SF contents (Bahmani and Mostofinejad 2022; Ge et al. 2023; Ju et al. 2017; Shen et al. 2022; Sultan et al. 2022).

Using 20% FA as a partial cement replacement modifies the ITZ microstructure and enhances mechanical properties to some degree, particularly under elevated temperatures and autoclave pressure. FA requires less water for reactions compared to SF (Golewski 2018; Hefni et al. 2018; Moffatt et al. 2017; Yazıcı et al. 2009; Yu et al. 2015).

The integration of nanoparticles into concrete is gaining recognition for its beneficial effects on fresh and hardened properties, attributed to their unique surface area characteristics. The most common nanoparticles used in concrete to enhance the cement matrix include nano-alumina, nano-titania, nano-iron oxide, nano-silica (NS), nano-zinc oxide, and nano-clay. Among these, NS, a conventional inorganic non-metallic oxide nanomaterial with high specific surface area and reactivity, is considered the most suitable nanoparticle for concrete applications (Rashad 2014). Through pozzolanic mechanisms, NS has been shown to improve the mechanical properties of cement-based materials (Balapour et al. 2018; Kong et al. 2012; Zhang et al. 2016). It has been concluded that the early compressive strength of high-performance concrete is more significantly affected by NS incorporation compared to later strength development. Furthermore, optimal mixing proportions are suggested to range between 3% and 5% NS (Wang 2011).

RPC compressive strength, flexural strength, and impact resistance all increase when the water-cement ratio is reduced, as this leads to greater density and lower porosity. The specimen with the highest overall mechanical performance had a 0.16 water-cement ratio, 134.4 MPa compressive strength, 16.86 MPa flexural strength, and the ability to withstand 1,150 destructive impacts (Tan et al. 2025).

Albakry and Abbas (2025) examined the influence of four different curing methods on RPC mechanical properties. The most substantial improvements in mechanical strength (compressive, flexural, and splitting tensile) were achieved in the Steam + Normal Curing (R-S) system, particularly with 1–3 day curing durations, followed by Normal Curing (R-N) at 28 and 90 days.

RPC offers exceptional strength and durability, making it ideal for constructing large-span lightweight structures and those required to withstand severe weather conditions, thus improving infrastructure longevity and reliability. The implementation of RPC aligns with sustainable development objectives by reducing the demand for natural resources, extending the service life of structures, and decreasing waste production, thereby fostering eco-friendly practices within the construction sector (Zhao 2024).

## 2. Material Properties

The materials used in this research to produce local RPC mixes were blast furnace slag cement, SF, FA, sand, NS, polypropylene fiber, superplasticizers, and water, as shown in Fig. 1.

### *2.1. Blast furnace slag cement*

The research used blast furnace slag cement (CEM III/A 42.5 N) with a specific gravity of 2.9, according to E.S.S. 4756-1 (2013). Its main properties are shown in Tables 1 and 2.

### *2.2. Silica fume*

Silica fume was used as a pozzolanic material meeting the requirements of E.S.S. 5129-1 (2006). Tables 3 and 4 show the chemical and physical properties of silica fume.

### *2.3. Fly ash*

Fly ash Class F was used as a pozzolanic material meeting the requirements of ASTM C618 (2019). Tables 5 and 6 show the chemical and physical properties of fly ash.

**Table 1.** Mechanical and physical properties of the cement used.

| Property | | Value | Limits |
|---|---|---|---|
| Specific gravity | | 2.9 | -- |
| Setting time | Initial (min) | 60 | Not less than 45 min |
| | Final (hrs) | 5.25 | Not more than 10 hrs |
| | Fineness | 3733 $cm^2/gm$ | Not less than 2500 $cm^2/gm$ |
| | Soundness (expansion) | 1 | Not more than 10 mm |
| Compressive strength ($N/mm^2$) | 2 days | 12.96 | -- |
| | 7 days | 27.33 | -- |
| | 28 days | 47.74 | -- |

**Table 2.** Chemical properties of the cement used.

| Oxides | Value % | % max |
|---|---|---|
| $SiO_2$ | 23.63 | -- |
| $Al_2O_3$ | 9.07 | -- |
| $Fe_2O_3$ | 3.45 | -- |
| CaO | 51.54 | -- |
| MgO | 4.66 | -- |
| SO3 | 2.71 | 4.0 |
| $K_2O$ | 0.35 | -- |
| Cl | 0.03 | 0.1 |
| $Na_2O$ | 0.34 | -- |
| (IR) Insoluble residue | 2.09 | 5.0 |
| (LOI) Loss on ignition | 2.02 | 5.0 |
| Equivalent Alkalis | 0.58 | -- |

**Table 3.** Chemical composition of silica fume.

| Chemical composition | Mass, % |
|---|---|
| $SiO_2$ | 92-94 |
| $Al_2O_3$ | 0.2-0.3 |
| $Fe_2O_3$ | 0.1- 0.5 |
| CaO | 0.1- 0.15 |
| MgO | 0.1-0.2 |
| $Na_2O$ | 0.1 |
| $K_2O$ | 0.1 |
| Carbon | 3-5 |
| MnO | 0.008 |

**Table 4.** Physical properties of silica fume.

| | |
|---|---|
| Moisture content, % | 0.5 max |
| Size above 45 µm | |
| Specific gravity | 2.13 |
| (BET) Particle Surface Area | 15.0 $m^2/g$ min |

**Table 5.** Chemical composition of fly ash.

| Chemical composition | Mass, % |
|---|---|
| $SiO_2$ | 55.71 |
| $Al_2O_3$ | 22.56 |
| $Fe_2O_3$ | 5.61 |
| Sum | 83.88 |
| MgO | 10.44 |
| $SO_3$ | 1.78 |
| $Na_2O$ | 0.54 |
| $K_2O$ | 0.79 |
| Total alkalis | 0.76 |
| Available alkalis | 0.26 |
| Loss on ignition (LOI) | 0.41 |

**Table 6.** Physical properties of fly ash.

| | |
|---|---|
| Moisture content, % | 0.16 |
| Amount retained on No. 325 sieve, % | 23.63 |
| Specific gravity | 2.2 |
| Autoclave soundness, % | |
| Strength activity index with portland cement at 7days, % of control | 77.1 |
| Strength activity index with portland cement at 28days, % of control | 85.5 |
| Water required, % of control | 94.6 |

### *2.4. Sand*

According to E.S.S. 1109 (2008), fine aggregate was used to produce the mortar specimens in this study. The particle size of the quartz sand used for producing RPC ranged from 150 to 650 µm, with a specific gravity of 2.65.

### *2.5. Nano-silica*

Nano-silica (NS) served as a concrete additive for enhancing cement hydration processes, improving durability characteristics, and optimizing the mechanical behavior of both fresh and hardened concrete. The chemical characteristics of NS are presented in Table 7.

Technical specifications include:

- Elevated purity levels ranging from 96.7% to 99%
- Completely natural sand composition (100%)
- Moisture-free sand with no water content
- Superior particle size gradation
- Spherical grain morphology
- Absence of organic matter and contaminants
- Non-radioactive material
- Non-hazardous composition
- Turbidity measurements below 100 units
- Dust-free condition
- Absence of heavy metals

### *2.6. Polypropylene fiber*

Fibers were graded in lengths of 6, 12, and 20 mm, with an average diameter of 0.034 mm. They had a tensile strength of 500–700 MPa, a density of 900 kg/m$^3$, a melting point of 162 °C, a modulus of elasticity of 2800 MPa, and an elongation of 25%, according to ASTM C1116 (2010) and ASTM C1339 (2008).

### *2.7. Superplasticizer*

As a superplasticizer, a high-range water-reducing admixture (HRWRA), according to ASTM C1017 (2013) (Type A and F), was used. The admixture is brown and weighs 1.18 kg per liter at room temperature. The amount of HRWRA was 2% of the total binder weight (fly ash, cement, silica fume, and nano-silica).

### *2.8. Water*

No impurities were allowed in the potable water used for making and curing the concrete. The water-to-binder ratio (silica fume + fly ash + cement + nano-silica) was set at 0.23.

**Table 7.** Chemical properties of nano-silica.

| Oxides | % min | % max |
|---|---|---|
| $SiO_2$ | 99.4 | 99.4 |
| $Al_2O_3$ | 0.06 | 0.09 |
| $Na_2O$ | 0.05 | 0.07 |
| $K_2O$ | 0.01 | 0.02 |
| CaO | 0.02 | 0.09 |
| MgO | 0.03 | 0.03 |
| $Fe_2O_3$ | 0.012 | 0.018 |
| $TiO_2$ | 0.017 | 0.021 |
| $Cr_2O_3$ | 2 ppm | 2 ppm |
| L.O.I. | 0.15 | 0.25 |

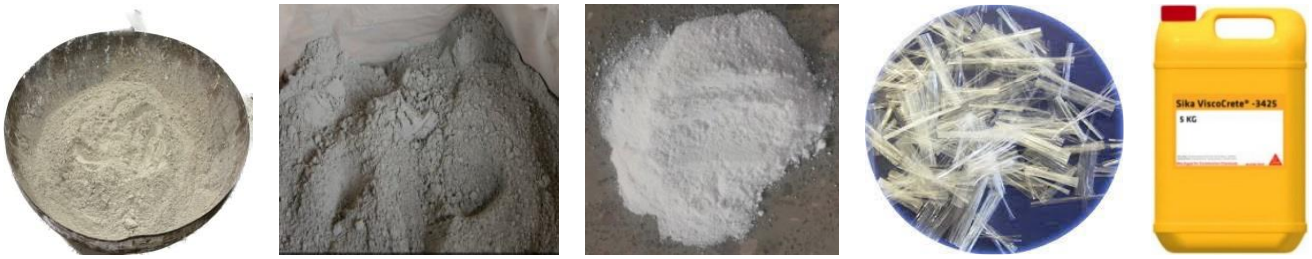


**Fig. 1.** Materials: Silica fume; Fly ash; Nano-silica; Polypropylene Fiber300–e3; Super-plasticizer.

## 3. Casting and Mix Proportion

Four RPC groups comprising 21 mixtures were examined to meet the study's objectives, as indicated in Table 8. With a cementitious content of 990.3 kg/m$^3$, the first group (SF) included mixes M01 to M05, in which SF partially replaced cement at 5, 10, 15, 20, and 25%. The second group (FA), also with a cementitious content of 990.3 kg/m$^3$, consisted of mixes M06 to M11, where FA partially replaced cement at 5, 10, 15, 20, 25, and 30%. The third group (SF+FA), with the same cementitious content, consisted of mixes M12 to M16, incorporating 10% SF and partial FA replacement at 10, 15, 20, 25, and 30%. The fourth group (SF+FA+NS) also had a cementitious content of 990.3 kg/m$^3$ and included mixes M17 to M21, containing 10% SF, 20% FA, and partial NS replacement at 1, 2, 3, 4, and 5%.

All mixes were cured in ordinary water at 25 °C. To prepare the mixtures, the sand and fine materials were blended in a mixer for two minutes. Water and superplasticizer were then added, and mixing continued for seven minutes until a uniform consistency was achieved. Polypropylene fiber was added next, and the mixture was blended for an additional five minutes to ensure homogeneity. An electric hand mixer was used to finalize the mix. The concrete was then poured into molds to create the specimens.

Specimens were demolded 24 hours after casting and cured in water at approximately 25 °C. At the time of testing, the specimens were removed from the water. To ensure consistent curing conditions, all specimens were treated in the same curing tanks.

## 4. Testing Method

Mechanical property evaluations were conducted using standard specimens in accordance with ASTM C109 (2020) for compressive strength, ASTM C348 (2021) for flexural strength, and ASTM C496 (2017) for splitting tensile strength. Strength assessments utilized cubic specimens (70×70×70 mm), cylindrical specimens (50×100 mm), and prismatic specimens (40×40×160 mm).

**Table 8.** Constituents of concrete mixes (kg/m$^3$) (sand/cement=1.1; water/binder=23%).

| Group | Mix No. | Cement (kg/m$^3$) | Sand (kg/m$^3$) | Water (kg/m$^3$) | HRWRA (kg/m$^3$) | PPF (kg/m$^3$) | SF (kg/m$^3$) | FA (kg/m$^3$) | $SiO_2$ (kg/m$^3$) |
|---|---|---|---|---|---|---|---|---|---|
| - | Control | 990.20 | 1089.2 | 227.75 | 19.8 | 2.7(0.3%) * | -- | -- | -- |
| Silica fume (SF) | M01 (5%) | 940.69 | 1089.2 | 227.75 | 19.8 | 2.7(0.3%) * | 49.51 | -- | -- |
| | M02 (10%) | 891.18 | | | | | 99.02 | -- | -- |
| | M03 (15%) | 841.67 | | | | | 148.53 | -- | -- |
| | M04 (20%) | 792.16 | | | | | 198.04 | -- | -- |
| | M05 (25%) | 742.65 | | | | | 247.55 | -- | -- |
| Fly Ash (FA) | M06 (5%) | 940.69 | 1089.2 | 227.75 | 19.8 | 2.7(0.3%) * | -- | 49.51 | -- |
| | M07 (10%) | 891.18 | | | | | -- | 99.02 | -- |
| | M08 (15%) | 841.67 | | | | | -- | 148.53 | -- |
| | M09 (20%) | 792.16 | | | | | -- | 198.04 | -- |
| | M10 (25%) | 742.65 | | | | | -- | 247.55 | -- |
| | M11 (30%) | 693.14 | | | | | -- | 297.06 | -- |
| Silica fume +Fly Ash (SF) + (FA) | M12 (10%SF + 10%FA) | 792.16 | 1089.2 | 227.75 | 19.8 | 2.7(0.3%) * | 99.02 | 99.02 | -- |
| | M13 (10%SF + 15%FA) | 742.65 | | | | | 99.02 | 148.53 | -- |
| | M14 (10%SF + 20%FA) | 693.14 | | | | | 99.02 | 198.04 | -- |
| | M15 (10%SF + 25%FA) | 643.63 | | | | | 99.02 | 247.55 | -- |
| | M16 (10%SF + 30%FA) | 594.12 | | | | | 99.02 | 297.06 | -- |
| Silica fume +Fly Ash + Nano-Silica (SF) + (FA) + (NS) | M17 (10%SF + 20%FA + 1%NS) | 683.24 | 1089.2 | 227.75 | 19.8 | 2.7(0.3%) * | 99.02 | 198.04 | 9.90 |
| | M18 (10%SF + 20%FA + 2%NS) | 673.47 | | | | | | | 19.80 |
| | M19 (10%SF + 20%FA + 3%NS) | 663.43 | | | | | | | 29.71 |
| | M20 (10%SF + 20%FA + 4%NS) | 653.53 | | | | | | | 39.61 |
| | M21 (10%SF + 20%FA + 5%NS) | 643.63 | | | | | | | 49.51 |

P.P: Poly Propylene; (*): Fiber volume fraction

### *4.1. Flow diameter assessment*

Flow testing procedures were carried out for each mixture composition. Through flow diameter determination protocols, the values shown in Fig. 2(a) were obtained. The results demonstrate that reactive powder concrete exhibits satisfactory workability characteristics.

### *4.2. Compressive strength test*

Compressive strength was evaluated using 70 mm cubic specimens at 7, 28, 56, and 90 days, as illustrated in Fig. 2(b).

### *4.3. Flexural strength test*

Flexural strength was determined at 28 days using 40×40×160 mm prismatic specimens, as shown in Fig. 2(c).

### *4.4. Splitting tensile strength test*

Splitting tensile strength was measured using cylindrical specimens measuring 50×100 mm at 28 days, as presented in Fig. 2(d).

### *4.5. Density*

Density measurements were conducted on three 70 mm cubic specimens. According to ASTM C642 (2013), density is defined as the ratio of concrete mass to its corresponding volume. Dry density was evaluated at 28 days.

## 5. Results and Discussion

Several conditions were used to evaluate the characteristics of RPC. The following sections detail the outcomes of the experimental program.

### *5.1. Workability of RPC*

The slump test was used to measure the fresh RPC properties for all mixes, considering the variety of binder materials (SF, FA, and NS) used at different ratios. The results are shown in Fig. 3. The flow diameter of the concrete decreases as the dosages of SF, FA, and NS increase. RPC mixes containing NS exhibit lower flowability than mixes containing only SF. This is explained by the fact that NS has a large surface area and requires more water to mix and flow properly (Ranjan et al. 2024).

RPC mixes containing FA show higher spread values than those containing SF. This is because excessive SF may reduce workability and increase fracture sensitivity, whereas FA improves fluidity without substantially affecting mechanical properties (Zhang et al. 2022). However, excessive fluidity may lead to concrete segregation. Therefore, when using FA, it is advisable to lower the dosage of superplasticizer. The surface area of cementitious materials increases with fineness, necessitating more water for hydration and workability. Chemical admixtures must be used in varying amounts depending on the type and proportion of cementitious materials.

**Fig. 2.** Testing: Slump flow test; Compressive strength test; Flexural strength test; Splitting tensile strength test.

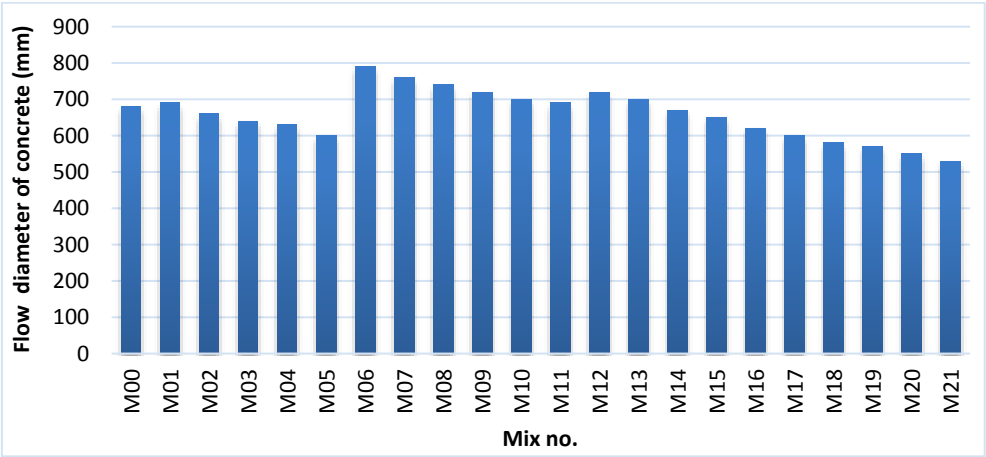


**Fig. 3.** The relation between the flow diameter of concrete and mix code for different mixes.

### *5.2. Compressive strength of RPC*

#### *5.2.1. Effect of the silica fume content*

It was observed that silica fume improves the compressive strength of reactive powder concrete, with the optimal replacement level at 25%, as shown in Fig. 4. For mix M05, the compressive strength increased by 56.37% at 7 days, 57.5% at 28 days, 59.09% at 56 days, and 60.16% at 90 days compared to the control mix M00 at the same ages. This improvement is attributed to the enhanced hydration and densification of the RPC matrix due to the extremely fine silica fume particles, which increase its strength (Danha et al. 2013). In addition, silica fume particles react effectively with calcium hydroxide, reducing small particles and microcracks, and strengthening the microstructure.

Because silica fume is extremely fine, calcium hydroxide is able to form nuclei on its surface, which accelerates cement hydration. Silica fume also provides physical improvements by enabling particles to pack more closely, thereby strengthening the RPC matrix, making it denser, and enhancing the adhesion between cement and fibers (Neville 2005).

#### *5.2.2. Effect of the fly ash content*

The results demonstrate that incorporating 20% fly ash into reactive powder concrete enhances compressive strength performance, as shown in Fig. 5. At testing intervals of 7, 28, 56, and 90 days, mixture M09 exhibited compressive strength improvements of 35.52%, 36.47%, 36.89%, and 37.42%, respectively, compared to the control mixture M00 at the corresponding ages. The pozzolanic activity of fly ash facilitates reactions involving $SiO_2$, $Al_2O_3$, calcium hydroxide, and calcium silicate hydrate formation, resulting in enhanced density with reduced porosity and, consequently, improved concrete strength (Malheiro et al. 2020), alongside improved particle packing efficiency. The micro-filler capability of fly ash within cement paste voids contributes to increased density and subsequent strength enhancement.

Fig. 6 reveals that increasing fly ash content from 10% through 15%, 20%, 25%, to 30%, while maintaining a constant 10% silica fume content, produced minimal impact on 28-day compressive strength development. Substituting silica fume with fly ash in RPC offers economic benefits but affects compressive strength performance.

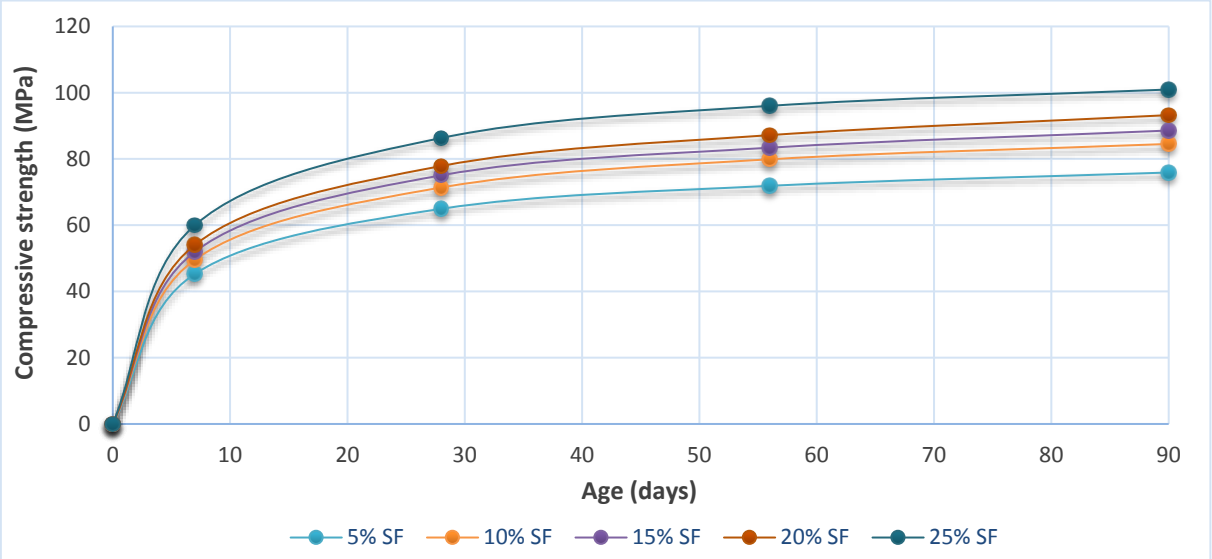


**Fig. 4.** Compressive strength of RPC using different ratios of silica fume.

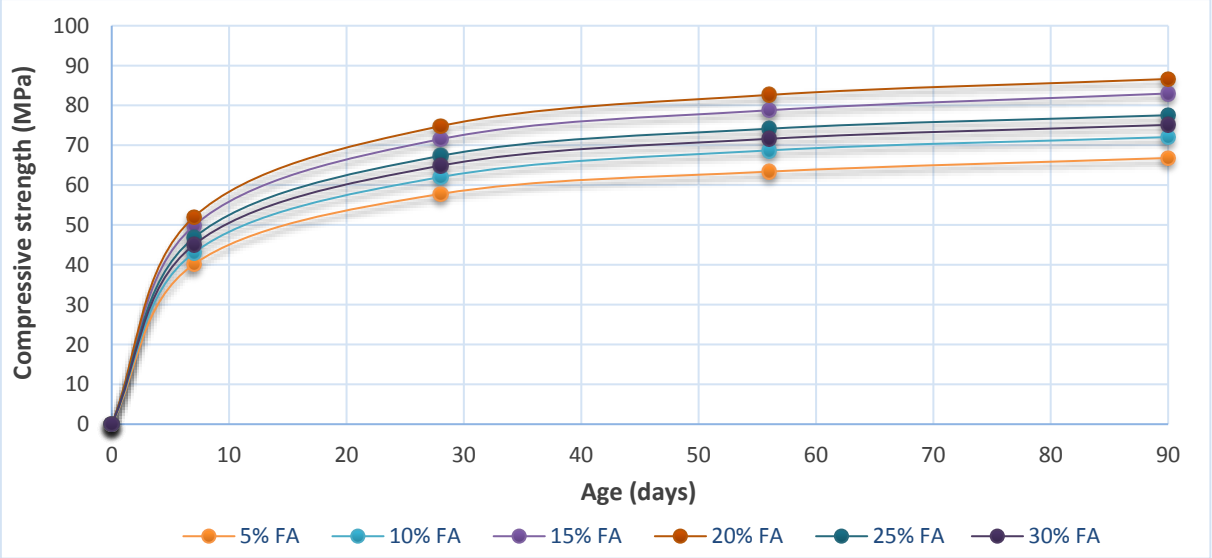


**Fig. 5.** Compressive strength of RPC using different ratios of fly ash.

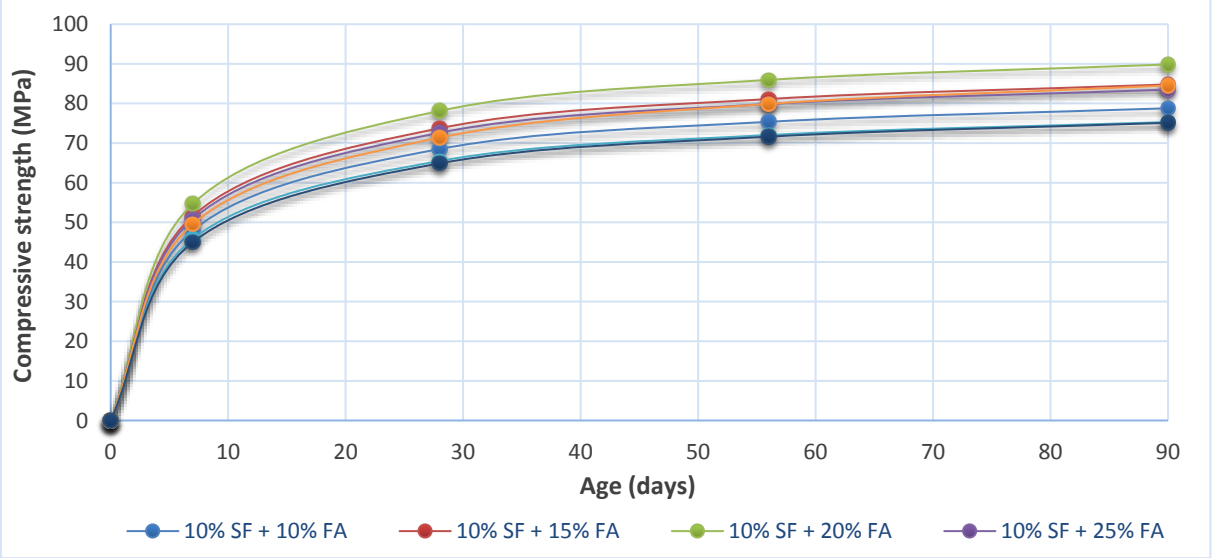


**Fig. 6.** Compressive strength of RPC using 10% silica fume with different ratios of fly ash.

The findings indicate that 30% fly ash replacement without silica fume achieved a 28-day compressive strength of 64.88 MPa, representing 16.96% lower performance compared to silica fume–fly ash combinations (10% SF + 20% FA). At equivalent ages and identical silica fume–fly ash proportions, silica fume demonstrated superior effectiveness in enhancing compressive strength. Specifically, compressive strength improvements of 12.88%, 15.27%, 4.42%, 4.00%, and 28.20% were observed at 7 days, as shown in Fig. 7(a), with corresponding improvements of 12.41%, 15.11%, 4.92%, 4.10%, and 28.20% at 28 days, as illustrated in Fig. 7(b). In addition, Fig. 7(c) and Fig. 7(d) provides the compressive strength alteration at 56 days and 90 days, respectively.

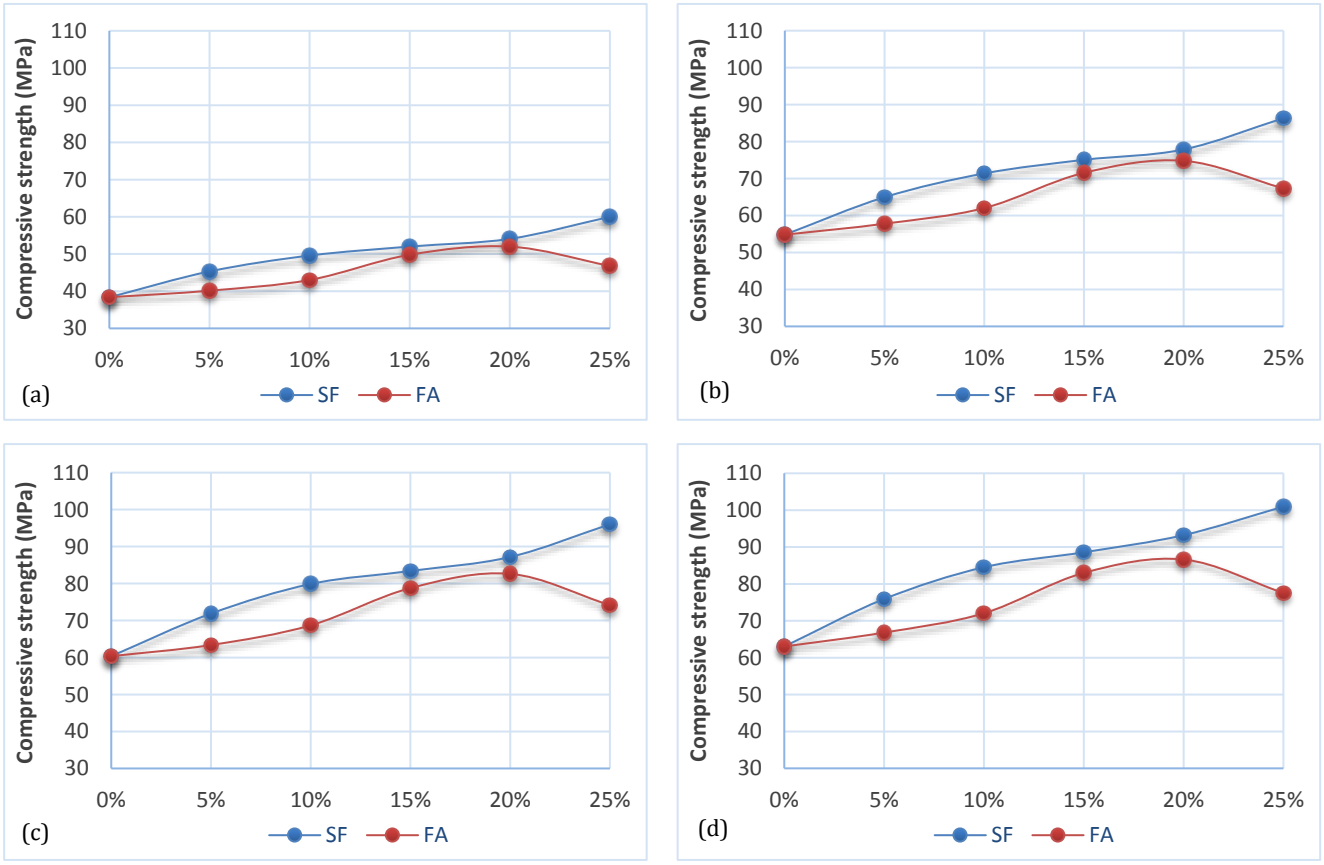


**Fig. 7.** Comparison between SF & FA at the same content: (a) at 7 days; (b) at 28 days; (c) at 56 days; (d) at 90 days.

*5.2.3. Effect of the nano-silica content*

Fig. 8 shows that nano-silica contents of 1%, 2%, 3%, 4%, and 5% were used together with 10% SF and 20% FA. The effect of this parameter on hardened concrete can be observed by examining mixes M17, M18, M19, M20, and M21. A maximum compressive strength of 103.13 MPa was recorded when 3% nano-silica was used. This was attributed to the optimal particle packing and the avoidance of strength reduction caused by particle agglomeration.

Nano-silica improved performance because it reacts with calcium hydroxide (CH) formed during cement hydration, producing additional calcium silicate hydrate (C-S-H) and strengthening the paste. With a stronger pozzolanic reaction, more C-S-H is generated, leading to greater overall strength (Rupasinghe et al. 2017). Nano-silica also enhances RPC by filling small pores and accelerating the formation of microstructural components that strengthen the concrete. As a result, the microstructure becomes denser, and the overall matrix strength increases (Ranjan et al. 2024).

### *5.3. Flexural strength of RPC*

*5.3.1. Effect of the silica fume content*

Fig. 9 shows the flexural strength at 28 days for various rapid hardening portland (RHP) cement mixes containing silica fume at 5%, 10%, 15%, 20%, and 25%. By examining mixes M01, M02, M03, M04, and M05, the effect of silica fume content on results can be observed. Increasing the silica fume content from 5% to 25% of the binder improved the flexural strength of RPC by 11.72%, 30.45%, 52.95%, 63.64%, and 76.48%, respectively, compared to the control mix M00.

Based on the test results, the optimal silica fume content was found to be 25%, as shown in Fig. 9. This improvement is attributed to the extremely fine silica fume particles, which facilitate hydration and densification of the RPC matrix, thereby enhancing its strength.

*5.3.2. Effect of the fly ash content*

Fig. 10 illustrates the flexural strength performance of RPC mixtures incorporating fly ash at concentra-

tions of 5%, 10%, 15%, 20%, 25%, and 30% at 28-day maturity. Progressive fly ash incorporation demonstrates an overall enhancement in flexural strength, with the maximum improvement of 49.10% observed at 20% fly ash replacement relative to the reference mixture M00.

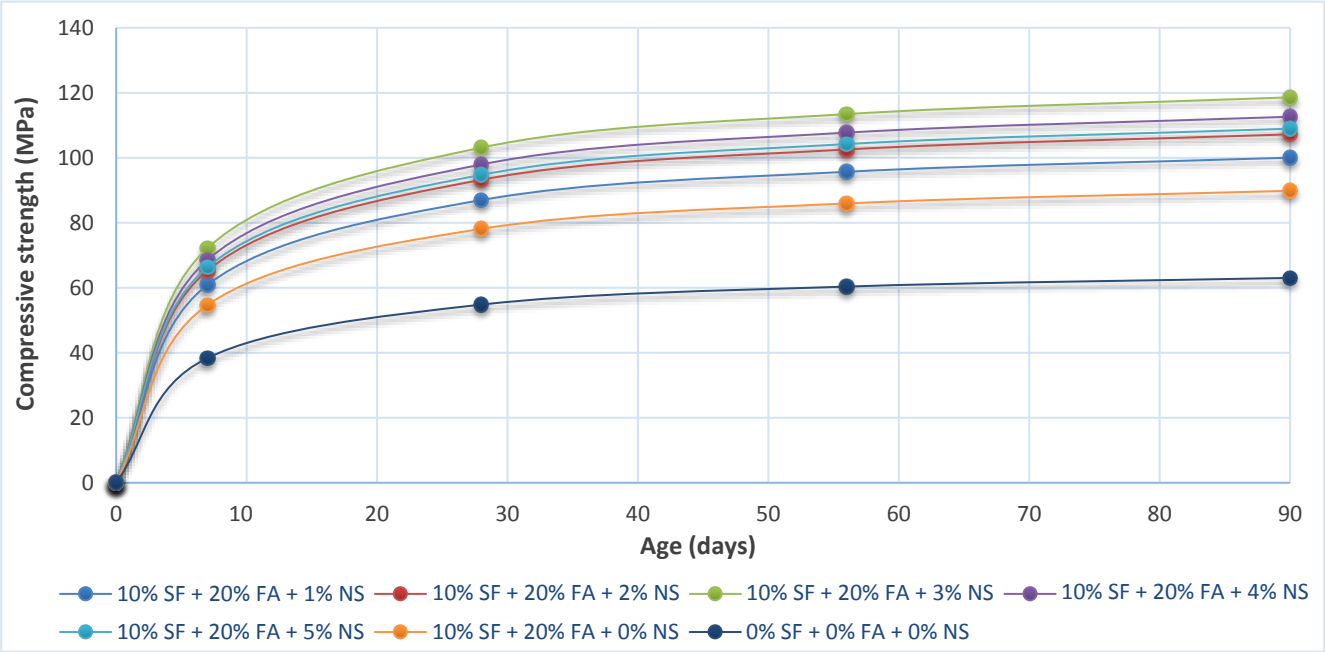


**Fig. 8.** Compressive strength of RPC using 10% SF + 20% FA with different ratios of nano-silica.

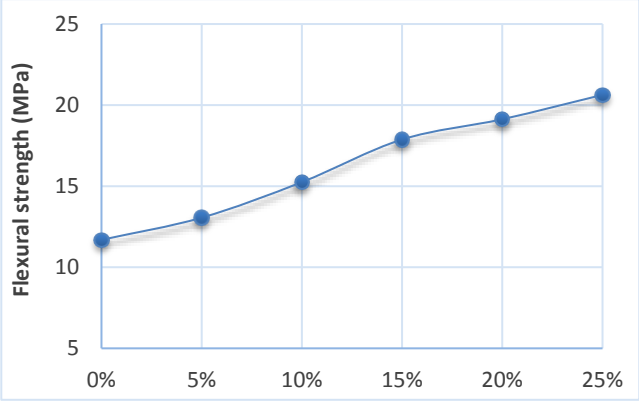


**Fig. 9.** Flexural strength of RPC using different ratios of silica fume.

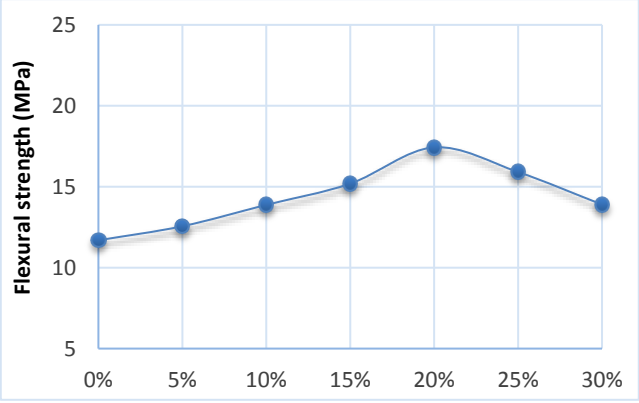


**Fig. 10.** Flexural strength of RPC using different ratios of fly ash.

Fig. 11 depicts flexural strength variations in concrete at 28 days as fly ash content increases from 10% to 30% while maintaining a constant 10% silica fume content. Although fly ash offers economic advantages over silica fume, it reduces the flexural resistance capacity of concrete. The 30% fly ash mixture achieved a flexural strength of 13.90 MPa, representing a 24.37% reduction compared to the 10% SF + 20% FA combination.

Comparative analysis reveals silica fume's superior effectiveness in enhancing mixture flexural strength performance. At 28 days, concrete strength improvements of 3.98%, 9.87%, 17.71%, 9.75%, and 29.67% are attributed to the pozzolanic activity of fly ash and its interactions with $SiO_2$, $Al_2O_3$, and calcium hydroxide, which collectively promote calcium silicate hydrate formation while reducing porosity and increasing density (Malheiro et al. 2020), in addition to improving particle packing. The incorporation of fly ash into the cement paste also provides micro-void filling capability, resulting in increased paste density and subsequent strength development.

### *5.3.3. Effect of the nano-silica content*

Nano-silica contents of 1%, 2%, 3%, 4%, and 5% were incorporated into mixes containing 10% SF and 20% FA to evaluate their effect on the flexural strength of RPC. Fig. 13 shows that 1% NS resulted in a 65% increase, 2% NS in a 77% increase, 3% NS in a 109% increase, 4% NS in an 86% increase, and 5% NS in a 77% increase in 28-day flexural strength compared with the control. The highest flexural strength, 24.35 MPa, was achieved with 3% NS, owing to nano-silica filling pores and promoting the formation of additional C-S-H gels (Keshavarzian et al. 2021).

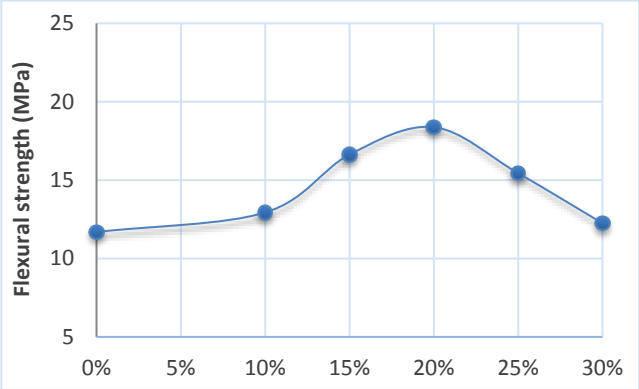


**Fig. 11.** Flexural strength of RPC using 10% silica fume with different ratios of fly ash.

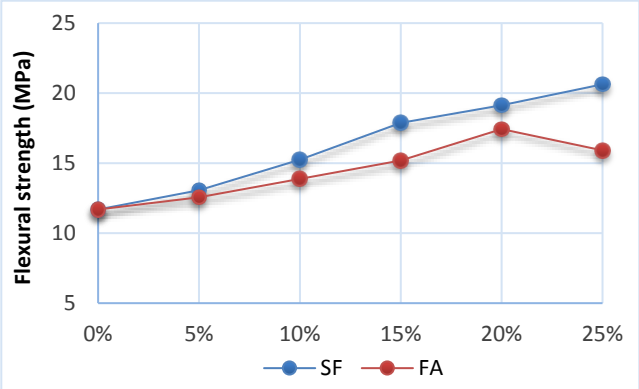


**Fig. 12.** Comparison between SF & FA at the same content at 28 days.

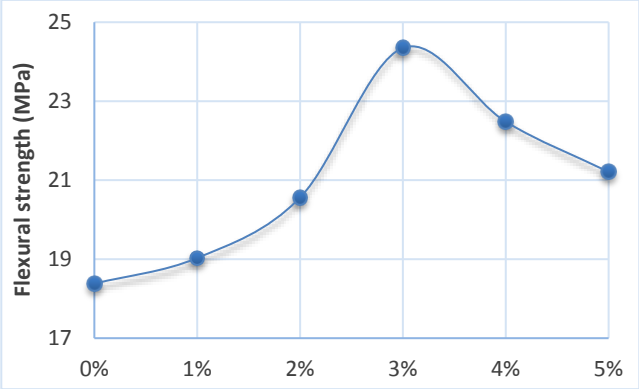


**Fig. 13.** Flexural strength of RPC using 10% SF + 20% FA with different ratios of nano-silica.

### *5.4. Splitting tensile strength of RPC*

#### *5.4.1. Effect of the silica fume content*

Fig. 14 presents the splitting tensile strength of RPC mixes containing 5% to 25% silica fume at 28 days. With 25% silica fume, tensile strength increased by 17.75% to 48% compared to the control mix M00, indicating that 25% silica fume provided the best performance. This improvement is attributed to the extremely fine silica fume particles, which enhanced hydration and densification of the RPC matrix, thereby increasing strength.

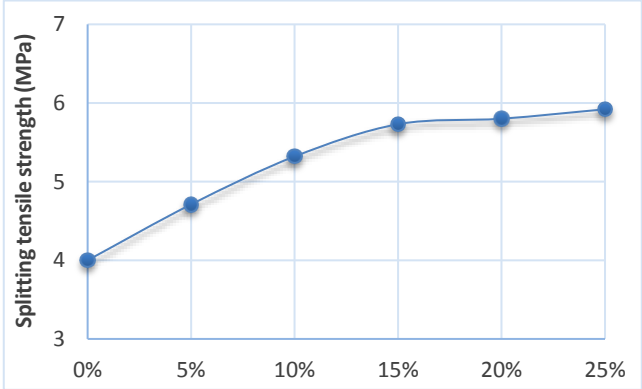


**Fig. 14.** Splitting Tensile strength of RPC using different ratios of silica fume.

#### *5.4.2. Effect of the fly ash content*

Fig. 15 shows the calculated splitting tensile strength of RPC mixes containing fly ash at 28 days, with fly ash content ranging from 5% to 30%. Compared to the control mix M00, tensile strength increased by 5%, 13%, 33.75%, 37%, 27.25%, and 13% for these respective replacement levels. The optimal performance was observed at around 20% fly ash content, where its pozzolanic activity—through reactions of $SiO_2$ and $Al_2O_3$ with calcium hydroxide (CH) to form C-S-H—produced a dense and less porous matrix, improving strength (Keshavarzian et al. 2021), alongside enhanced particle packing capacity.

Incorporating fly ash into the cement paste allowed void filling within the matrix, which increased density and consequently improved strength. However, when the fly ash content was increased from 10% to 30% while maintaining 10% silica fume, the 28-day splitting tensile strength remained nearly unchanged (Fig. 16). The strength was 4.52 MPa for the mix containing 30% fly ash, which was lower than that of the 10% SF + 20% FA combination.

When compared to fly ash, silica fume demonstrated a much greater improvement in splitting tensile strength, with increases of 12.14%, 17.70%, 7.10%, 5.84%, and 16.31% at 28 days (Fig. 17).

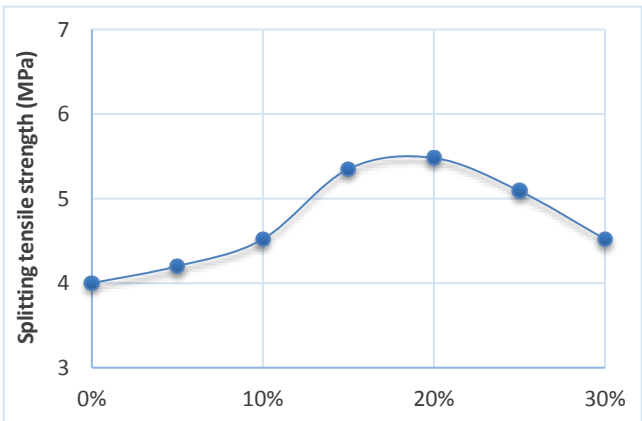


**Fig. 15.** Splitting tensile strength of RPC using different ratios of fly ash.

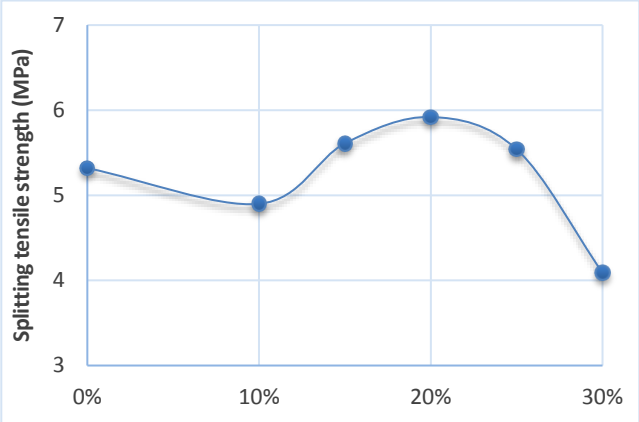


**Fig. 16.** Splitting tensile strength of RPC using 10% silica fume with different ratios of fly ash.

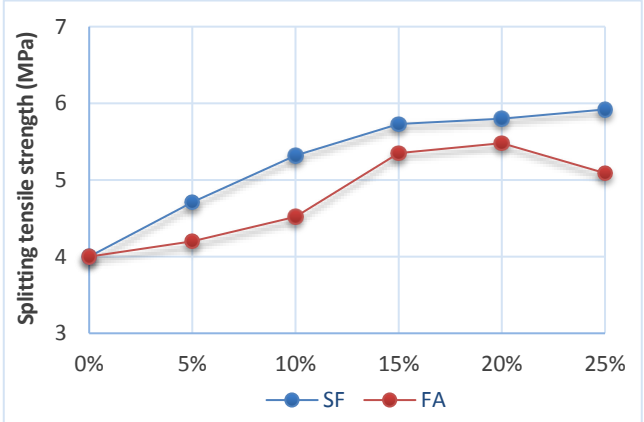


**Fig. 17.** Comparison between SF & FA at the same content at 28 days.

*5.4.3. Effect of the nano-silica content*

With 10% SF + 20% FA, compared to the control mixture, 1% NS resulted in a 76.50% increase in splitting tensile strength, 2% NS in a 122.25% increase, 3% NS in a 212% increase, 4% NS in a 155.75% increase, and 5% NS in a 127.25% increase after 28 days (Fig. 18). The mix containing 3% nano-silica achieved the highest splitting tensile strength, which was 24.35 MPa. This improvement is attributed to nano-silica filling pores and promoting the formation of additional C-S-H gels (Keshavarzian et al. 2021).

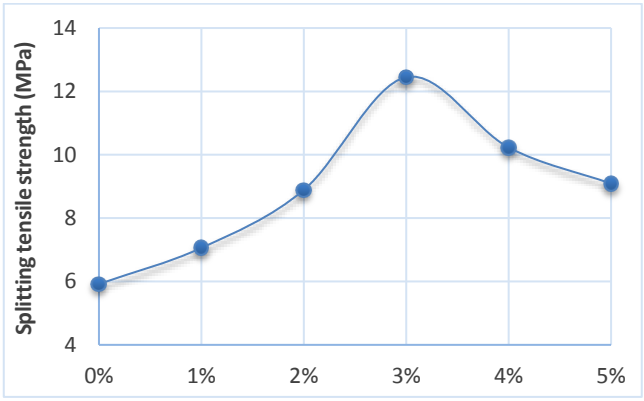


**Fig. 18.** Splitting tensile strength of RPC using 10% SF + 20% FA with different ratios of nano-silica.

### *5.5. Density of RPC*

The density values shown in Fig. 19 indicate that RPC mixes containing only silica fume had densities between 2344 and 2401 kg/m$^3$, those containing only fly ash had densities between 2375 and 2450 kg/m$^3$, mixes with silica fume + fly ash had densities between 2436 and 2495 kg/m$^3$, and those with silica fume + fly ash + nano-silica g had densities between 2533 and 2600 kg/m$^3$.

When pozzolanic materials are added, they increase density because their reaction with calcium hydroxide seals small air pockets and microcracks. Due to its extremely fine and smooth particles, RPC containing nano-silica exhibits higher density than the other mixtures, according to the results.

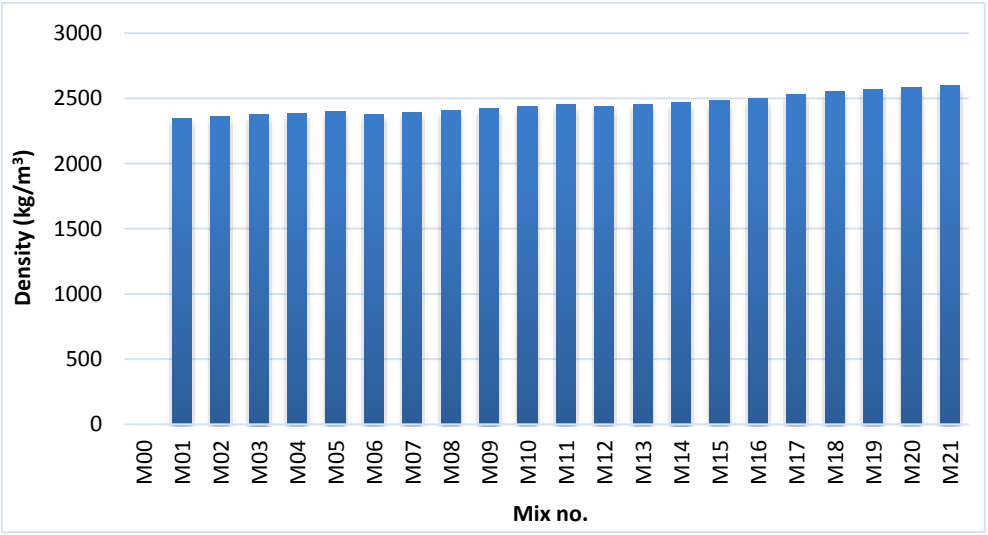


**Fig. 19.** Density of RPC.

## 6. Conclusions

Based on the research findings and analyses presented in this investigation, the following conclusions are drawn:

- Increased concentrations of silica fume, fly ash, and nano-silica reduced RPC workability, with fly ash demonstrating superior workability performance, followed by silica fume and then binary combinations.
- Nano-silica incorporation alongside fly ash and silica fume enhanced mixture density characteristics.
- Increased fineness of cementitious materials correlates with reduced workability while producing denser materials and final products.
- Increasing silica fume content within the binder system from 5% to 25% improved RPC performance in compressive, splitting tensile, and flexural strength evaluations.
- Progressive increases in fly ash content from 5% to 20% within the binder enhanced RPC compressive, tensile, and flexural strength properties. Further increases from 20% to 25% or 30% resulted in marginal reductions in compressive, splitting tensile, and flexural strength. Experimental evidence indicates an optimal fly ash content of approximately 20%.
- Fly ash substitution for silica fume in RPC provides economic benefits but compromises compressive strength performance.
- A complete 30% binder replacement with fly ash alone achieved a compressive strength of 64.88 MPa at 28 days, significantly lower than the 10% SF + 20% FA combination (72.65 MPa).
- The maximum compressive strength of 103.13 MPa at 3% nano-silica replacement resulted from effective nanoparticle packing and reduced agglomeration phenomena.
- Nano-silica produces superior strength enhancement through calcium hydroxide reactions, accelerated cement hydration, and increased calcium silicate hydrate formation within the paste matrix. Continued pozzolanic reactions generate additional strength-contributing C-S-H, improving overall mixture performance.
- Regional material sources can be employed for RPC production.
- Alternative curing methodologies, such as steam curing, are feasible.
- Hybrid fiber combinations utilizing polypropylene and steel fibers can further enhance mechanical property development.

***Acknowledgements***

*None declared.*

***Funding***

*The authors received no financial support for the research, authorship, and/or publication of this manuscript.*

***Conflict of Interest***

*The authors declared no potential conflicts of interest with respect to the research, authorship, and/or publication of this manuscript.*

***Author Contributions***

*All of the authors made substantial contributions to conception and design, or acquisition of data, or analysis and interpretation of data; were involved in drafting the manuscript or revising it critically for important intellectual content; and gave final approval of the version to be published.*

***Data Availability***

*The datasets created and/or analyzed during the current study are not publicly available, but are available from the corresponding author upon reasonable request.*

## REFERENCES

Aïtcin PC (2000). Cements of yesterday and today. *Cement and Concrete Research*, 30(9), 1349-1359.

Aïtcin PC (2016). Supplementary cementitious materials and blended cements. In: Aïtcin PC, Flatt RJ, editors. *Science and Technology of Concrete Admixtures*. Elsevier, Amsterdam, Netherlands, 53-73.

Albakry BA, Abbas ZK (2025). Evaluation of reactive powder concrete strength using various curing methods. *Engineering, Technology & Applied Science Research*, 15(2), 21685-21690.

ASTM C1017 / C1017M – 13 (2013). Standard specification for chemical admixtures for use in producing flowing concrete. ASTM International, West Conshohocken, PA, USA.

ASTM C109 / C109M – 20b (2020). Standard test method for compressive strength of hydraulic cement mortars (using 2-in. or [50-mm] cube specimens). ASTM International, West Conshohocken, PA, USA.

ASTM C348 – 21 (2021). Standard test method for flexural strength of hydraulic-cement mortars. ASTM International, West Conshohocken, PA, USA.

ASTM C496 / C496M – 17 (2017). Standard test method for splitting tensile strength of cylindrical concrete specimens. ASTM International, West Conshohocken, PA, USA.

ASTM C618 – 19 (2019). Standard specification for coal fly ash and raw or calcined natural pozzolan for use in concrete. ASTM International, West Conshohocken, PA, USA.

ASTM C642 – 13 (2013). Standard test method for density, absorption, and voids in hardened concrete. ASTM International, West Conshohocken, PA, USA.

ASTM C1116 / C1116M – 10a (2010). Standard specification for fiber-reinforced concrete. ASTM International, West Conshohocken, PA, USA.

ASTM C1339 / C1339M – 08 (2008). Standard specification for thin bonded overlays for bridge decks using hydraulic cement concrete. ASTM International, West Conshohocken, PA, USA.

Bahmani H, Mostofinejad D (2022). Microstructure of ultra-high-performance concrete (UHPC) – A review study. *Journal of Building Engineering*, 50, 104118.

Balapour M, Joshaghani A, Althoey F (2018). Nano-$SiO_2$ contribution to mechanical, durability, fresh and microstructural characteristics of concrete: A review. *Construction and Building Materials*, 181, 27-41.

Chandra S, Berntsson L (1996). Use of silica fume in concrete. In: Chandra S, Berntsson L, editors. *Waste Materials Used in Concrete Manufacturing*. Elsevier, Amsterdam, Netherlands, 554-623.

Danha LS, Khalil WI, Al-Hassani HM (2013). Mechanical properties of reactive powder concrete (RPC) with various steel fiber and silica fume contents. *Engineering and Technology Journal*, 31(16), 3090–3108.

E.S.S. 1109 (2008). Aggregates for concrete. Egyptian Organization for Standardization and Quality (EOS), Cairo, Egypt.

E.S.S. 4756-1 (2013). Plain and reinforced concrete – Part 1: Specifications, performance, production and conformity. Egyptian Organization for Standardization and Quality (EOS), Cairo, Egypt.

E.S.S. 5129-1 (2006). Products and systems for the protection and repair of concrete structures – Definitions, requirements, quality control and evaluation of conformity – Part 1: Definitions. Egyptian Organization for Standardization and Quality (EOS), Cairo, Egypt.

Ge W, Wang A, Zhang Z, Ge Y, Chen Y, Li W, Jiang H, Shuai H, Sun C, Yao S, Qiu L (2023). Study on the workability, mechanical property and water absorption of reactive powder concrete. *Case Studies in Construction Materials*, 18, e01777.

Golewski GL (2018). An assessment of microcracks in the interfacial transition zone of durable concrete composites with fly ash additives. *Composite Structures*, 200, 515-520.

Hefni Y, Zaher YA El, Wahab MA (2018). Influence of activation of fly ash on the mechanical properties of concrete. *Construction and Building Materials*, 172, 728-734.

Ju Y, Tian K, Liu H, Reinhardt HW, Wang L (2017). Experimental investigation of the effect of silica fume on the thermal spalling of reactive powder concrete. *Construction and Building Materials*, 155, 571-583.

Keshavarzian F, Saberian M, Li J (2021). Investigation on mechanical properties of steel fiber reinforced reactive powder concrete containing nano-$SiO_2$: An experimental and analytical study. *Journal of Building Engineering*, 44, 102601.

Kong D, Du X, Wei S, Zhang H, Yang Y, Shah SP (2012). Influence of nano-silica agglomeration on microstructure and properties of the hardened cement-based materials. *Construction and Building Materials*, 37, 707-715.

Kurdowski W (2014). Mineral additions for cement production. In: Kurdowski W, editor. *Cement and Concrete Chemistry*. Springer Netherlands, Dordrecht, Netherlands, 533-583.

Malheiro R, Camões A, Meira G, Pinto J (2020). Durability of fly ash ecofriendly cement mortars in severe environment. *Procedia Manufacturing*, 46, 122-130.

Moffatt EG, Thomas MDA, Fahim A (2017). Performance of high-volume fly ash concrete in marine environment. *Cement and Concrete Research*, 102, 127-135.

Neville AM (2005). Properties of Concrete (4th and final edition). Pearson Education Limited, Harlow, England.

Ranjan M, Kumar S, Sinha S (2024). Nanosilica's influence on concrete hydration, microstructure, and durability: A review. *Journal of Applied Engineering Sciences*, 14(2), 322-335.

Rashad AM (2014). A comprehensive overview about the effect of nano-$SiO_2$ on some properties of traditional cementitious materials and alkali-activated fly ash. *Construction and Building Materials*, 52, 437-464.

Richard P, Cheyrezy M (1995). Composition of reactive powder concretes. *Cement and Concrete Research*, 25(7), 1501-1511.

Rupasinghe M, Mendis P, Ngo T, Nguyen TN, Sofi M (2017). Compressive strength prediction of nano-silica incorporated cement systems based on a multiscale approach. *Materials & Design*, 115, 379-392.

Sadrekarimi A (2004). Development of a light weight reactive powder concrete. *Journal of Advanced Concrete Technology*, 2(3), 409-417.

Sarika S, Elson J (2015). A study on properties of reactive powder concrete. *International Journal of Engineering Research & Technology*, 4(11), 110-113.

Shen M, Zhou L, Chen Z, Shen Y, Huang B, Lv J (2022). Effects of basalt powder and silica fume on ultra-high-strength cementitious matrix: A comparative study. *Case Studies in Construction Materials*, 17, e01397.

Sultan HK, Zinkaah OH, Rasheed AA, Alridha Z, Alhawat M (2022). Producing sustainable modified reactive powder concrete using locally available materials. *Innovative Infrastructure Solutions*, 7(6), 342.

Tan H, Yuan P, Sun D, Fan X, Wang C, Liu J (2025). Ratio of water to cement and supplementary cementitious materials on mechanical and impact resistance properties of reactive powder concrete. *Scientific Reports*, 15(1), 7480.

Ullah R, Qiang Y, Ahmad J, Vatin NI, El-Shorbagy MA (2022). Ultra-high-performance concrete (UHPC): A state-of-the-art review. *Materials*, 15(12), 4131.

Wang BM (2011). Influence of nano-$SiO_2$ on the strength of high performance concrete. *Materials Science Forum*, 686, 432-437.

Yazıcı H, Yardımcı MY, Aydın S, Karabulut AŞ (2009). Mechanical properties of reactive powder concrete containing mineral admixtures under different curing regimes. *Construction and Building Materials*, 23(3), 1223-1231.

Yu R, Spiesz P, Brouwers HJH (2015). Development of an eco-friendly ultra-high performance concrete (UHPC) with efficient cement and mineral admixtures uses. *Cement and Concrete Composites*, 55, 383-394.

Zhang L, Ma N, Wang Y, Han B, Cui X, Yu X, Ou J (2016). Study on the reinforcing mechanisms of nano silica to cement-based materials with theoretical calculation and experimental evidence. *Journal of Composite Materials*, 50(29), 4135-4146.

Zhang Y, Wang J, Wang J, Qian X (2022). Preparation, mechanics and self-sensing performance of sprayed reactive powder concrete. *Scientific Reports*, 12(1), 7787.

Challenge Journal of Concrete Research Letters

Case Study

# Exploring deflection challenges: A case study on the influence of heavy concrete weight on profiled steel deck slabs

Sudhakaran Arumugam [a], Vijayaprabha Chakrawarthi [b,*], Manicka Mamallan Andavar [c]

[a] *Department of Mechanical Engineering, Indian Institute of Technology, 826004 Dhanbad, India*
[b] *Department of Civil Engineering, Alagappa Chettiar Government College of Engineering and Technology, 630003 Karaikudi, India*
[c] *Department of Civil Engineering, Ramco Institute of Technology, 626117 Rajapalayam, India*

## ABSTRACT

This paper presents a case study of a deflection challenge in a profiled steel deck slab subjected to heavy concrete loads, as observed during a field investigation. In recent decades, such slabs have gained popularity in both the construction and industrial sectors due to advantages such as being lightweight, cost-effective, quick to install, and capable of resisting natural disasters. However, field observations indicate that when these slabs are subjected to heavy concrete weight, they may experience significant deflection, raising concerns about long-term performance, durability, and serviceability. Excessive deflection can lead to cracking, reduced structural stability, and increased maintenance costs. It is therefore critical to understand the factors influencing deflection by examining key parameters such as material properties, slab geometry, reinforcement detailing, and load distribution characteristics. This study provides a comprehensive assessment of the structural response of such slabs. Field observations suggest that optimizing the L-angle section and C-channel section in areas where the concrete width increases can effectively reduce structural deflection. This approach helps structural elements resist excessive flexural behavior, and when combined with the use of lightweight materials, offers an innovative structural solution that highlights the importance of modern construction practices.

## ARTICLE INFO

**Article history:**
Received – March 5, 2025
Revision requested – April 10, 2025
Revision received – April 15, 2025
Accepted – April 28, 2025

**Keywords:**
Profiled sheet deck slab
Heavy concrete
Deflection challenges
Structural stability



**Citation:** Arumugam S, Chakrawarthi V, Andavar MM (2025). Exploring deflection challenges: A case study on the influence of heavy concrete weight on profiled steel deck slabs. *Challenge Journal of Concrete Research Letters*, 16(3), 155–163.

## 1. Introduction

In recent decades, steel–concrete composite slabs have become increasingly popular in the construction sector due to the combined advantages of two effective building materials. These composite slabs consist of a profiled steel deck topped with reinforced structural concrete. The decking serves as permanent formwork for the concrete and provides adequate shear bonding while functioning as a composite component. The main advantages of using such slabs include being lightweight, cost-effective, fast to construct, and offering good ductility and seismic performance (Hu and Wang 2017; Wan and Yu 2022; Xiong et al. 2022; Liu et al. 2017; Deng et al. 2022).

Once the concrete has cured and the components of the structural system act together as a composite structural system, the steel deck serves as positive reinforcement. However, certain aspects of composite systems that attract structural experts—particularly reinforcement moments and the formwork required for casting concrete—are often overlooked or significantly minimized during the construction phase. The use of steel deck concrete floors dates back to 1950, when concrete was used as a filling agent over steel decks (Porter and Ekberg 1976).

To ensure composite action, a shear connection is necessary to link the concrete slab with the steel section. Traditionally, this connection is achieved by welding

* *Corresponding author*. E-mail address: vijayaprabhac@accet.ac.in (V. Chakrawarthi)
ISSN: 2548-0928 / DOI: https://doi.org/10.20528/cjcrl.2025.03.005

steel studs to the steel parts (Shin 2015; Wang and Yu 2017). However, when a composite slab is demolished at the end of its service life, welded shear connections make it difficult to separate the concrete slab from the steel section (Lam et al. 2013).

From a sustainability perspective, traditional construction methods that generate significant waste are becoming less acceptable. Construction and demolition (C&D) waste constitutes one of the largest waste streams globally, accounting for 30% to 40% of total waste (Nair 2024). In India, C&D waste was estimated at 24 million tonnes in 2010 (Shrivastava and Chini 2009), with other estimates suggesting between 11.1 and 14.69 million tonnes generated annually (Raja et al. 2012). Such practices are unsustainable because they not only harm the environment but also affect future generations.

To address this, Lam et al. (2021) proposed an innovative approach involving the use of composite slabs with demountable shear connectors. This design replaces welded connections with bolted ones, allowing the slab to be dismantled at the end of its service life. These connectors function similarly to prefabricated composite structures, improving upon traditional methods for composite element construction (Li et al. 2023).

A critical aspect of composite profiled steel slabs is the bonding behavior between the concrete and steel (Zhu et al. 2012). Studying bonding performance is challenging due to slip behavior at the steel–concrete interface (Shahezad 2014; Patil and Shahezad 2014). The design of the deck slab is also important, as there are three main failure modes: longitudinal shear, vertical shear, and flexural failure (Patrick and Bridge 1993). The strength of a composite slab primarily depends on the connection between the steel sheet and concrete, which governs the longitudinal shear strength. This failure mode determines the ultimate load-bearing capacity of the structure (Siva et al. 2016) and can occur when mechanical connections cannot transfer shear forces until bending failure takes place.

To investigate these shear behavior characteristics, Xian-tie (2011) conducted experimental studies on factors such as slab thickness, sheet thickness, and shear span. The results showed that increasing slab and sheet thickness enhances longitudinal shear capacity, while increasing span length reduces it. Vertical shear failures, on the other hand, occur with shorter spans and increased height under the same loads, particularly near the support region (Kataoka et al. 2017). The shear resistance of composite profiled sheet decking depends largely on the shape of the profile, its height, and the wavelength of the sheeting. Behr et al. (1989) analyzed how various composite structural forms are affected by shear-bearing capacity through both theoretical analysis and experimental testing. Flexural failure is typically associated with excessive deflection, with a peak deflection corresponding to a fraction of the span length.

Other parameters influencing load-bearing capacity and stiffness include slab thickness, sheet thickness, polyurethane foam density, and span length (Qiao et al. 2024). Based on field research, this case study investigates how deflection behavior caused by high-strength concrete in a profiled steel sheet composite slab affects the structural integrity and overall performance.

### *1.1. Research background*

The application of heavy concrete layers impacts the deflection behavior of profiled steel deck slabs, potentially leading to long-term serviceability issues. Excessive deflection can cause cracking, aesthetic concerns, and durability problems (Sun et al. 2024; Porter and Ekberg 1990).

This study investigates deflection challenges in profiled steel deck slabs subjected to heavy concrete loads, focusing on a real-world construction site in Tamil Nadu, India. The selected steel decking system has a span length of 22.87 m, with an external width of 10.61 m on one side and 9.51 m on the other, and a concrete thickness of 127 mm. Fig. 1 illustrates the profile of the steel deck slab at the swimming pool site.

Field visits and virtual observations from real-time construction sites provided an in-depth understanding of how heavy concrete weight influences structural integrity and performance. By analyzing these findings, this case study aims to optimize steel deck slab design and material selection, minimize serviceability failures, and propose effective reinforcement strategies for practical application in the construction sector.

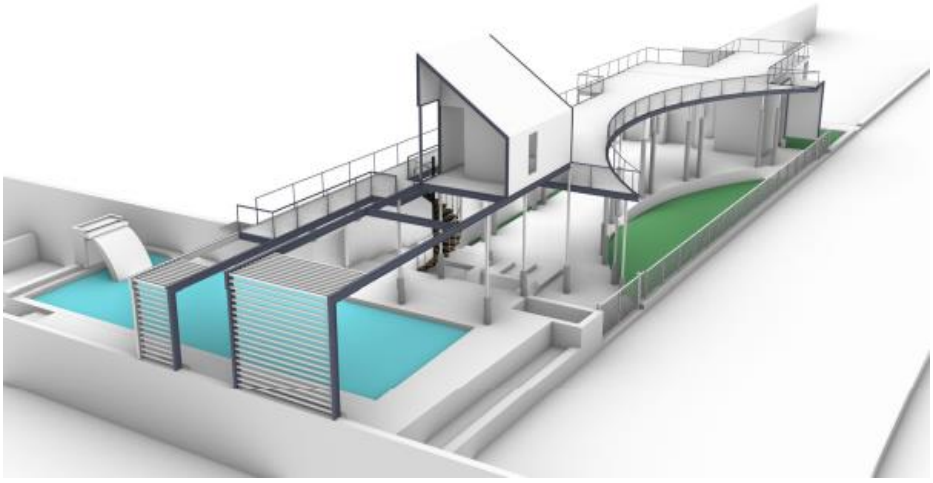

**Fig. 1.** 3D rendered model of the swimming pool site.

### *1.2. Research significance*

- To understand how heavy concrete weight affects the deflection behavior of steel deck slabs.
- To identify deflection issues that arise from excessive concrete loads.
- To explore potential material alternatives or reinforcement methods that minimize excessive deflection while maintaining structural integrity.

## 2. Literature Study

As an advanced technology in the construction industry, profiled steel deck slabs are widely used as structural members (Hedaoo and Gupta 2008). The use of slab sheeting helps reduce the quantity of reinforcement steel bars in composite construction systems. Once the concrete has hardened, the steel deck acts as tensile reinforcement for the structure. This type of composite deck slab flooring system is widely used in buildings across the USA and Canada (Schuster 1976).

According to the research board of the Steel Deck Institute (SDI), a standardized procedure exists for composite slab research and testing, providing design criteria based on reinforced cement concrete (RCC) methodologies (Heagler 1993). Based on this study, design recommendations were drafted for long-span composite slabs with deep profiled steel decks, having a depth of at least 200 mm (Brekelmans et al. 1997).

Kubic and Daniels (1979) developed an elastically orthotropic finite element model (FEM) to simulate the behavior of orthotropic steel deck reinforced concrete slabs with uniform thickness. Previous research data effectively predicted the behavior of almost all the models. The research examined a single panel of a typical slab under simply supported and fixed boundary conditions, comparing deflections and bending moments for two-way flexural action versus one-way bending behavior. Additionally, an expression for the optimal aspect ratio of steel-deck-reinforced concrete slabs was proposed. The findings highlight the feasibility of incorporating two-way action in the design process, thereby enhancing structural efficiency.

Nie et al. (2008) examined 13 steel–concrete composite beams, both simply supported and continuous, tested under positive and negative bending. The results indicated that slip at the steel–concrete interface increased deflection by 45% to 90% at 50% of the ultimate load compared to full shear connections. Predictions from Eurocode 4 (EN 1994-1-1 (2004)) and AISC (1999) generally aligned with experimental findings, confirming the feasibility of partial shear connections for achieving structural efficiency while reducing costs and simplifying construction.

Cold-formed sheet behavior in composite deck slabs has also been evaluated using bolted shear connectors. Various profiles were tested for load capacity, deflection, slip, strain energy, and failure modes (Fig. 2). Results show that dovetailed profiles exhibited superior load resistance—5.35% and 22.03% higher than rectangular and trapezoidal profiles, respectively—with lower deflection and slip. Trapezoidal slabs stored the highest strain energy (2.98 kNm) but predominantly failed in shear bond mode. Ductility ratios increased with the rib-to-flange opening width ratio, with trapezoidal profiles showing 36.3% and 55% higher ductility than rectangular and dovetailed slabs, respectively.


**Fig. 2.** Delamination and end slip in profiled sheet deck slab (Avudaiappan et al. 2021).

He et al. (2019) investigated the structural performance of 26 composite slab specimens with trapezoidal and dovetail profiles, examining the effects of span, end anchorage, and cross-sectional depth. The results indicated that end anchorage significantly enhances load-bearing capacity, although its influence diminishes with increasing span length. Longitudinal shear failure was prevalent in slabs without end anchorage, while slabs with anchorage exhibited either ductile shear or flexural failure. Increasing the thickness of profiled steel sheets and adding reinforcement at the troughs improved bearing capacity and slip resistance, although gains in rigidity were minimal. Overall, dovetail-profiled slabs outperformed trapezoidal ones in long-span flooring systems, offering superior structural efficiency (Gholamhoseini et al. 2014).

The literature review highlights that limited experimental research has been conducted on the time-dependent, in-service behavior of concrete composite slab sections. While advancements in permanent formwork techniques have been made, there is little guidance on calculating long-term deflection. Additionally, Gilbert et al. (2012) determined that the presence of a steel deck slab slightly influences the drying shrinkage profile across the thickness of the composite slab, thereby affecting its overall long-term performance.

## 3. Effects of Heavy Concrete Weight on Structural Deflection

With an emphasis on mid-span serviceability, Jaffar et al. (2015) examined the impact of geopolymer concrete infill on the Profile Steel Sheeting Dry Board (PSSDB) system with the half board (PSSHB). Due to its higher compressive strength, geopolymer concrete was selected, and an OPC-free composition was used in a modified PSSHDB panel. Experimental results demonstrated that the geopolymer infill improved the stiffness and performance of the system, reducing mid-span deflection by 41%.

In profiled sheet slabs, the use of heavier concrete, which increases deflection, has led to a stronger focus on serviceability considerations in design, particularly when using higher-strength concrete and shallower sections, as studied by Lamport and Porter (1990). In current composite concrete slab construction, thin-walled, cold-formed profiled steel decking plays a critical role, and significant research has been conducted using analytical, numerical, and experimental methods.

Many design codes, such as IS 801 (1975), Eurocode 3 (EN 1993-1-1, 2001), BS 5950-1 (1995), AS/NZS 4600 (2005), and AISI (2007), address various aspects of steel deck design, including limitations related to bending moment, web crippling, and distortional buckling. Indian Standard IS 801-1975 specifies the design of steel decks, whereas Eurocode 3 (EN 1993-1-1, 2001) and AS/NZS 4600 (2005) present improved techniques such as the Direct Strength Method (DSM) for cross-section capacity prediction. The AISI (2007) specification refines calculations for distortional buckling, combined bending, and torsional stress by integrating Allowable Stress Design (ASD), Load and Resistance Factor Design (LRFD), and Limit State Design (LSD) methods. BS 5950-1 (1995) emphasizes balancing safety and material efficiency while also incorporating factors such as local buckling, torsional-flexural buckling, and material non-linearity in a structured manner.

Studies by Hedaoo and Gupta (2008) indicate the need for further investigation into bending moments, internal responses, and embossment effects, with finite element methods showing strong potential for addressing these research areas.

## 4. Improving Load–Slip Behavior and Strengthening Composite Slabs

Shahezad (2014) investigated the shear bond behavior of lightweight aggregate concrete composite slabs commonly used with profiled steel sheets to improve performance. The research indicates that various types of concrete and strengthening techniques can enhance the load–slip behavior of composite construction. Additionally, the use of stainless-steel decks has been shown to offer higher strength and corrosion resistance, making them a valuable alternative for long-term durability.

In one study, three types of profiled steel sheet composite concrete slabs (PSSCCS)—with studs, with minimum reinforcement, and without reinforcement—were tested under static loading. The results indicated that slabs with reinforcement and studs exhibited two to three times higher load-carrying capacity than non-reinforced slabs. Failure modes, including shear bond failure, bending failure, and end-slip, were analyzed, revealing that shear studs enhance composite action by preventing debonding. Load–deflection curves demonstrated increased linearity in stud-reinforced slabs prior to shear bond failure. Analytical models aligned well with experimental findings, accurately predicting structural behavior. Increasing the thickness of steel sheets further enhanced slab strength, making PSSCCSs a viable solution for high-rise buildings (Islam et al. 2020).

Controlling slippage in composite deck slabs is crucial, as it directly impacts central deflection and overall structural stability (Vohra and Dhankot 2015). To address failure mechanisms, one study introduced a reinforced concrete infill strengthening method, effectively delaying premature failure modes. Furthermore, Bavan and Baharom (2014) proposed a novel approach for predicting short-term deflections in composite cold-formed steel decks, demonstrating significant improvements over conventional methods and ensuring better performance and serviceability.

## 5. Methodology

The procedure for this case study, following a structural approach, is illustrated in Fig. 3 as a flowchart diagram.

## 6. Profiled Steel Deck Specifications

A composite structural system consists of a profiled galvanized iron (GI) decking sheet, reinforced concrete, structural steel elements, and shear connectors to achieve effective composite action. Fig. 4 shows a section view of the concrete slab, designed using M30-grade concrete (Table 1), which provides compression resistance and structural integrity. Reinforcement is provided by 8 mm diameter bars positioned to resist tensile stresses.

The structural steel framework includes primary and secondary I-beams that support the composite slab. Figs. 5 and 6 illustrate the main I-beams (8″×4″) acting as the primary load-bearing members, distributing loads to the supporting columns, while the secondary I-beams (4″×2″) transfer loads from the slab to the main beams, minimizing deflection. Additional structural support is provided by C-channel sections (3″×1.5″), which enhance lateral stability, and L-angles (1″×1″), which reinforce slab edges and connection points.

To ensure proper composite behavior, shear connectors—typically in the form of shear studs—are installed at the steel–concrete interface to prevent slip and enhance load transfer efficiency.

Key observations include flexural failure due to bending, shear bond failure at the interface, and brittle failure in extreme cases. The inclusion of shear connectors significantly improves load-carrying capacity by minimizing slip and increasing ductility, while reinforcement enhances flexural resistance.

The advantages of this system include:

- Structural efficiency by eliminating the need for temporary formwork.
- Enhanced strength through composite action.
- Cost-effectiveness by reducing material consumption.
- Improved durability due to the steel–concrete interface.

These benefits make profiled steel deck composite slabs ideal for high-rise buildings, industrial structures, and bridges where strength, speed, and economic feasibility are critical design considerations.

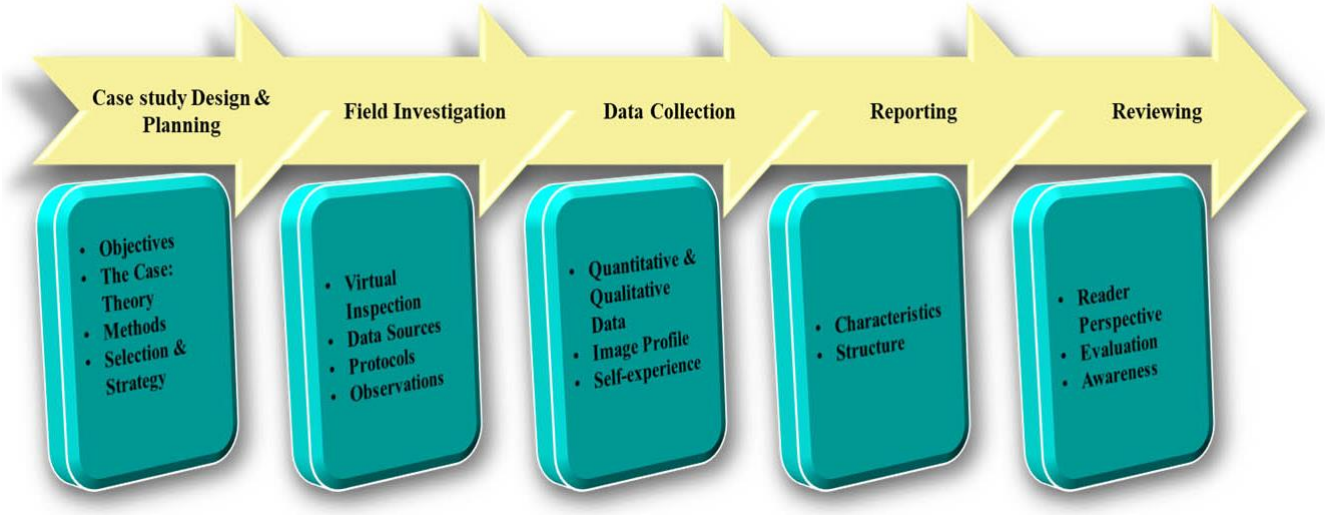


**Fig. 3.** Stepwise approach to case study investigation.

**Table 1.** Concrete mix properties.

| Property | Specification | Remarks |
|---|---|---|
| Grade of concrete | M30 (30 MPa or 300 kg/cm$^2$) | Based on the characteristic compressive strength at 28 days |
| Nominal mix ratio | Design mix as per IS 10262 (2019) | Mix proportion determined by lab trials |
| Cement content | 350–450 kg/m$^3$ | Min. 300 kg/m$^3$ as per IS 456 (2000) |
| Water-cement ratio | 0.40–0.45 | Adjusted based on workability and exposure conditions |
| Fine aggregate (sand) | 600–800 kg/m$^3$ | Well-graded sand (zone II or III as per IS 383 (2016)) |
| Coarse aggregate (20 mm) | 1200-1350 kg/m$^3$ | Crushed angular aggregates preferred |
| Water content | 150–180 litres/m$^3$ | Based on workability requirements |
| Admixtures (if used) | Superplasticizer (0.5–1% by cement weight) | Improves workability and reduces water demand |
| Slump value | 75–125 mm | Depends on placement method (pumped/hand-placed) |
| Compressive strength | 30 MPa (at 28 days) | Achieved under standard curing conditions |
| Curing period | Min. 7 days (with curing compounds)<br>Min. 14 days (for normal curing) | Longer curing enhances durability as per IS 456 (2000) |

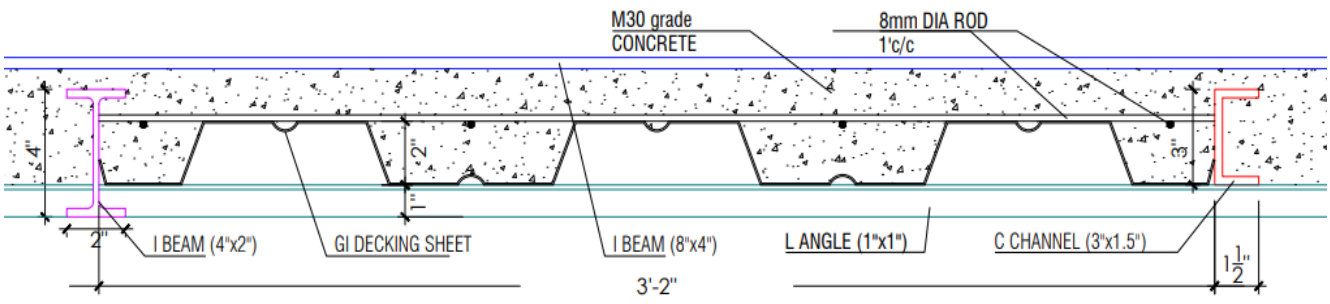


**Fig. 4.** Sectional view of profile sheet.

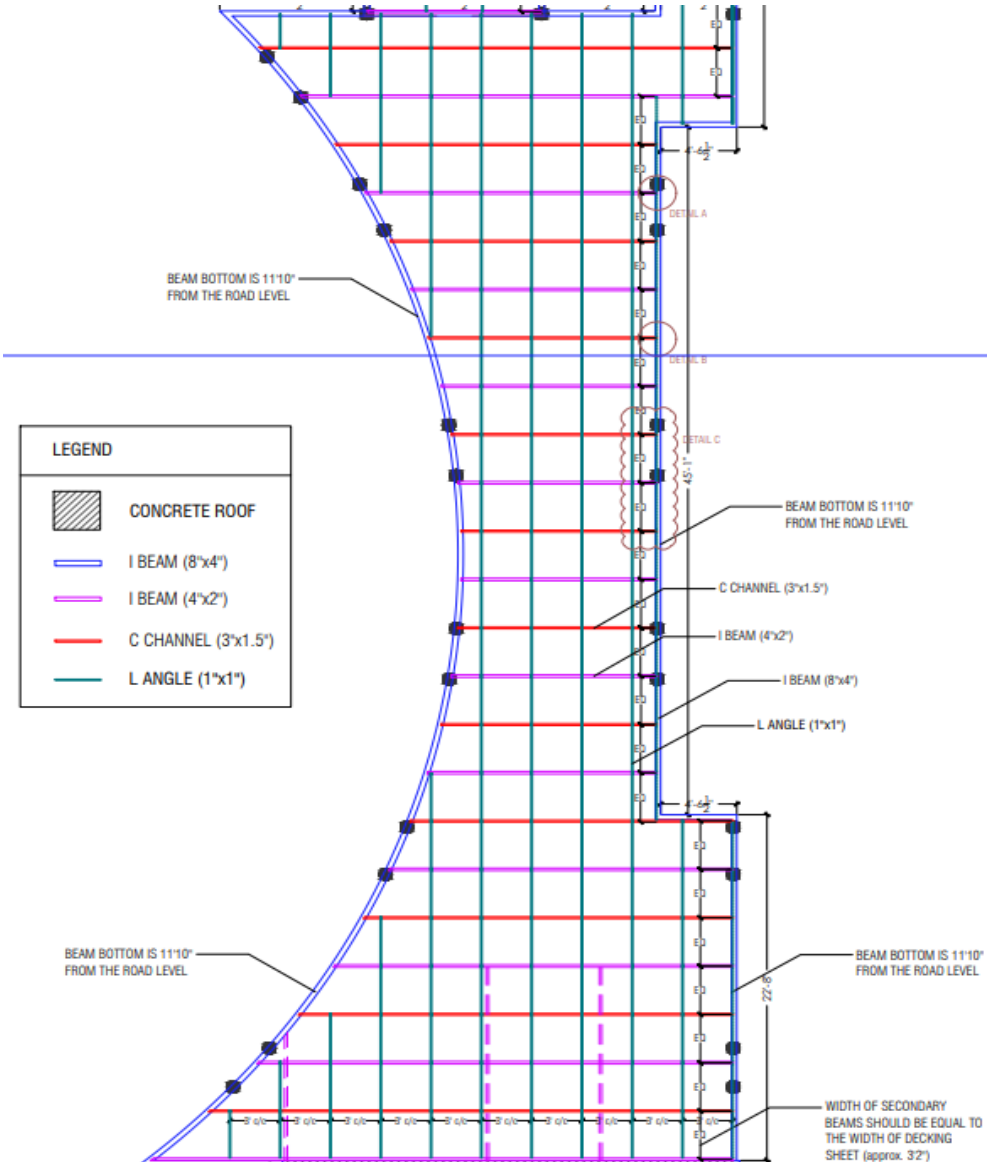


**Fig. 5.** Plan view of details of the deck slab.

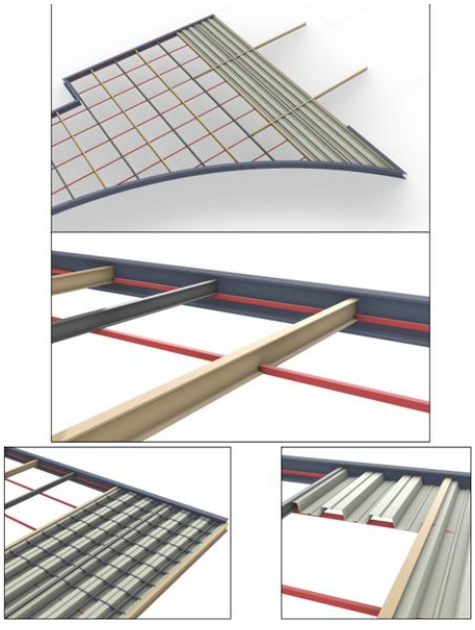

**Fig. 6.** 3D view of deck slab detailing.

### *6.1. Proposed design criteria*

Moments of inertia for rectangular section;

$$I = \frac{bd^3}{12} \tag{1}$$

Maximum deflection;

$$\delta_{im} = \frac{5wl^4}{384EI} \tag{2}$$

Long-term deflection;

$$\delta_{tt} = \lambda\delta_{im} \tag{3}$$

where:

- $\lambda$ is the creep coefficient, which depends on the concrete age and loading duration.
- Typical values for creep coefficient ($\lambda$);
  Short-term (1 month) : $\lambda$=1.2–1.5
  Medium-term (6 months to 1 year) : $\lambda$=2.0–2.5
  Long-term (5+ years) : $\lambda$=2.5–3.0

## 7. Cause of Structural Issues

Based on on-site observations and structural virtualization, it is evident that the composite deck slab experienced significant deflection due to its inability to adequately withstand the applied concrete loads, as shown in Fig. 7. This issue was particularly pronounced in areas with larger span widths, where increased bending stresses were observed. The slab is supported by a combination of structural members, with longitudinal and transverse supports intended to distribute loads effectively. However, the observed excessive deflection suggests that the existing support configuration does not provide sufficient flexural rigidity, resulting in structural deformation beyond permissible limits.

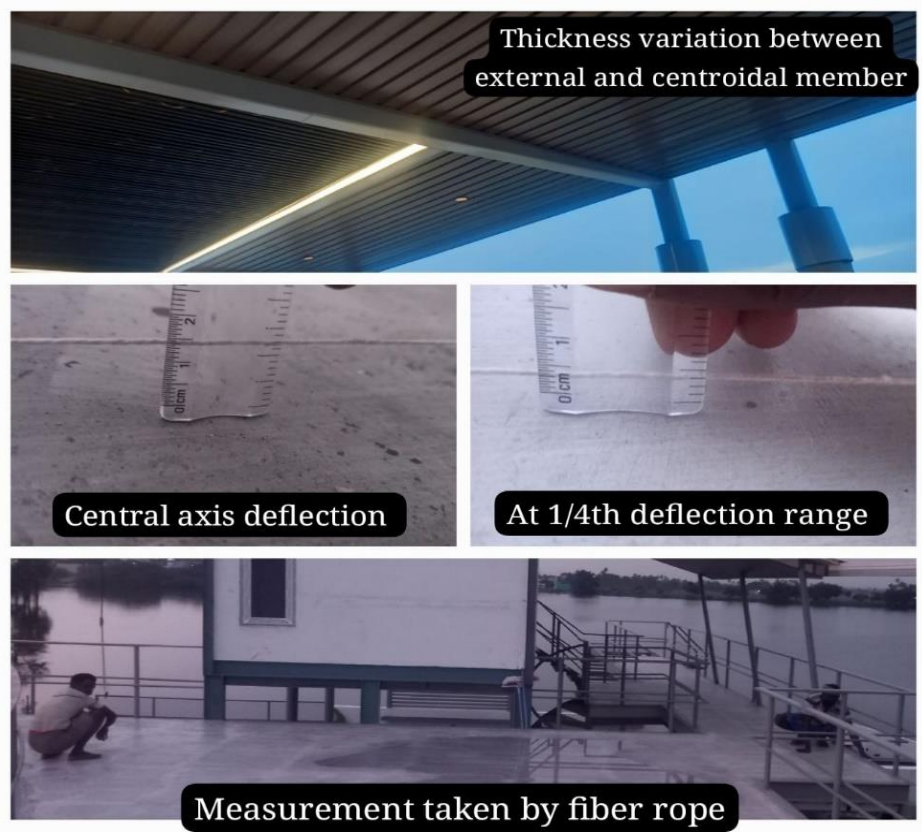


**Fig. 7.** Field deck slab deflection.

A critical factor contributing to this issue is the non-uniform load distribution caused by variations in slab thickness between external and central regions. This imbalance likely induced differential bending stresses, leading to localized weaknesses in the slab. The deflection was further exacerbated after the placement of terrace tiles, which involved layering waste aggregate, moisture conditioning for compaction, and applying mortar with a low water–cement ratio. The additional weight from this process intensified bending deformations, particularly above the galvanized iron (GI) decking sheets. Once the deflection became visibly apparent, corrective measures were immediately implemented by removing the waste aggregate layer, which helped reduce bending to some extent. However, residual structural deformations remain, indicating the need for further assessment and reinforcement.

Several technical deficiencies likely contributed to this anomaly. An inadequate structural system and improper or excessive reinforcement may have reduced the slab's flexural rigidity. In addition, the composite action between the concrete and steel deck is a critical factor in such systems. Any insufficiencies in shear connection can cause inadequate interlocking or reduced bonding between materials, resulting in ineffective load transfer and increased deflection. Furthermore, material-related issues such as improper mix proportioning, inadequate curing conditions, or uneven reinforcement placement may have weakened the slab's performance under service loads.

Long-term environmental factors have also influenced the structure's performance. Over time, deflection may have been gradually induced by thermal expansion, shrinkage, and differential settlement of supporting materials. On-site deflection measurements confirm departures from design tolerances, especially at the central axis and at one-fourth of the span length, highlighting the necessity for structural intervention.

A comprehensive structural assessment—including finite element analysis (FEA) simulations and in-situ load testing—is required to evaluate the slab's actual performance under service conditions. To restore serviceability and ensure compliance with safety regulations, strengthening techniques such as additional reinforcement, structural retrofitting using external post-tensioning, or polymer-based overlays should be considered.

## 8. Conclusions

This case study determined that inadequate structural components combined with the excessive weight of concrete were the primary causes of deflection in the profiled sheet deck slab. Excessive deflection compromises the serviceability of the structure and poses a risk to its long-term durability. Inefficient load transfer can result from several contributing factors, including variations in slab thickness, insufficient reinforcement detailing, and inadequate shear connections between the concrete and steel deck.

The flexural stiffness required to resist bending forces—particularly over larger spans—was found to be insufficient in the current support configuration. Site observations indicated that this problem was further aggravated by the additional weight of terrace tiles, moisture retention, and mechanical applications, which induced localized bending deformations. In response, corrective actions were taken by removing these additional materials, leaving the slabs finished only with concrete surfaces. This outcome reinforces the need for detailed structural evaluation and targeted reinforcement strategies.

To improve performance, it is recommended that structural components be enhanced through the use of L-angle and C-channel sections, which can increase flexural stiffness and reduce excessive bending, especially in areas with greater slab width. Verification of the slab's performance should be conducted through comprehensive finite element analysis (FEA) and in-situ load testing. Strengthening measures such as external post-tensioning and polymer-based overlays should also be considered to enhance stability, ensure compliance with safety standards, and extend the service life of composite deck slabs in modern construction.

**Suggestions:**

This study observed that the current design approach for such structures is relatively simple and lacks provisions for future adaptability or enhancement. Therefore, engineers should perform detailed structural analyses before initiating composite slab projects to ensure optimal performance. Alternative reinforcement strategies—such as double-layer steel mesh or Fiber-Reinforced Polymer (FRP) bars—should be explored to reduce the overall density of the slab. In parallel, research into lightweight aggregates as a substitute for natural aggregates could help lower concrete weight and improve long-term serviceability. Additionally, all structural details should be enriched and validated using structural design software to ensure consistency with intended performance requirements.

**Note:**

While clients may prioritize an architectural design that conveys luxury and aesthetics, structural engineering must ultimately prioritize safety, durability, and long-term stability.

***Acknowledgements***

*None declared.*

***Funding***

*The authors received no financial support for the research, authorship, and/or publication of this manuscript.*

***Conflict of Interest***

*The authors declared no potential conflicts of interest with respect to the research, authorship, and/or publication of this manuscript.*

***Author Contributions***

*All of the authors made substantial contributions to conception and design, or acquisition of data, or analysis and interpretation of data; were involved in drafting the manuscript or revising it critically for important intellectual content; and gave final approval of the version to be published.*

***Data Availability***

*The datasets created and/or analyzed during the current study are not publicly available, but are available from the corresponding author upon reasonable request.*

## REFERENCES

AISC (1999). Load and resistance factor design specification for structural steel buildings (LRFD). American Institute of Steel Construction (AISC), Chicago, IL, USA.

AISI (2007). North American specification for the design of cold-formed steel structural members (NAS). American Iron and Steel Institute, Washington, DC, USA.

AS/NZS 4600 (2005). Cold-formed steel structures. Standards Australia/Standards New Zealand, Sydney, Australia / Wellington, New Zealand.

Avudaiappan S, Saavedra Flores EI, Araya-Letelier G, Jonathan Thomas W, Raman SN, Murali G, Amran M, Karelina M, Fediuk R, Vatin N (2021). Experimental investigation on composite deck slab made of cold-formed profiled steel sheeting. *Metals*, 11(2), 229.

Bavan M, Baharom S (2014). Improvement of ultimate strength of continuous profiled steel sheet dry board (PSSDB) floor slab. *Proceedings of the International Conference on Civil and Architecture Engineering*, Cairo, Egypt.

Behr RA, Goodspeed CH, Yari N (1989). Shear connector design for composite flexural members. *Journal of Structural Engineering*, 115(2), 483-489.

Brekelmans JWPM, Daniels BJ, van Hove BWEM, Koukkari HH, Stark JWB, Schuurman RG (1997). Design recommendations for long-span composite slabs with deep profiled steel sheets. *Proceedings of the Engineering Foundation Conference on Composite Construction in Steel and Concrete III*, Irsee, Germany, ASCE, 660-671.

BS 5950-1 (1995). Structural use of steelwork in building – Part 1: Code of practice for design – Rolled and welded sections. British Standards Institution (BSI), London, UK.

Deng XF, Dong TF, Fu F, Weng YH (2022). Resilience of prefabricated concrete frames using hybrid steel-concrete composite connections. *Journal of Building Engineering*, 59, 105119.

EN 1993-1-1 (2001). Eurocode 3: Design of steel structures – Part 1-1: General rules and rules for buildings. European Committee for Standardization (CEN), Brussels, Belgium.

EN 1994-1-1 (2004). Eurocode 4: Design of composite steel and concrete structures – Part 1-1: General rules and rules for buildings. European Committee for Standardization (CEN), Brussels, Belgium.

Gholamhoseini A, Gilbert I, Bradford MA (2014). Time-dependent deflection of composite concrete slabs: A simplified design approach. *Australian Journal of Structural Engineering*, 15, 287-298.

Gilbert RI, Bradford MA, Gholamhoseini A, Chang ZT (2012). Effects of shrinkage on the long-term stresses and deformations of composite concrete slabs. *Engineering Structures*, 40, 9-19.

He X, Li GC, Yang Z (2019). Experimental study of the bearing capacity of long-span profiled steel sheet concrete composite slabs. *Advanced Steel Construction*, 15(3), 288-296.

Heagler RB (1993). The Steel Deck Institute method for designing composite slabs. *Thin-Walled Structures*, 16, 319-326.

Hedaoo NA, Gupta LM (2008). State of the art report on thin-walled cold-formed profiled steel decking. *Proceedings of the 19th International Specialty Conference on Cold-Formed Steel Design and Construction*, St. Louis, MO, USA, 307-323.

Hu B, Wang J (2017). Experimental investigation and analysis on flexural behavior of CFSTTC beams. *Thin-Walled Structures*, 116, 277-290.

IS 383 (2016). Coarse and fine aggregate for concrete – Specification. Bureau of Indian Standards (BIS), New Delhi, India.

IS 456 (2000). Plain and reinforced concrete – Code of practice. Bureau of Indian Standards (BIS), New Delhi, India.

IS 801 (1975). Code of practice for use of cold formed light gauge steel structural members in general building construction. Bureau of Indian Standards (BIS), New Delhi, India.

IS 10262 (2019). Concrete mix proportioning – Guidelines. Bureau of Indian Standards (BIS), New Delhi, India.

Islam SMZ, Ahmed B, Mahbub ASM, Siddique MJ, Alam S (2020). Structural strength and behavior of profiled steel sheet-concrete composite slab. *Proceedings of the 5th International Conference on Civil Engineering for Sustainable Development*, Bangladesh.

Jaffar MI, Badaruzzaman WHW, Abdullah MMAB, Kamarulzaman K, Seraji M (2015). Effect of geopolymer concrete infill on profiled steel sheeting half dry board (PSSHDB) floor system subjected to bending moment. *Applied Mechanics and Materials*, 754-755, 354-358.

Kataoka MN, Friedrich JT, Debs A (2017). Experimental investigation of longitudinal shear behavior for composite floor slab. *Steel and Composite Structures*, 23, 351-362.

Kubic CR, Daniels JH (1979). Two-way flexure of steel-deck-reinforced slabs. *Journal of the Structural Division*, 105, 1039-1054.

Lam D, Dai X (2013). Demountable shear connectors for sustainable composite construction. *Proceedings of the World Congress on Advances in Structural Engineering and Mechanics (ASEM13)*, Jeju, Korea.

Lam D, Yang J, Wang Y, Dai X, Sheehan T, Zhou K (2021). New composite flooring system for the circular economy. *Steel and Composite Structures*, 40(5), 649-661.

Lamport WB, Porter ML (1990). Deflection predictions for concrete slabs reinforced with steel decking. *ACI Structural Journal*, 87, 564-571.

Li C, Zhou Z, Wang H, Gao Y, Fan L (2023). Numerical investigation on novel shear connectors in prefabricated composite beams. *Applied Sciences*, 13(10).

Liu X, Bradford MA, Ataei A (2017). Flexural performance of innovative sustainable composite steel-concrete beams. *Engineering Structures*, 130, 282-296.

Nair S (2024). A study on C&D waste generation and recycling potential in Gujarat. *ITM Web of Conferences*, 65.

Nie J, Fan JS, Cai CS (2008). Experimental study of partially shear-connected composite beams with profiled sheeting. *Engineering Structures*, 30, 1-12.

Patil SM, Shahezad M (2014). Experimental study on cold-formed steel composite metal deck slab. *International Journal of Engineering Sciences & Research Technology*, 3(6), 201-205.

Patrick M, Bridge RQ (1992). Design of composite slabs for vertical shear. *Proceedings of the Engineering Foundation Composite Construction Conference*, Missouri, USA; *Proceedings of the Pacific Structural Steel Conference*, Tokyo, Japan.

Porter ML, Ekberg CE (1976). Design recommendations for steel deck floor slabs. *Journal of the Structural Division*, 102(11), 2121-2136.

Porter ML, Lamport WB (1990). Deflections for composite steel deck floors. *Proceedings of the 10th International Specialty Conference on Cold-Formed Steel Structures*, St. Louis, Missouri, USA.

Qiao W, Huang ZY, Wang T, Cui KL, Meng LJ (2024). Study on flexural capacity of profiled steel sheet-polyurethane sandwich slabs. *Advanced Steel Construction*, 20(1), 53-59.

Raja CM, Shanmugavelu VA, Lenin P (2012). New approach for using C&D waste. *International Journal of Scientific Research*, 2(5), 153-155.

Schuster RM (1976). Composite steel-deck concrete floor systems. *Journal of the Structural Division*, 102, 899-917.

Shahezad M (2014). Investigation on composite metal deck slab of cold-formed steel. *International Journal of Science, Technology & Management*, 3(12), 307-314.

Shin HS (2015). Influence of tensile behavior of slab on the structural behavior of shear connection in composite beam subjected to hogging moment. *International Journal of Engineering Research and Development*, 11(9), 6-15.

Shrivastava S, Chini A (2009). Construction materials and C&D waste in India. *Lifecycle Design of Buildings, Systems and Materials*, 72, 74-78.

Siva A, Senthil R, Swaminathan S (2016). Assessment of longitudinal shear strength of composite deck slab. *International Journal of Innovation and Scientific Research*, 24, 277-284.

Sun J, Yu Y, Li RYM, Wang Z, Li L, Guo F, Yu L, Deng C (2024). Study on the flexural deformation behavior of high-titanium heavy-slag concrete composite beams: Material application, experimental investigation, and theoretical refinement. *Materials*, 17(19), 4721.

Vohra HS, Dhankot MA (2015). Shear connectors and composite deck slab experimental study: State of the art review. *International Journal of Scientific Engineering and Research*, 3(3), 21-24.

Wan Z, Fang Z, Liang L, He S, Sun X (2022). Structural performance of steel–concrete composite beams with UHPC overlays under hogging moment. *Engineering Structures*, 270, 114866.

Wang Y, Yu J (2017). Punching shear behavior of an innovative connection between steel tubular column to flat concrete slab. *ce/papers - Proceedings in Civil Engineering*, 1(2-3), 721-728.

Xian-tie W (2011). Study on the longitudinal shear behavior of closed profiled steel sheet-concrete composite slab. *Journal of Xi'an University of Architecture & Technology (Natural Science Edition)*, 43(3), 335-341.

Xiong G, Li W, Wang X, Liu J, Bai Y, Chen YF (2022). Flexural behavior of prefabricated high-strength steel-concrete composite beams with steel block connectors. *Journal of Constructional Steel Research*, 197, 107507.

Zhu D, Liu J, Liu Z (2012). Properties of profiled steel sheet-concrete structure under high temperature. *Applied Mechanics and Materials*, 174-177, 113-116.